The structure of galactic disks - Studying late-type spiral galaxies using SDSS

Pohlen, M.; Trujillo, I.

Published in:
Astronomy & astrophysics

DOI:
10.1051/0004-6361:20064883

Astronomy & Astrophysics manuscript no. SDSS May 5, 2006
(DOI: will be inserted by hand later)

The structure of galactic disks

Studying late-type spiral galaxies using SDSS

M. Pohlen[1,2] and I. Trujillo[3,4]

[1] Kapteyn Astronomical Institute, University of Groningen, P.O. Box 800, NL–9700 AV Groningen, The Netherlands
e-mail: pohlen@astro.rug.nl
[2] Instituto de Astrofísica de Canarias, C/ Via Láctea s/n, E–38200 La Laguna, Tenerife, Spain
[3] Max–Planck–Institut für Astronomie, Königstuhl 17, D–69117 Heidelberg, Germany
[4] School of Physics and Astronomy, University of Nottingham, University Park, Nottingham, NG7 2RD, UK
e-mail: ignacio.trujillo@nottingham.ac.uk

Received January 23, 2006; accepted April 26, 2006

Abstract. Using imaging data from the SDSS survey, we present the g′ and r′ radial stellar light distribution of a complete sample of ∼ 90 face-on to intermediate inclined, nearby, late-type (Sb–Sdm) spiral galaxies. The surface brightness profiles are reliable (1σ uncertainty less than 0.2 mag) down to $\mu \sim 27$ mag/$\square''$. Only ∼ 10% of all galaxies have a *normal/standard* purely exponential disk down to our noise limit. The surface brightness distribution of the rest of the galaxies is better described as a broken exponential. About 60% of the galaxies have a break in the exponential profile between ∼ 1.5 – 4.5 times the scalelength followed by a *downbending*, steeper outer region. Another ∼ 30% shows also a clear break between ∼ 4.0 – 6.0 times the scalelength but followed by an *upbending*, shallower outer region. A few galaxies have even a more complex surface brightness distribution. The shape of the profiles correlates with Hubble type. Downbending breaks are more frequent in later Hubble types while the fraction of upbending breaks rises towards earlier types. No clear relation is found between the environment, as characterised by the number of neighbours, and the shape of the profiles of the galaxies.

Key words. Galaxies: photometry – Galaxies: structure – Galaxies: fundamental parameters – Galaxies: evolution – Galaxies: formation

1. Introduction

The structural properties of the faintest regions of galactic disks must be intimately linked to the mechanisms involved in the growing and shaping of galaxies. These *outer edges* are easily affected by interactions with other galaxies and, consequently, their characteristics must be closely connected with the evolutionary path followed by the galaxies. Together with their stellar halos, the study of the outer edges allows the exploration of the so-called fossil evidence imprinted by the galaxy formation process.

Most of the detailed structural studies of nearby disk galaxies so far (Courteau, 1996; de Jong, 1996; Graham, 2001; Jansen & Kannappan, 2001; Trujillo et al., 2002; MacArthur et al., 2003; Möllenhoff, 2004) have been concentrated on the (most easily accessible) inner parts of the galaxies. These studies of the brightest region of the stellar disk show that its light distribution is almost always well described by a simple exponential decline going back to Patterson (1940), de Vaucouleurs (1959) or Freeman (1970). This simple description, however, has now been shown to fail at fainter surface brightness. In fact, since van der Kruit (1979) we know that this decline does not continue to the last measured point, but is *truncated* after several radial scalelengths.

The main concern with current, larger statistical studies exploring the faintest surface brightness region of the galaxies is that they are based on edge-on galaxies (Barteldrees & Dettmar, 1994; Pohlen et al., 2000a; Florido et al., 2001; de Grijs et al., 2001; Pohlen, 2001; Kregel, van der Kruit, & de Grijs, 2002). This geometry facilitates the discovery of the truncation in the surface brightness profiles, but introduces severe problems caused by the effects of dust and the line–of–sight integration (Pohlen et al., 2004, for a recent review), such as masking the actual shape of the truncation region, or interfering with the identification of other important disk features (e.g. bars, rings, or spirals).

Only few works have probed the faintest regions of the disk galaxies in low inclination systems. Pohlen et al. (2002) demonstrated for a small sample of face-on galaxies that the so-called cut-offs in the surface brightness profiles discovered by van der Kruit are in fact not complete but better described by a broken exponential with a shallow inner and a steeper outer exponential region separated at a relatively well defined

Send offprint requests to: M. Pohlen

break radius. However, not all the galaxies seem to have a break or a truncation in their surface brightness profiles. Just recently Bland-Hawthorn et al. (2005) found (using star counts) again a galaxy (NGC 300) for which the exponential decline simply continues down to $\sim$ 10 radial scalelength. Together with earlier measurements by Barton & Thompson (1997) or Weiner et al. (2001) (using surface photometry) this provides evidence that indeed there are prototypical, model exponential disks.

Our picture of the faintest regions of spiral galaxies have been even broadened with some recent studies. Erwin et al. (2005a), studying a large sample of early-type barred S0–Sb galaxies, discovered that there is more than *truncated* or *untruncated* galaxies. They report the detection of *antitruncated* galaxies, which show also a broken exponential but having the opposite behaviour, an outer upbending profile. Similar structures are also found for a large sample of irregular systems (Im) and BCDs by Hunter & Elmegreen (2005).

The disk structures we describe in this study are the result of initial conditions, infalling matter and/or redistribution of gas and stars, already settled in the disk, triggered by internal (e.g. bars) or external (e.g. interaction) forces. All these processes are linked to the detailed mechanism of forming the stars which build up the observed brightness distribution. To explain for example the observed truncation in the surface brightness profiles radial star-formation thresholds (e.g. Kennicutt, 1989; Schaye, 2004) have been suggested (see Pohlen et al., 2004). However, there is compelling evidence of star-formation in the far outer regions of spiral galaxies (e.g. Ferguson et al., 1998; Cuillandre et al., 2001; Thilker et al., 2005; Gil de Paz et al., 2005), well beyond the break of the observed broken exponential structure (Pohlen et al., 2002). The outer star formation activity argues against a simple threshold scenario. Just recently, though, Elmegreen & Hunter (2006) show that their model of star-formation is able to produce the variety of observed radial profiles. Alternatively, Debattista et al. (2005) also find downbending breaks using purely collisionless N-body simulations.

The main goal of the present study is to conduct a complete census of the outer disk structure of late-type galaxies –together with a complementary study by Erwin et al. (2006) for early-type (barred) galaxies– in the local universe. The objective is to provide the frequencies of the different surface brightness profile types, the structural disk parameters, and search for correlations (if any) between them.

Aside from the observations showing the increasing complexity of radial surface brightness profiles, the breaks in the surface brightness distribution can be used to directly constrain galaxy evolution. Pérez (2004) showed that it is possible to detect stellar truncations even out to higher redshift ($z \sim 1$). So using the radial position of the truncation as a direct estimator of the size of the stellar disk, Trujillo & Pohlen (2005) infer a moderate ($\sim$ 25%) inside-out growth of the disk galaxies since $z \sim 1$, using as a local reference the galaxies studied in this paper.

The remainder of this paper is organised as follows. In Sect. 2 we describe the sample selection and our environment parameter. In Sect. 3 we give the details about the ellipse fitting and the SDSS imaging used, characterising their quality and addressing the crucial issue of sky subtraction. The applied classification schema of the observed profiles and the derived parameters are discussed in Sect. 4. The results are presented in Sect. 5 and briefly discussed in Sect. 6. The colour profiles and the physical implications derived from them will be discussed in a subsequent paper. In Appendix A we give detailed comments for all galaxies, show their r' and g'-band surface brightness profiles and reproduce their SDSS colour pictures.

2. The sample

2.1. Selection

We selected our initial galaxy sample from the LEDA[1] online galaxy catalogue (version Nov. 2004), since this is the richest catalogue with homogeneous parameters of galaxies for the largest available sample. We restricted the Hubble type (T parameter), the mean heliocentric radial velocity relative to the Local Group (corrected for virgocentric inflow, $v_{\rm vir}$), the axis ratio (major axis/minor axis), the absolute B-magnitude ($M_{\rm abs}$), and the Galactic latitude ($b_{\rm II}$).

The Hubble type is chosen to be between $2.99 < T < 8.49$ (corresponding to Sb to Sdm galaxies) building an intermediate- to late-type galaxy sample. This allows a complementary study to the work by Erwin et al. (2006) on the disk structure of early type (barred) galaxies. To have some, but not too much, overlap with their sample we did not include all Sb galaxies by excluding the range $2.49 < T < 2.99$. The axis ratio is selected to be $\log r_{25} < 0.301$ (equal to $a/b < 2$ or $e < 0.5$, which corresponds to an inclination of $\lesssim 61^\circ$ assuming an intrinsic flattening of $q_0 = 0.14$) bringing a face-on to intermediate inclined galaxy sample. This is necessary to avoid the influence of the dust and is convenient to provide reliable information on the morphological features such as bars, rings, or spiral arm structure. The recession velocity is chosen to be $v_{\rm vir} < 3250$ km/s and the galaxies brighter than -18.4 $M_{\rm abs}$ in B band (the total B-magnitude, provided by LEDA, is corrected for galactic and internal extinction, k corrected, and the distance modulus is derived from the recession velocity corrected for Virgo infall with a Hubble constant of $H_0 = 70$ km s^{-1}Mpc^{-1}). We did not apply a diameter limit. Since SDSS, our data source, is a survey of the high Galactic latitude sky, visible from the northern hemisphere, there is no worry about incompleteness there. In any case, we restricted the initial sample to $|b_{\rm II}| > 20^\circ$.

To assess the completeness of the LEDA catalogue Baryshev & Paturel (2001) draw several cumulative curves $\log N$ versus $\log r$ (N is the total number of observed galaxies within the radius r in Mpc) for different absolute magnitudes and compare these with an expected galaxy distribution. Using the same approach we have confirmed that LEDA (version Nov. 2004) is almost complete for galaxies of $M_{\rm abs} < -18.4$ within our $\sim$ 46 Mpc survey distance (estimated following the Hubble relation with $H_0 = 70$ km s^{-1}Mpc^{-1}).

Our selection criteria results in a total number of 655 galaxies, of which 98 (15%) are part of the SDSS Second

[1] http://leda.univ-lyon1.fr

Data Release (DR2), surveying the north Galactic cap and three stripes in the southern Galactic cap (York et al., 2000; Abazajian et al., 2004). The global parameters[2] for this subsample of 98 galaxies are presented in Table 1. Histograms showing the distribution of Hubble type and absolute magnitude (cf. Fig. 1) reveal that the subsample restricted by the SDSS DR2 coverage is apparently unbiased in this sense. There is a lack of very bright galaxies ($M_{\rm abs} < -21.9$ B-mag) due to the small number statistics. Plotting absolute magnitude $M_{\rm abs}$ with Hubble Type T reveals –although with a lot of scatter– a mild trend of earlier Hubble type galaxies being on average brighter.

Only three galaxies (NGC 4273, NGC 4480, NGC 4496A) are possible members of the Virgo Cluster according to their VCC numbers by Binggeli et al. (1985). In this sense our sample is a faithful representation of the local spiral galaxy population providing a volume limited sample ($D \lesssim 46$ Mpc) of late-type, intermediate inclined to face-on nearby galaxies brighter than −18.4 B-mag. The Appendix A and B show colour images for all galaxies.

2.2. Environment

To characterise the environment we counted neighbours around our sample galaxies using the SDSS database from a more recent Data Release (DR3, Abazajian et al., 2005). According to the distance, derived from the infall corrected velocity, we sum all the DR3 galaxies within a projected radius of 1 Mpc that satisfy the following criteria: the difference in velocity with respect to the targeted galaxy is less than 350 km s^{-1} (Giuricin et al., 2000) and their absolute magnitude is brighter than $M_{\rm abs} < -16$ r'-mag. It is important to note, however, that the density of galaxies could be affected by the position of the galaxy within the survey. If the targeted galaxy is close to the edge of the survey or to a region where the redshift completeness (fraction of photometrically detected galaxies with redshifts) is not high, the number of neighbours could be underestimated. To eliminate such a problem we have estimated whether the distance of our galaxy to the edge of the survey or to a redshift incomplete region is less than 1 Mpc. If this is the case this galaxy is not used in the analysis of the effect of the density on the galaxy profile type.

3. Data and profile extraction

3.1. The data

The Sloan Digital Sky Survey (SDSS) (York et al., 2000) will map one-quarter ($\sim 10^4 \square^\circ$) of the entire sky mainly around the north galactic cap (above Galactic latitude $\sim 30^\circ$) in five bands, u', g', r', i' and z' (Fukugita et al., 1996; Smith et al., 2002). SDSS imaging are obtained using a drift-scanning mosaic CCD camera (Gunn et al., 1998) with a pixel size of 0.396″. We downloaded the g' and r' band images (which have a median PSF of ∼1.4″in r') of the night sky ("corrected frames") in fits format using the Data Archive Server[3]. The u', i' and z' bands images are less sensitive and, consequently, less useful to study the profile towards the outer disk. The corrected frames, having been bias subtracted, flat-fielded, and purged of bright stars are stored at SDSS in integer format to save disk space. According to the SDSS helpdesk the pixel values get randomised appropriately before being rounded to make sure that the statistics of the background counts are what they should be. An additional offset (SOFTBIAS) of 1000 counts is added to each pixel to avoid negative pixel values and should be subtracted together with the sky value (as described in Sect. 3.3).

After inspecting all images for the 98 galaxies we had to remove 13 galaxies (marked with a ⋆ in Table 1) from further analysis (cf. Appendix B). For four galaxies (NGC 0988, NGC 4900, UGC 04684, and UGC 06162) there are one (or more) very bright foreground stars too close to the galaxy preventing any useful surface brightness measurement. Another six galaxies (NGC 0428, NGC 2712, NGC 4116, NGC 4496A, NGC 5364, and UGC 09215) are very close to the border of the SDSS field (more than 1/3 of the galaxy is off the image). To avoid any problems while trying to recover the galaxies with a mosaic out of two or even three images we discarded them. Two peculiar galaxies (NGC 3023 and NGC 5218) are removed since they are clearly interacting systems. They are gravitationally highly distorted and in the case of NGC 5218 connected by an intergalactic bridge to its companion. One galaxy (PGC 032356 ≡ UGCA 219) turns out to be a BCD galaxy and probably even a double system. This leave 85 galaxies for the final analysis.

3.2. Photometric calibration

The photometric calibration is done using the *aa*, *kk*, and *airmass* coefficients (the photometric zeropoint, the extinction term and the airmass) out of the associated TsField table file for each image. From this we calculated[4] our surface brightness zeropoints as: $-2.5 * (0.4 * [aa + kk * airmass]) + 2.5 * \log\left(53.907456 * 0.396^2\right)$ using the pixel scale of 0.396″/pixel and the exposure time of 53.907456 *s* for each SDSS pixel. Our magnitudes are the conventional Pogson astronomical magnitudes in the SDSS g' and r' AB system in contrast to the asinh magnitudes used in the SDSS database. The applied zero points are given in Table 2. To transform the SDSS g' and r' standard-star system magnitudes into the commonly used Johnson-Cousins B, R system, we applied the transformation equations given in Smith et al. (2002): $B = g' + 0.47(g' - r') + 0.17$ and $R = g' - 1.14(g' - r') - 0.14$. For eight galaxies of the final SDSS sample we found aperture measurements in the literature. Synthetic aperture measurements on the SDSS images agree with these previous published values in the majority of cases to better than 0.1 mag. All profiles and surface brightness results, given in Table 3, are the measured values from the uncorrected SDSS data. Only at calculating mean values and plotting histograms we applied the galactic extinction correction according to Schlegel et al. (1998) using

[2] Note: Some of the bar classifications from LEDA have slightly changed after our study. Table 1 still shows the 2004 version. For comparison we always listed the RC3 classification.

[3] http://www.sdss.org/dr2/access/index.html#DAS

[4] http://www.sdss.org/dr2/algorithms/fluxcal.html

Galaxy	RA	DEC	RC3	LEDA	T	$M_{\rm abs}$	Diam.	$v_{\rm vir}$	Dist.	$v_{\rm rot}$
	(J2000.0)		type	type		[B-mag]	[′]	[km s^{-1}]	[Mpc]	[km s^{-1}]
(1)	*(2)*	*(3)*	*(4)*	*(5)*	*(6)*	*(7)*	*(8)*	*(9)*	*(10)*	*(11)*
NGC 0428*	01 12 55.7	+00 58 54	.SXS9..	SBd	8.2	−19.39	3.6	1118	16.0	90
NGC 0450	01 15 30.8	−00 51 38	.SXS6*.	SBc	6.0	−19.63	3.0	1712	24.5	118
PGC 006667†	01 49 10.2	−10 03 45	.SBS7..	SBcd	7.1	−18.77	2.9	1887	27.0	129
NGC 0701	01 51 03.8	−09 42 09	.SBT5..	SBc	5.1	−19.74	2.5	1729	24.7	140
NGC 0853	02 11 41.5	−09 18 17	.S..9P?	Sd	8.3	−18.42	1.5	1405	20.1	...
NGC 0941	02 28 27.9	−01 09 06	.SXT5..	SBc	5.4	−19.02	2.5	1535	21.9	91
NGC 0988*	02 35 27.4	−09 21 17	.SBS6*.	SBc	5.8	−20.72	4.5	1392	19.9	135
UGC 02081	02 36 00.9	+00 25 12	.SXS6..	Sc	5.8	−18.56	1.8	2549	36.4	100
NGC 1042	02 40 23.9	−08 25 58	.SXT6..	SBc	6.1	−19.83	4.4	1264	18.1	50
NGC 1068†	02 42 40.8	−00 00 48	RSAT3..	Sb	3.0	−21.69	7.6	1068	15.3	310
NGC 1084	02 45 59.7	−07 34 37	.SAS5..	Sc	5.1	−20.20	3.2	1299	18.6	173
NGC 1087	02 46 25.2	−00 29 55	.SXT5..	SBc	5.3	−20.46	3.7	1443	20.6	125
NGC 1299	03 20 09.4	−06 15 50	.SBT3?.	Sb	3.2	−19.25	1.2	2197	31.4	...
NGC 2543	08 12 58.0	+36 15 16	.SBS3..	SBb	3.1	−20.66	2.5	2590	37.0	158
NGC 2541	08 14 40.1	+49 03 41	.SAS6..	SBc	6.2	−18.50	5.8	734	10.5	97
UGC 04393	08 26 04.3	+45 58 03	.SB?...	SBc	5.5	−19.49	2.2	2290	32.7	70
NGC 2684	08 54 54.1	+49 09 37	.S?....	Sd	7.8	−19.76	1.0	3043	43.5	99
UGC 04684*	08 56 40.7	+00 22 30	.SAT8*.	Sd	7.9	−18.86	1.4	2477	35.4	108
NGC 2701	08 59 05.9	+53 46 16	.SXT5*.	SBc	5.1	−20.36	2.1	2528	36.1	168
NGC 2712*	08 59 30.5	+44 54 50	.SBR3*.	SBb	3.2	−20.02	2.9	1987	28.4	171
NGC 2776	09 12 14.3	+44 57 17	.SXT5..	SBc	5.1	−21.04	2.9	2796	39.9	118
NGC 2967	09 42 03.3	+00 20 11	.SAS5..	Sc	4.8	−20.26	2.6	1858	26.5	172
NGC 3023*	09 49 52.6	+00 37 05	.SXS5P*	SBc	5.4	−19.20	2.6	1852	26.5	67
NGC 3055	09 55 17.9	+04 16 11	.SXS5..	SBc	5.0	−19.90	2.1	1816	25.9	155
NGC 3246	10 26 41.8	+03 51 43	.SX.8..	SBd	8.0	−18.91	2.2	2138	30.5	117
NGC 3259	10 32 34.8	+65 02 28	.SXT4*.	SBbc	4.0	−19.84	2.1	1929	27.6	119
NGC 3310	10 38 45.8	+53 30 12	.SXR4P.	SBbc	4.0	−20.25	2.8	1208	17.3	280
NGC 3359	10 46 36.3	+63 13 28	.SBT5..	SBc	5.0	−20.42	7.2	1262	18.0	139
PGC 032356†*	10 49 04.6	+52 19 57	.S?....	Sc	6.0	−18.46	0.8	2679	38.3	...
NGC 3423	10 51 14.3	+05 50 24	.SAS6..	Sc	6.0	−19.54	3.9	1032	14.7	122
NGC 3488	11 01 23.6	+57 40 39	.SBS5*.	SBc	5.1	−18.80	1.6	3226	46.1	132
UGC 06162*	11 06 54.7	+51 12 12	.S..7..	SBcd	6.7	−19.08	2.3	2426	34.7	105
NGC 3583	11 14 11.0	+48 19 06	.SBS3..	SBb	3.2	−19.57	2.3	2347	33.5	194
NGC 3589	11 15 13.2	+60 42 01	.S..7*.	SBcd	7.0	−18.49	1.5	2217	31.7	75
UGC 06309	11 17 46.4	+51 28 36	.SB?...	SBc	5.0	−19.63	1.3	3097	44.2	124
NGC 3631	11 21 02.4	+53 10 08	.SAS5..	Sc	5.1	−20.62	4.9	1388	19.8	82
NGC 3642	11 22 18.0	+59 04 27	.SAR4*.	Sbc	4.0	−20.60	5.5	1831	26.2	45
UGC 06518	11 32 20.4	+53 54 17	.....	Sbc	4.3	−18.94	1.0	3044	43.5	84
NGC 3756	11 36 48.3	+54 17 37	.SXT4..	SBbc	4.3	−19.89	3.8	1525	21.8	153
NGC 3888	11 47 34.7	+55 58 00	.SXT5..	SBc	5.3	−20.43	1.8	2648	37.8	191
NGC 3893	11 48 38.4	+48 42 34	.SXT5*.	SBc	4.8	−20.33	4.1	1193	17.0	175
UGC 06903	11 55 36.9	+01 14 15	.SBS6..	SBc	5.8	−18.80	2.5	1916	27.4	158
NGC 3982	11 56 28.3	+55 07 29	.SXR3*.	SBb	3.2	−19.54	2.3	1351	19.3	193
NGC 3992†	11 57 35.9	+53 22 35	.SBT4..	SBbc	3.8	−20.98	6.9	1286	18.4	285
NGC 4030	12 00 23.4	−01 06 03	.SAS4..	Sbc	4.1	−20.27	3.9	1476	21.1	231
NGC 4041	12 02 12.2	+62 08 14	.SAT4*.	Sbc	4.3	−19.92	2.7	1486	21.2	284
NGC 4102	12 06 23.1	+52 42 39	.SXS3$.	SBb	3.0	−19.38	3.1	1082	15.5	169
NGC 4108	12 06 44.0	+67 09 44	PSA.5*.	Sc	5.0	−20.13	1.7	2828	40.4	242

Table 1. Global parameters of the LEDA–SDSS DR2 subsample: *(1)* Principal name in LEDA, *(2)* right ascension, and *(3)* declination, *(4)* RC3 de Vaucouleurs et al. (1991) Hubble-type, and *(5)* LEDA Hubble-type, *(6)* coded LEDA Hubble parameter T, *(7)* absolute B band magnitude, corrected for galactic plus internal extinction, and k-corrected, *(8)* apparent diameter, defined by the isophote at the brightness of 25 B-mag/$\square''$, *(9)* heliocentric radial velocities corrected for the Local Group infall onto Virgo, *(10)* estimated distance according to the Hubble relation with the Hubble constant of $H_0 = 70$ km s^{-1}Mpc^{-1}, *(11)* weighted average of

Galaxy	RA	DEC	RC3	LEDA	T	$M_{\rm abs}$	Diam.	$v_{\rm vir}$	Dist.	$v_{\rm rot}$
	(J2000.0)		type	type		[B-mag]	[′]	[km s^{-1}]	[Mpc]	[km s^{-1}]
(1)	(2)	(3)	(4)	(5)	(6)	(7)	(8)	(9)	(10)	(11)
NGC 4108B	12 07 11.3	+67 14 10	.SXS7P?	SBcd	7.0	−18.46	1.3	2840	40.6	212
NGC 4116⋆	12 07 37.0	+02 41 29	.SBT8..	SBd	7.5	−19.32	3.5	1346	19.2	104
NGC 4123	12 08 11.1	+02 52 42	.SBR5..	SBc	4.8	−19.55	4.1	1364	19.5	134
NGC 4210	12 15 15.9	+65 59 08	.SBR3..	SBb	3.0	−19.89	2.0	3000	42.9	202
NGC 4273	12 19 56.2	+05 20 36	.SBS5..	SBc	5.1	−20.41	2.1	2435	34.8	187
NGC 4480	12 30 26.8	+04 14 47	.SXS5..	SBc	5.1	−20.14	2.1	2494	35.6	169
NGC 4496A⋆	12 31 39.5	+03 56 22	.SBT9..	SBd	8.2	−20.25	3.8	1780	25.4	95
NGC 4517A	12 32 28.1	+00 23 25	.SBT8*.	SBd	7.9	−19.18	3.8	1562	22.3	73
UGC 07700	12 32 32.8	+63 52 38	.SBS8..	SBd	7.8	−18.50	1.8	3239	46.3	94
NGC 4545	12 34 34.2	+63 31 30	.SBS6*.	SBc	5.9	−20.49	2.5	3000	42.9	136
NGC 4653	12 43 50.9	−00 33 41	.SXT6..	SBc	6.1	−20.37	3.0	2658	38.0	181
NGC 4668	12 45 32.0	−00 32 09	.SBS7*.	SBcd	7.1	−18.88	1.5	1654	23.6	63
UGC 08041	12 55 12.7	+00 07 00	.SBS7..	SBcd	6.8	−18.62	3.2	1376	19.7	93
UGC 08084	12 58 22.4	+02 47 33	.SBS8..	SBd	8.1	−18.61	1.3	2824	40.3	90
NGC 4900⋆	13 00 39.2	+02 30 02	.SBT5..	SBc	5.2	−19.01	2.2	1020	14.6	185
NGC 4904	13 00 58.6	−00 01 38	.SBS6..	SBc	5.7	−18.69	2.1	1213	17.3	122
UGC 08237	13 08 54.5	+62 18 23	PSB.3*.	SBb	3.2	−19.61	0.9	3120	44.6	...
NGC 5147	13 26 19.2	+02 06 04	.SBS8..	SBd	7.9	−18.77	1.8	1154	16.5	118
NGC 5218⋆	13 32 10.4	+62 46 04	.SBS3$P	SBb	3.1	−20.46	1.9	3154	45.1	243
UGC 08658†	13 40 39.9	+54 19 59	.SXT5..	SBc	5.1	−19.91	2.6	2285	32.6	126
NGC 5300	13 48 16.1	+03 57 03	.SXR5..	SBc	5.0	−18.93	3.5	1246	17.8	124
NGC 5334	13 52 54.4	−01 06 51	.SBT5*.	SBc	5.0	−19.22	3.9	1433	20.5	145
NGC 5376	13 55 16.1	+59 30 24	.SXR3$.	SBb	3.0	−20.00	2.1	2293	32.8	216
NGC 5364⋆	13 56 11.9	+05 00 55	.SAT4P.	Sbc	4.4	−20.53	6.0	1322	18.9	157
NGC 5430	14 00 45.8	+59 19 43	.SBS3..	SBb	3.1	−20.86	2.2	3238	46.3	195
NGC 5480	14 06 21.5	+50 43 32	.SAS5*.	Sc	5.0	−19.72	1.7	2119	30.3	138
NGC 5584	14 22 23.8	−00 23 15	.SXT6..	SBc	6.1	−19.80	3.2	1702	24.3	136
UGC 09215⋆	14 23 27.3	+01 43 32	.SBS7..	SBcd	6.6	−18.81	2.2	1462	20.9	102
NGC 5624	14 26 35.3	+51 35 03	.S?....	Sc	5.0	−18.69	1.1	2186	31.2	67
NGC 5660	14 29 49.8	+49 37 22	.SXT5..	SBc	5.1	−20.62	2.8	2585	36.9	138
NGC 5667	14 30 22.9	+59 28 11	.S..6*P	SBc	5.8	−19.69	1.7	2222	31.7	119
NGC 5668	14 33 24.4	+04 27 02	.SAS7..	Scd	6.7	−19.65	2.8	1672	23.9	87
NGC 5693	14 36 11.2	+48 35 04	.SBT7..	SBcd	6.8	−18.64	1.9	2537	36.2	39
NGC 5713	14 40 11.4	−00 17 25	.SXT4P.	SBbc	4.1	−20.50	2.8	1958	28.0	135
NGC 5768	14 52 07.9	−02 31 47	.SAT5*.	Sc	5.0	−19.24	1.6	2018	28.8	122
IC 1067	14 53 05.2	+03 19 54	.SBS3..	SBb	3.0	−18.97	2.0	1665	23.8	158
NGC 5774	14 53 42.6	+03 35 00	.SXT7..	SBcd	6.9	−19.09	2.8	1655	23.6	91
NGC 5806	15 00 00.4	+01 53 29	.SXS3..	SBb	3.3	−19.74	3.0	1440	20.6	182
NGC 5850	15 07 07.7	+01 32 40	.SBR3..	SBb	3.0	−21.43	4.3	2637	37.7	133
UGC 09741†	15 08 33.5	+52 17 46	.S?....	Sc	6.0	−18.54	0.9	2735	39.1	...
UGC 09837	15 23 51.7	+58 03 11	.SXS5..	Sc	5.1	−19.45	1.8	2938	42.0	221
NGC 5937	15 30 46.1	−02 49 46	PSXT3P.	Sb	3.2	−20.90	1.9	2870	41.0	202
IC 1125	15 33 05.6	−01 37 42	.S..8*.	SBd	7.7	−20.05	1.7	2868	41.0	106
IC 1158	16 01 34.1	+01 42 28	.SXR5*.	SBc	5.3	−19.36	2.2	2018	28.8	125
NGC 6070	16 09 58.9	+00 42 34	.SAS6..	Sc	6.0	−21.04	3.4	2085	29.8	215
NGC 6155	16 26 08.3	+48 22 01	.S?....	Sd	7.8	−19.45	1.3	2684	38.3	105
UGC 10721	17 08 25.6	+25 31 03	.S..6?.	Sc	5.8	−19.68	1.2	3118	44.5	144
NGC 7437	22 58 10.0	+14 18 32	.SXT7..	Scd	7.1	−18.88	1.8	2190	31.3	175
NGC 7606	23 19 04.8	−08 29 06	.SAS3..	Sb	3.2	−21.38	4.3	2187	31.2	291
UGC 12709	23 37 24.0	+00 23 27	.SXS9..	Sd	8.3	−19.05	3.0	2672	38.2	70

Table 1. (continued): Global parameters of the LEDA–SDSS DR2 subsample
(⋆): Galaxy removed from further analysis (see text).
(†): Galaxy with relevant alternative name: NGC 1068 ≡ M 77; NGC 3992 ≡ M 109; PGC 006667 ≡ UGCA 021; PGC 032356 ≡ UGCA 219; UGC 08658 ≡ Holmberg V; UGC 09741 ≡ NGC 5975 A

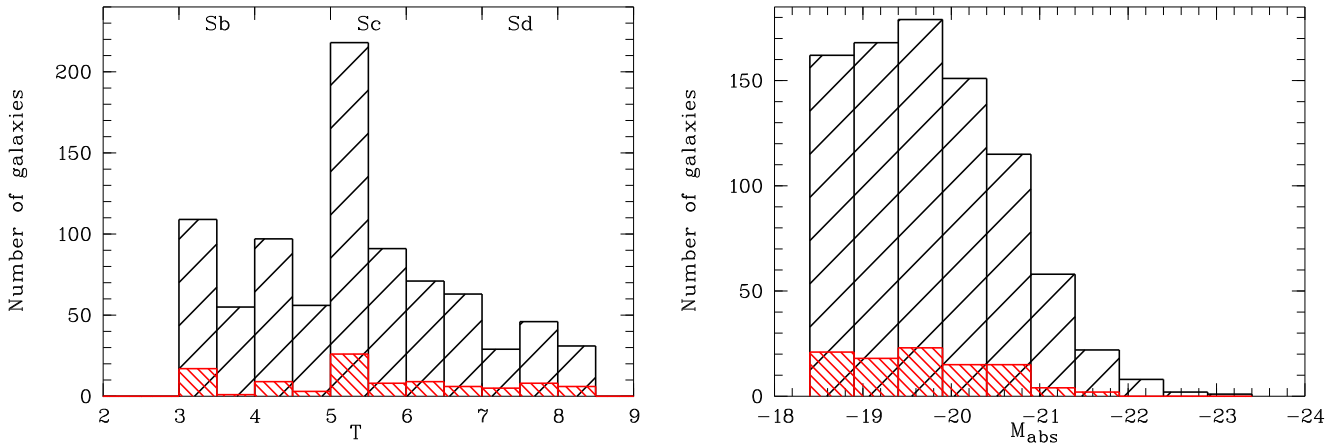

Fig. 1. Histogram showing the distribution of galaxies covering the morphological types (T) and absolute magnitude ($M_{\rm abs}$) for the full LEDA sample *(rising hashed lines)* and the studied SDSS DR2 subsample *(falling hashed lines)*.

$\mu_{\rm corrected} = \mu_{\rm measured} - A_{r'/g'}$. The values we used for $A_{r'}$ and $A_{g'}$ are also shown in Table 3. No attempt was made to correct the surface brightness measurements for internal extinction, since no unique recipe is available to do this. In addition, the galaxies studied here are all fairly face-on systems ($< e >= 0.3 \Leftrightarrow i \sim 46^\circ$) so the expected corrections are only small. Since we are working with a local sample ($z \lesssim 0.01$) we also do not correct for the cosmological surface brightness dimming.

3.3. Sky subtraction

The crucial point in using SDSS data (and in general) to study surface brightness profiles at very faint levels is the measurement of an appropriate sky value. SDSS provides in the header of each image a first estimate of such a value. However, this is just a global value which is in more than half of the cases off by more than ±0.2 counts ($\gtrsim$ 0.2% level) and therefore for our purposes not accurate enough. We need a more elaborated value depending on the size of the galaxy, thus the area of sky covered by the galaxy, and the exact position on the chip. This means that for different galaxies on the same chip we may derive different sky values.

In deep surface photometry the quality (flatness and noise) of the background around (and 'below') the galaxy determines the surface brightness level down to which one can trust the profiles. A common way of measuring the sky is, after the removal of a possible large scale gradient (typically of only first order), to manually place several small boxes homogeneously around –*but outside*– the galaxy, avoiding foreground stars or obvious background galaxies, and measure the median of the pixel distribution in each box. The best sky value is then the mean value of all median measurements. However, the fact of storing SDSS data as integer not real numbers (cf. Sect. 3.1) hampers the use of median values in small boxes. Only by using a large number of pixels (or an inappropriate high number of boxes dealing with about 100 galaxies) one is able to recover an accurate estimate of the mean value of the background pixel distribution.

Therefore we decided to use two independent methods to determine the sky value. First, we strategically placed 2-5 large, rectangular sky boxes (of roughly 100k-200k pixels) as close as possible to the galaxy avoiding bright foreground stars or obvious structure in the background (e.g. from halos of very bright foreground stars) while trying to match the brightness of the sky around the galaxy. Within each box we derived the mean sky after three, 3σ, clipping iterations to remove the unavoidable contamination by faint foreground stars. The mean value of all boxes serves as the first estimate of the sky. For the second method we applied a free ellipse fit to the original image. Using the ellipse task in IRAF[5] we calculated the flux in linear steps of 10 pixels between successive ellipses forcing the program to extend the fit well beyond the galaxy with the fixed ellipticity and PA of the outer disk (see Fig. 2). By plotting the flux at these ellipses as a function of radius it becomes clear at which radial distance the ellipses leave the galaxy and enters the background, flat flux (noise), region. After visual confirmation that these ellipses are really outside the galaxy, by overplotting the ellipses on the image, the mean value and standard deviation of the fluxes within the above radius and the radius extended by ~ 20% are used as the final sky values. In most cases the two methods agree well within ±0.15 counts (~ 0.15% of the sky). Since it is possible to automatise it, we choose the ellipse method to fix our final sky values. They are listed in Table 2 together with a limiting surface brightness ($\mu_{\rm lim}$) due to a 3σ-sky error, which is used to constrain the outer boundary for the exponential fits. Our sky values can be easily inspected by downloading the public SDSS images.

To specify the error on the profiles from our sky estimate (which is much larger than the statistical errors produced by e.g. photon noise) in more detail we defined a more conservative critical surface brightness ($\equiv \mu_{\rm crit}$) up to where we really trust the final profile. This is placed where the profiles obtained by either over- or undersubtracting the sky by $\pm 1\sigma$ start to deviate by more than 0.2 mag, which is at 0.54 mag above the limiting surface brightness defined above. So the typical

[5] Image Reduction and Analysis Facility (IRAF) http://iraf.noao.edu/

value for the full sample of this critical surface brightness is $\mu_{\rm crit} \sim 27.0$ r'-mag/$\square''$. This is the limit down to which the slope of the outer profile could be traced confidently.

The pure background noise in the r' band images is typically slightly higher compared to the g' band image, which is expected for images taken at new moon. However, the g' band images suffer often from an electronic noise pattern in addition to the normal patchy background. Typically 6-8 more or less pronounced stripes are visible where all rows show a slightly different background level, alternating between being higher or lower. Unfortunately, this structure is not common on all images so there is no way to properly remove it by combining several images as usually done for fringe patterns. In many cases the galaxies are small compared to the strip size and the above pattern is not an issue. In other cases only small parts of the galaxies reach another strip and can be masked. However, there are some galaxies extended over two or more stripes. For these systems the sky estimate is less reliable because the contribution of each region changes with changing size of the ellipse.

For five galaxies (NGC 1042, NGC 1084, NGC 5480, NGC 5624, and PGC 006667) we had to remove at first a large scale gradient (from top to bottom) in the background of the r' band images (for NGC 1042 also in the g' band) with a linear fit (using IRAFs *imsurfit*).

3.4. Data quality

We have checked our sky estimation method comparing the profiles obtained from the SDSS images with deep surface photometry. We have used the profiles of three face-on Sbc–Sc galaxies from Pohlen et al. (2002), from which UGC 9837 is also part of our sample.

The photometrically transformed SDSS profiles match the deep R-band surface brightness profiles in all three cases quite well (two of the galaxies are shown in Fig. 3). The remaining differences visible are easily explained by the two very different methods applied to extract these profiles. Whereas the SDSS profiles are standard fixed ellipse fits to the images, the deep R-band comparison profiles are obtained by vertically averaging after polar transformation (see Pohlen et al., 2002). This test confirms that SDSS profiles can be obtained reliably down to ~ 27.0 r'-mag/$\square''$.

3.5. Ellipse fitting and Masking

We used the IRAF task *ellipse* (STSDAS package) on the sky subtracted images to produce our final surface brightness profiles. We apply an extensive manual masking for each galaxy image. This is necessary to remove contamination from different sources. We masked all non-galaxy components like foreground stars, companion galaxies, or faint background galaxies. Not masked are extended spiral arms, or outer asymmetries clearly belonging to the galaxy itself. The masking is primarily done in a 9x9 pixel (3.6″ x 3.6″) median smoothed version of the image, ideally suited to visualise structure in the background. This step also ensures to reliably trace the halos of the foreground stars to large radii. Whereas this is necessary for bright stars it is a conservative measure for fainter ones. In a second round any remaining stars in the unsmoothed image are also masked.

The common center for each concentric ellipse is fixed by a Gaussian fit to the bright nucleus of the galaxy. For 21 galaxies (marked in Table 2 with a †) the disk is lopsided or there is no bright center visible so we first allowed the ellipse centers to vary, choosing the best center representative for the outer disk.

We used a logarithmic radial sampling with steps of 0.03 to increase the S/N especially in the outer parts at cost of larger radial bins compared to linear sampling. Iterative 3σ rejection along the ellipse is applied to minimise the influence of cosmic rays or any remaining faint foreground stars.

We fitted two different sets of ellipses (three in case of a necessary free center fit) to each galaxy image (for general information on ellipse fitting see Erwin et al., 2006). The first, free ellipse fit tends to follow morphological features like bars, spirals, or asymmetries so it is not ideal to characterise the outer, underlying disk component, which we want to address in this work. Therefore we used a fixed ellipse fit to produce our final surface brightness profiles which will be the only ones discussed in the following sections. Fixing a single ellipticity and position angle for a galaxy is based on the assumption that the disk is axisymmetric and round and the ellipticity and PA values are representative for the orientation (inclination angle) of the galaxy.

The initial free ellipse fit (fixed center, free ellipticity and PA) is used to determine the best set of ellipticity and PA describing the outer disk. These values are typically taken at the radius where the mean flux of the best fitted free ellipse reaches the value of the standard deviation of our background measurement in large boxes (1σ criterion). This limit ensures enough S/N to fit a free ellipse but is small enough to be in the radial region dominated by the outer disk. Ideally one would like to determine the ellipticity and PA of the outer disk not photometrically, but by means of kinematical informations. Since this is not possible for the whole sample we used only the photometric way to get a set of homogeneous values for all our galaxies. However, for some galaxies the 1σ criterion clearly marked a radius in a region with rapidly changing ellipticity and PA values, or a region which is not representative to the outer disk. In this cases we chose, after visual inspection, a different radius to represent the disk, which is typically the outermost successfully fitted free ellipse.

The r' band and g' band ellipticity and PA values are determined independently. Since a galaxy should have only a single pair of PA and ellipticity (depending on the inclination and intrinsic circularity) independent of the wavelength used, we averaged the two values in case of no major problem in one of the bands. The fixed ellipse fits to the r' and g' band is therefore repeated using these mean values (see Table 2) and the resulting profiles are shown in Appendix A.

	r' band				g' band						
Galaxy	ZP [$\frac{\mathrm{mag}}{\square''}$]	sky [ADU]	σ [ADU]	μ_{lim} [$\frac{\mathrm{mag}}{\square''}$]	ZP [$\frac{\mathrm{mag}}{\square''}$]	sky [ADU]	σ [ADU]	μ_{lim} [$\frac{\mathrm{mag}}{\square''}$]	R_{ell} [$''$]	PA [$^\circ$]	ME
(1)	*(2)*	*(3)*	*(4)*	*(5)*	*(6)*	*(7)*	*(8)*	*(9)*	*(10)*	*(11)*	*(12)*
NGC 0450	26.267	165.11	0.14	27.2	26.686	99.19	0.09	28.1	84	-8.8	0.36
PGC 006667	26.213	175.59	0.06	28.1	26.451	74.16	0.12	27.6	67	35.8	0.19
NGC 0701†	26.136	157.72	0.08	27.7	26.343	69.07	0.09	27.8	74	-41.9	0.49
NGC 0853†	26.293	144.89	0.11	27.5	26.542	75.84	0.07	28.2	59	-11.7	0.36
NGC 0941	26.114	99.42	0.02	29.2	26.507	68.58	0.11	27.7	69	78.6	0.30
UGC 02081	26.106	99.91	0.03	28.7	26.282	56.34	0.08	27.8	51	-18.8	0.42
NGC 1042	26.266	175.77	0.09	27.7	26.508	75.11	0.07	28.2	136	-69.0	0.20
NGC 1068	26.248	186.31	0.12	27.4	26.551	94.08	0.09	28.0	312	9.8	0.09
NGC 1084	26.259	170.55	0.18	26.9	26.416	70.41	*	*	80	-46.9	0.39
NGC 1087†	26.246	175.97	0.09	27.7	26.533	92.17	0.08	28.1	114	-88.4	0.39
NGC 1299	26.275	190.56	0.13	27.3	26.480	82.11	0.14	27.4	43	-35.0	0.45
NGC 2543	26.271	129.29	0.17	27.0	26.563	79.22	0.09	28.0	108	-3.1	0.50
NGC 2541†	26.259	181.06	0.10	27.6	26.532	91.73	0.04	28.8	135	-53.5	0.52
UGC 04393†	26.345	116.47	0.08	27.9	26.564	66.68	0.07	28.3	61	11.9	0.45
NGC 2684	26.314	122.01	0.08	27.9	26.591	70.12	0.19	27.2	35	8.7	0.18
NGC 2701†	26.360	162.44	0.09	27.8	26.653	86.65	0.08	28.2	60	-19.3	0.32
NGC 2776	26.291	156.28	0.05	28.4	26.508	67.37	0.05	28.6	83	30.8	0.05
NGC 2967	26.278	150.33	0.06	28.1	26.605	106.62	0.12	27.7	77	-70.7	0.07
NGC 3055	26.255	117.73	0.11	27.5	26.566	73.52	0.11	27.8	65	-24.1	0.42
NGC 3246†	26.281	125.07	0.11	27.5	26.539	72.34	0.09	28.0	65	8.0	0.48
NGC 3259	26.260	158.22	0.14	27.2	26.530	70.55	0.07	28.2	53	-47.0	0.43
NGC 3310	26.229	134.53	0.07	27.9	26.527	70.73	0.24	26.9	83	-50.2	0.05
NGC 3359	26.274	150.77	0.08	27.8	26.623	84.83	0.10	27.9	236	-80.9	0.48
NGC 3423	26.286	103.65	0.07	28.0	26.720	75.84	0.10	28.0	112	-53.5	0.19
NGC 3488	26.266	119.86	0.10	27.6	26.548	70.64	0.08	28.1	52	-75.8	0.34
NGC 3583	26.270	104.52	0.11	27.5	26.550	59.18	0.08	28.1	81	46.1	0.32
NGC 3589†	26.312	139.12	0.10	27.6	26.567	60.49	0.03	29.2	46	-21.9	0.50
UGC 06309	26.241	109.30	0.07	27.9	26.569	58.96	0.05	28.6	50	45.8	0.31
NGC 3631	26.261	140.70	0.07	28.0	26.661	77.36	0.06	28.5	129	32.1	0.16
NGC 3642	26.266	94.01	0.05	28.3	26.569	54.00	0.04	28.9	77	5.1	0.05
UGC 06518	26.263	137.25	0.13	27.3	26.514	65.27	0.08	28.1	31	-59.0	0.39
NGC 3756	26.205	135.84	0.17	26.9	26.507	67.02	0.14	27.4	118	-82.2	0.50
NGC 3888	26.223	133.12	0.07	27.9	26.512	65.09	0.05	28.6	52	30.9	0.26
NGC 3893	26.279	107.16	0.09	27.7	26.691	66.61	0.10	28.0	133	83.6	0.41
UGC 06903	26.264	136.09	0.04	28.6	26.571	76.94	0.08	28.1	69	48.1	0.12
NGC 3982	26.204	133.59	0.11	27.4	26.540	68.43	0.04	28.8	58	-87.4	0.11
NGC 3992	26.235	113.06	0.09	27.7	26.517	59.44	0.18	27.2	264	-15.4	0.42
NGC 4030	26.261	137.95	0.06	28.1	26.707	96.55	0.09	28.1	124	-59.6	0.20
NGC 4041	26.353	152.10	0.05	28.4	26.596	62.19	0.07	28.3	84	-8.5	0.05
NGC 4102	26.267	123.57	0.06	28.1	26.594	68.12	0.08	28.1	94	-47.9	0.43
NGC 4108†	26.317	174.08	0.11	27.5	26.603	92.76	0.06	28.5	55	13.2	0.22
NGC 4108B†	26.317	173.86	0.06	28.2	26.603	92.71	0.03	29.2	37	39.8	0.23
NGC 4123	26.195	161.48	0.09	27.6	26.524	90.50	0.11	27.7	111	36.1	0.33
NGC 4210	26.290	119.97	0.04	28.6	26.607	62.28	0.05	28.7	55	9.3	0.24
NGC 4273†	26.252	130.84	0.10	27.6	26.566	73.89	0.11	27.8	72	-83.3	0.39
NGC 4480	26.228	143.92	0.08	27.8	26.489	77.53	0.08	28.0	65	87.2	0.50

Table 2. Background (sky) and ellipse parameters: *(1)* Principal name in LEDA, *(2+6)* photometric r' and g' band zero points, *(3+7)* background value estimated around each galaxy, *(4+8)* σ of background from the ellipse method (cf. Sect. 3.3), *(5+9)* limiting surface brightness due to this background, used to constrain the outer boundary of the exponential fits, *(10)* radius used for fixing the ellipse parameters (cf. Sect. 3.5), *(11)* mean position angle PA (for r' and g' band) of the fixed ellipse (as measured on the SDSS image), *(12)* mean ellipticity ME (r' and g' band) of the fixed ellipse.

Galaxy	r' band				g' band				$R_{\rm ell}$	PA	ME
	ZP [$\frac{\rm mag}{\square''}$]	sky [ADU]	σ [ADU]	$\mu_{\rm lim}$ [$\frac{\rm mag}{\square''}$]	ZP [$\frac{\rm mag}{\square''}$]	sky [ADU]	σ [ADU]	$\mu_{\rm lim}$ [$\frac{\rm mag}{\square''}$]	[$''$]	[$^\circ$]	
(1)	(2)	(3)	(4)	(5)	(6)	(7)	(8)	(9)	(10)	(11)	(12)
NGC 4517A	26.278	136.44	0.07	28.0	26.605	78.57	0.08	28.2	113	-61.4	0.43
UGC 07700†	26.346	124.40	0.02	29.4	26.766	71.96	0.13	27.8	66	-23.6	0.24
NGC 4545	26.225	115.06	0.04	28.5	26.541	54.71	0.07	28.2	66	-87.9	0.42
NGC 4653	26.292	135.45	0.05	28.4	26.584	75.43	0.08	28.1	79	78.5	0.17
NGC 4668	26.292	135.17	0.07	28.0	26.584	75.49	0.09	28.0	53	-85.5	0.48
UGC 08041	26.253	127.60	0.11	27.5	26.566	78.23	0.14	27.5	101	70.0	0.48
UGC 08084†	26.195	157.33	0.05	28.3	26.524	86.02	0.01	30.3	43	-30.9	0.18
NGC 4904	26.322	142.49	0.08	27.9	26.588	75.36	0.06	28.4	70	-63.4	0.29
UGC 08237	26.228	103.85	0.11	27.4	26.574	56.11	0.03	29.2	35	30.7	0.22
NGC 5147	26.242	179.24	0.04	28.5	26.494	92.26	0.06	28.4	60	28.8	0.21
UGC 08658	26.174	122.81	0.13	27.2	26.465	66.52	0.07	28.2	65	3.2	0.39
NGC 5300	26.235	146.52	0.09	27.7	26.495	81.87	0.09	27.9	100	58.5	0.33
NGC 5334	26.261	125.54	0.07	28.0	26.707	86.37	0.05	28.8	107	-76.0	0.23
NGC 5376	26.237	108.94	0.11	27.4	26.528	56.56	0.03	29.1	63	-49.8	0.39
NGC 5430	26.237	108.70	0.07	27.9	26.528	55.89	0.05	28.6	69	70.5	0.35
NGC 5480	26.226	149.31	0.08	27.8	26.670	69.86	0.08	28.2	60	-73.3	0.15
NGC 5584	26.312	135.42	0.08	27.9	26.567	74.06	0.07	28.3	106	67.9	0.26
NGC 5624†	26.163	147.69	0.09	27.6	26.487	63.15	0.09	27.9	38	82.8	0.34
NGC 5660	26.199	123.03	0.06	28.1	26.488	64.66	0.08	28.0	69	24.3	0.05
NGC 5667	26.216	99.47	0.09	27.6	26.566	55.67	0.04	28.9	55	51.3	0.47
NGC 5668	26.257	117.18	0.05	28.3	26.578	70.51	0.09	28.0	95	43.2	0.15
NGC 5693†	26.225	151.52	0.08	27.8	26.669	74.68	0.09	28.1	61	13.2	0.05
NGC 5713†	26.312	134.21	0.04	28.6	26.567	73.88	0.06	28.4	88	-81.6	0.13
NGC 5768†	26.212	128.52	0.07	27.9	26.493	76.07	0.03	29.1	70	24.1	0.11
IC 1067	26.261	123.11	0.09	27.7	26.537	69.83	0.17	27.3	60	25.8	0.26
NGC 5774†	26.254	173.84	0.06	28.1	26.522	85.40	0.06	28.4	87	41.8	0.22
NGC 5806†	26.246	179.83	0.09	27.7	26.518	82.76	0.06	28.4	79	73.7	0.46
NGC 5850	26.241	195.14	0.09	27.7	26.492	94.97	0.06	28.4	141	74.9	0.22
UGC 09741	26.192	126.43	0.04	28.5	26.548	56.25	0.05	28.6	45	42.2	0.11
UGC 09837	26.246	115.43	0.08	27.8	26.731	62.31	0.07	28.4	53	20.9	0.05
NGC 5937	26.232	121.74	0.07	27.9	26.650	84.21	0.12	27.8	61	-69.1	0.44
IC 1125	26.189	113.30	0.12	27.3	26.525	74.76	0.09	27.9	46	56.0	0.44
IC 1158	26.233	164.49	0.10	27.5	26.689	112.46	0.12	27.8	69	39.1	0.44
NGC 6070	26.296	149.32	0.15	27.2	26.519	63.01	0.13	27.5	114	-30.8	0.57
NGC 6155†	26.304	125.81	0.07	28.0	26.584	63.54	0.11	27.8	47	-7.7	0.28
UGC 10721	26.198	118.98	0.10	27.5	26.524	55.93	0.05	28.6	38	-31.0	0.33
NGC 7437	26.191	153.77	0.12	27.3	26.495	87.08	0.09	27.9	57	-65.7	0.10
NGC 7606	26.278	225.46	0.12	27.4	26.576	89.15	0.17	27.3	146	51.7	0.62
UGC 12709†	26.236	154.79	0.11	27.4	26.565	80.44	0.07	28.3	71	50.4	0.39

Table 2. (continued): Background and ellipse parameters
†: The centers for these galaxies are not obtained by a Gaussian fit to the central region but by a free ellipse fit to determine the best center representative for the outer disk.

4. Analysis

4.1. Classification

We have classified (following Erwin et al., 2006) each profile according to observed break feature using the following nomenclature: Type I (no break), Type II (downbending break), and Type III (upbending break). A schematic view of our classification is shown in Fig. 4. Images and profiles for some typical examples of each class are given in Fig. 5.

The **Type I** classification follows the nomenclature established by Freeman (1970). Aside from a varying bulge com-

ponent these galaxies exhibit a region well described by a single exponential allowing for some wiggles associated with substructure in the disk such as spiral arms or prominent star forming regions.

The galaxies displaying a break with a downbending steeper outer region could be labelled **Type II** as (Freeman, 1970) originally proposed. Although he states at some point the inner deficit is *not far from the center of the system* there is no further restriction on this distance. In addition, for the three most prominent Type II galaxies in his sample he states that the outer exponential disk *begins outside the main region of spiral-arm activity*, so clearly outside a central region.

Following Erwin et al. (2006) the Type II class is subdivided into two groups in case the galaxy is barred. A **Type II.i** (inside) and a **Type II.o** (outside) depending on the position of the break in respect to the bar length (inside or outside the bar region). Moreover, we tried to subclassify the Type II and Type II.o profiles even further into additional three groups, which now tend to categorise the observed profiles according to their potential physical origin. First, profiles where the apparent break can be associated with large scale asymmetries of the galaxy in itself (only present in Sc–Sd galaxies). These are either associated to a lopsided disk having a well defined center, which is different from the applied ellipse centered on the outer disk, or to some large scale asymmetries in (or beyond) the main body of the outer disk (cf. extended spiral arms). These profiles are called **Type II-AB**, for *A*pparent (or *A*symmetric) *B*reak. Another group, showing the break radius at around $2-2.5$ times the bar radius, is probably related to a resonance of the bar as described in Erwin et al. (2006). The bar itself is most often nicely marked by the presence of an additional inner ring. These profiles are classified as **Type II.o-OLR**, for *O*uter *L*indblad *R*esonance which happens to be at the position of ~ 2 times the bar radius. The remaining profiles revealing a broken exponential behaviour are called **Type II-CT**, since they are best associated to what we call now *C*lassical *T*runcations discovered by van der Kruit (1979). Three nice examples of unbarred Sbc–Sc face-on galaxies are presented by Pohlen et al. (2002). For Type II-CT galaxies with bars we made sure that the break is significantly further out than typical for the Type II.o-OLR breaks.

The galaxies with a break followed by an upbending (shallower outer) profile are called **Type III** according to Erwin et al. (2005a) who find two sub-classes. One (**Type III-s**) showing a fairly gradual transition and outer isophotes that are progressively rounder than the isophotes in the main disk, suggesting a disk embedded within a more spheroidal outer zone associated to a halo or an extended bulge component. The other type (**Type III-d**) exhibits a rather sharp transition with the outer isophotes being not significantly rounder. Whereas measuring the ellipticity is an appropriate way to disentangle for early-type galaxies, devoid of prominent spiral arm structure misleading the free ellipse fits, it will most probably fail for late-types. So we decided here to classify them all as Type III only subclassifying those with visible spiral arm structure beyond the break radius, obviously associated with an outer disk-like region, as Type III-d (cf. Appendix A). In our subsequent paper we will study if colour variations at and beyond the break could potentially be used to decide between these subclasses. The colour profile of a transition between a star-forming inner disk and a halo/envelope (**Type III-s**) may look different from a transition between an intermediate-age inner disk to a predominantly younger outer disk (**Type III-d**).

Some galaxies have a more complex surface brightness distribution. They are better described with two breaks each of which could be associated to an individual type (as described above). These are called *mixed* classification (see Fig. 5). For all the galaxies with a break in the profile we verified that changes in the sky value (e.g. subtracting $\pm 3\sigma$ to the sky level) will not produce an untruncated Type I profile (see Fig. 2).

Please note that our classification Type I and Type II are used slightly different from MacArthur et al. (2003). Our Type II-CT class is called Type I with truncation in their study and their Type II is a mix of our Type II.i and all other Type II.o classes. Since we do not have infrared images we cannot comment on their 'transition' class. However, we note that for IC 1067 (see Appendix A for a detailed discussion) the r'-band profile is barely consistent with being Type I whereas in the g'-band it is clearly a Type II.o-OLR which is consistent with the profile shown by Erwin et al. (2006). This might imply that in very few cases dust is playing a role in shaping the observed profile close to the center. So this profile could be a Type I in the K-band, which has to be investigated in further studies.

4.2. Deriving break radius, break region and scalelengths

In addition to our pure identification –break (down- or upbending) *yes* or *no*– we have quantified the radial distance $R_{\rm br}$ where the break occurs, characterised its sharpness and derived an inner and outer scalelength ($h_{\rm in}$, $h_{\rm out}$) (see Fig. 6).

To determine the scalelengths we restricted our fits, to the 1D, azimuthally averaged, surface brightness profiles obtained with fixed ellipse fits (cf. Sect. 3.5). Since a detailed bulge to disk decomposition is beyond the scope of this paper, we used the so called "marking the disk" method by applying boundaries and fitting simple exponential functions: $\mu(R) = \mu_0 + 1.086 * R/h$. The inner boundary ($b_1$) is chosen manually to exclude the region obviously dominated by the bulge plus bar (shoulder) component. The outer boundary (b_4) is taken where the surface brightness profile reaches (3σ) of the noise level obtained from the sky ellipse fitting described in Sect. 3.3.

If the profile shows a broken exponential we need an additional boundary marking the break. This could be placed by eye, but to obtain the break radius objectively we used the following approach. At first an approximated derivative of the profile is calculated at each point, by fitting a straight line including four points around each radius. This provides a measure of a local scalelength ($h_{\rm local}$) along the radial axis (cf. Fig. 6). To get a linear spacing of surface brightness measurements along the radial axis and to decrease the noise in the $h_{\rm local}$ distribution we first rebinned the profile to linear units using a spline function and then median smoothed the $h_{\rm local}(R)$ profile adapting the smoothing length to 5% of the full extent of the profile.

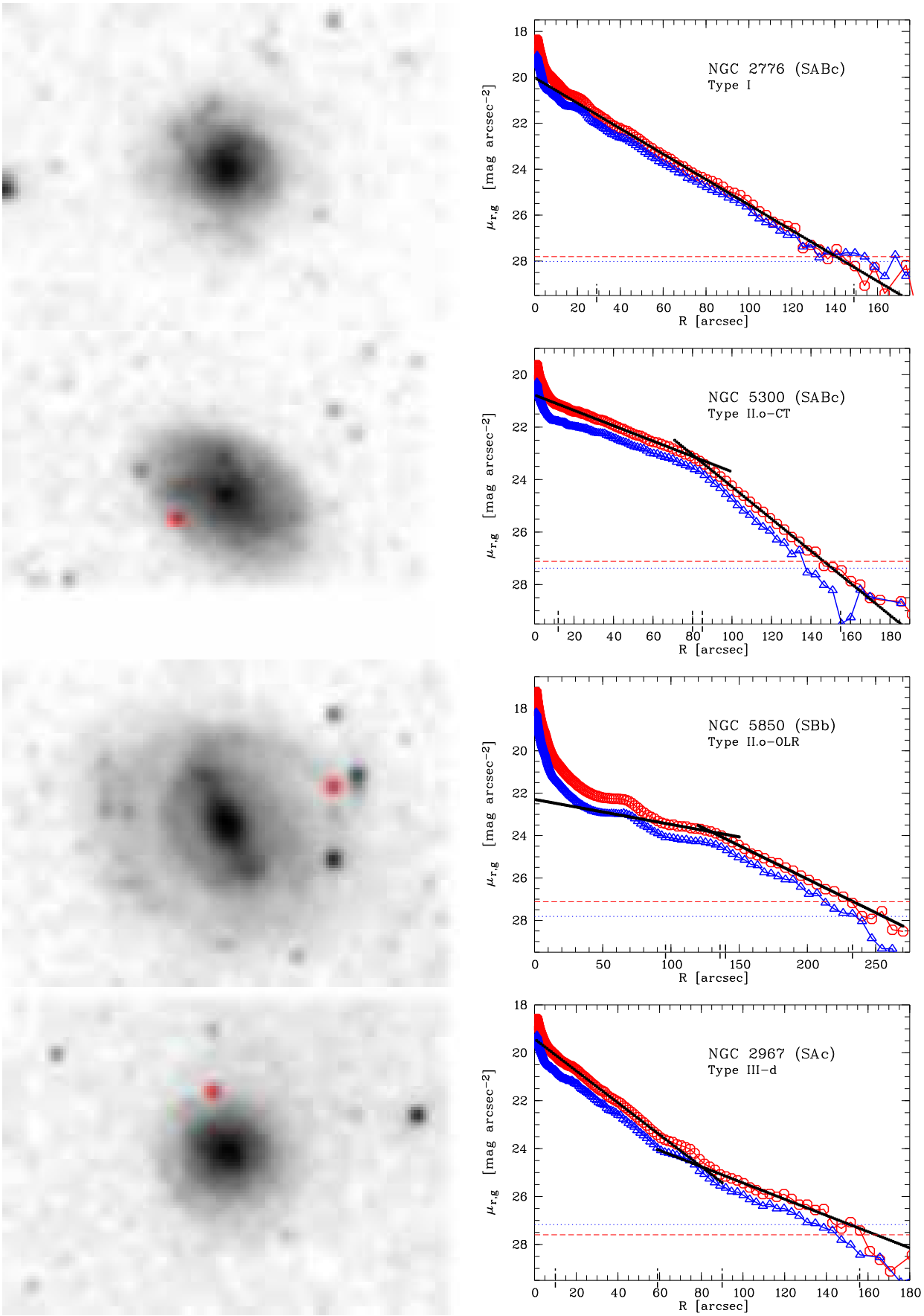

Fig. 5. Prototypical examples for each class of profiles: Type I, Type II-CT, Type II.o-OLR, and Type III *(top to bottom)*. (*Left panels):* r'-band images (unrotated cut-outs from the SDSS fields) with the break radius marked with an ellipse. The ellipse for the first Type I profile corresponds to the seeing limit at $\approx 140''$. *(Right panels)*: A simultaneously averaged radial SDSS surface

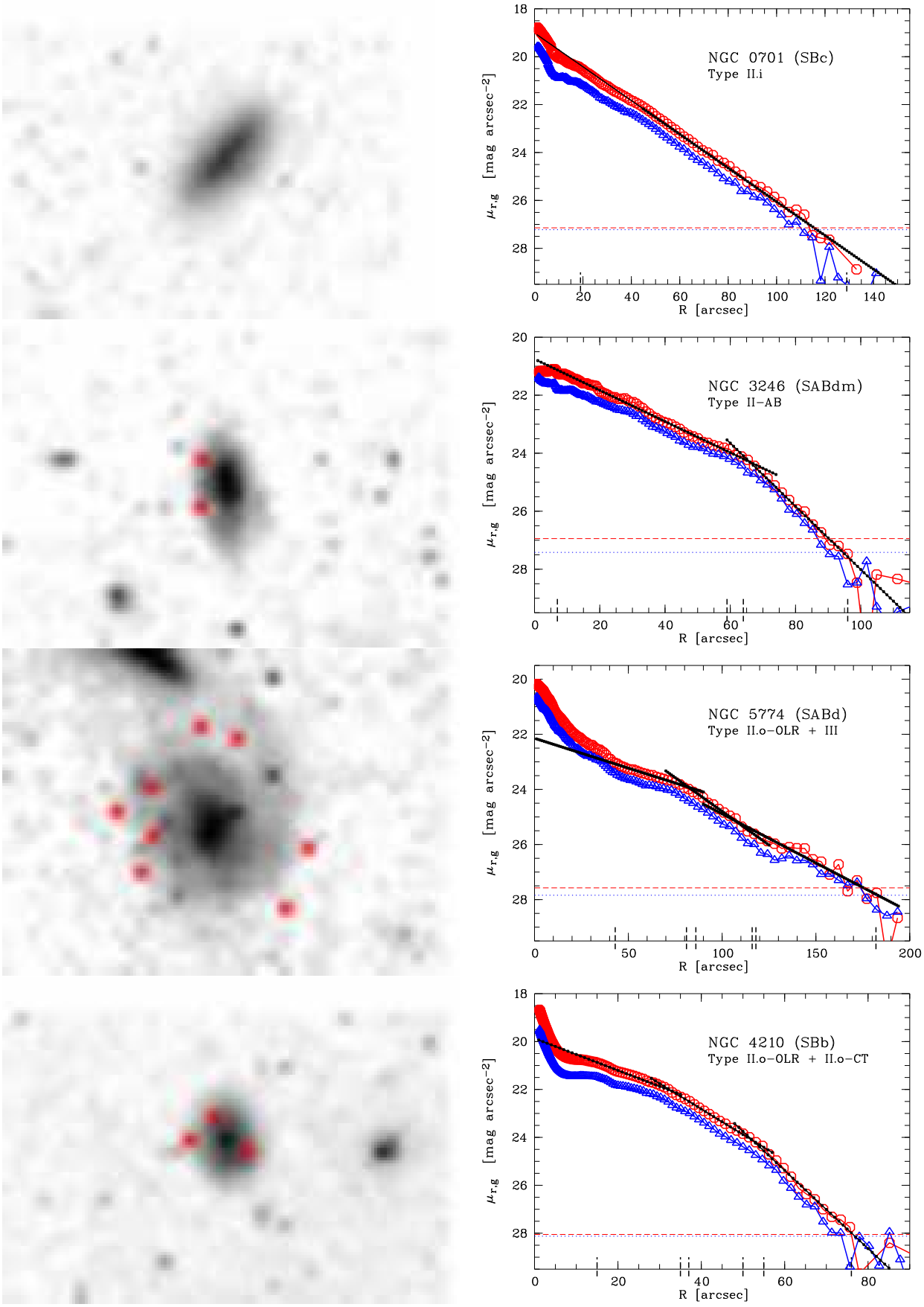

Fig. 5. (continued): Prototypical examples: Type II.i, Type II-AB, Type II.o-OLR + III, and Type II.o-OLR + II.o-CT *(top to bottom)*. The ellipse for the first Type II.i galaxy corresponds to the inner boundary at $\sim$ 20″. For the mixed classifications two ellipses are shown corresponding to the associated bulge.

Our general assumption is now that we have two regions with nearly constant scalelength together with a change (up- or downbending) in the profile. This will be reflected by two plateaus in the plot of $h_{\rm local}(R)$ (see Fig. 6). Depending on the actual shape (e.g. sharpness) of the transition region $h_{\rm local}(R)$ will move from one scalelength region around $h_{\rm in}$ to another region around $h_{\rm out}$. To quantify a single radius defining this break we used then the radius where the $h_{\rm local}(R)$ profile crosses the horizontal line set by a characteristic value. In case the two regions do not cover the same radial range, the characteristic value is always taken as the median of the $1/h_{\rm local}$ distribution, to avoid a bias towards the more extended region.

To characterise the shape of the break we defined an additional region around the break. Ideally a sharp break would translate into a step function in the $h_{\rm local}(R)$ profile whereas a smooth transition would cross the line set by the weighted mean value with a finite slope. Therefore we defined an inner and outer boundary of the break region where the profile, starting from the break, reaches a value within two standard deviations away from the mean calculated for the inner/outer region separately (cf. Fig. 6). The derived break radii are almost always consistent with those derived by eye, but of course fail if one of the regions is very small (e.g. in the case of IC 1067, see Appendix A) or get uncertain if more than two regions with roughly constant scalelengths are involved (as for the mixed classifications, see below and Sect. 5).

Using the boundaries of the break region (b_2 and b_3) to mark the separation of an inner and outer exponential disk, the final scalelengths are derived from two simple exponential fits ($\mu(R) = \mu_{0,\rm in} + 1.086 * R/h_{\rm in}$ and $\mu(R) = \mu_{0,\rm out} + 1.086 * R/h_{\rm out}$) to the original profile. To decrease the noise we give priority to this classical approach to determine the scalelength over using a weighted mean from the $h_{\rm local}$ values inside the now defined inner and outer region. Fitting the two exponentials one could alternatively define the break radius, as the meeting point of the two exponential fits. However, since this would add an influence by the actual shape of the two disk regions into the positioning of the break radius we decided against it.

In cases where the derivative profile ($h_{\rm local}(R)$) crosses the horizontal line set by the characteristic value twice (three or more times is considered to be explained by wiggles caused by asymmetries such as spiral arms) we check if we could apply a mixed classification. This implies assigning two breaks associated to the individual types as discussed in Sect. 4.1 which significantly improve the overall fit. The boundaries for both breaks are then used to fit three exponential regions.

The final results for all the galaxies are given in Table 3. We do not provide individual errors for the fitting parameters in Table 3, since their uncertainty is a complex combination of random and systematic errors. Typical random errors of the exponential fitting routine alone are 2% for $h_{\rm in}$, 3% for $h_{\rm out}$, $\pm$0.04mag for $\mu_{0,\rm in}$, and $\pm$0.17mag for $\mu_{0,\rm out}$. The uncertainty in the sky subtraction, however, translates to a clearly systematic error. In the case of over/under-subtraction the measured scalelengths are systematically smaller/larger and the central surface brightnesses are systematically lower/higher. To estimate how the error on the sky subtraction alone effects our parameters we have over/under-subtracted the measured sky level by $\pm 1\sigma$. Typical errors are then only $\pm$1% for $h_{\rm in}$ and $\pm$0.02mag for $\mu_{0,\rm in}$, but $\pm$7% for $h_{\rm out}$ and $\pm$0.38mag for $\mu_{0,\rm out}$. Another source of uncertainty is generated by the positioning of the boundaries (b_{1-4}). This uncertainty can not be easily quantified since it depends on the shape (up/down-bending) of, and features (bulges, bars, etc.) in, the surface brightness profiles and cause systematic errors. To minimise their contribution in our determination of the structural parameters each fit is verified by eye.

5. Results

Our final classifications are presented in Table 3 and discussed in more detail individually in Appendix A. For four galaxies in common with Erwin et al. (2006) the classification (as well as the final profiles) agree very well. All features in the surface brightness profiles classified here are always consistently found in deep surface photometry profiles available (cf. Appendix A) in the literature (e.g. Courteau, 1996).

About 90% of our sample can be classified into one of the classes described in Sect. 4.1. However, the remaining galaxies are better described with two breaks in their surface brightness profiles. Galaxies with extra breaks are classified as *mixed*. In almost all cases this is a combination of a downbending break, either Type II-CT, Type II.o-OLR, Type II-AB, or Type II.i, classified as described in Sect. 4.1, followed by an additional upbending break in the very outer parts. These galaxies are classified as e.g. Type II.o-OLR + III. Interestingly, none of the Type III profiles show an additional outer truncation within our sensitivity limit.

Only two galaxies (see detailed explanation in Appendix A) exhibit an inner downbending break followed by an additional outer downbending break. In one case (NGC 4517A) the outer sharp drop is clearly associated to a Type II-AB, whereas the inner break is consistent with being a Type II.o-OLR or Type II-CT. The other case is NGC 4210, where the inner boundary of an extended, exponential, break region is consistent with a Type II.o-OLR break leaving the outer break to be Type II-CT. This galaxy could be the ideal test object to study the difference between Type II.o-OLR and Type II-CT breaks. Finally, for only one galaxy, IC 1067, the classification in the r' and g'-band could be different (see Sect. 4.1).

5.1. Frequencies

The vast majority (almost 90%, see Table 4) of the galaxies exhibit surface brightness profiles with breaks, only 9 (11% $\pm$ 4%) are reasonably well described (allowing sometimes for quite extensive deviations) as being purely single-exponential (Type I). Even adding the barred galaxies showing only a dip inside the bar radius (Type II.i), their frequency increases up to merely 15% $\pm$ 4%.

66% $\pm$ 5% of the galaxies are classified as Type II with a break and downbending profiles (61% excluding Type II.i). The frequencies of the three main subgroups are the following: a) 33% $\pm$ 5% (from the full sample) exhibit a classical truncations (Type II-CT), b) 15% $\pm$ 4% (from the full sample) are classified as having breaks with downbending profiles that could be (size

Galaxy	Break type	b_1 [″]	b_2 [″]	b_3 [″]	b_4 [″]	$R_{\rm br}$ [″]	$R_{\rm br}$ [kpc]	$h_{\rm in}$ [″]	$h_{\rm in}$ [kpc]	$h_{\rm in}$ [$h_{\rm out}$]	$\mu_{0,\rm in}$ [$\frac{\rm mag}{\square''}$]	$\mu_{0,\rm out}$ [$\frac{\rm mag}{\square''}$]	$\mu_{\rm br}$ [$\frac{\rm mag}{\square''}$]	$A_{r'/g'}$ [mag]
(1)	(2)	(3)				(4)		(5)		(6)	(7)		(8)	(9)
NGC 0450	II.o-CT	16	79	88	120	80	9.5	31.3	3.7	2.7	21.0	16.0	24.0	0.11
		16	78	89	128	79	9.4	34.5	4.1	2.9	21.5	16.3	24.2	0.15
PGC 006667	II-AB	10	70	77	108	74	9.7	22.6	2.9	1.9	21.1	18.0	24.7	0.14
		10	72	78	96	73	9.5	22.7	3.0	1.8	21.5	18.7	25.1	0.19
NGC 0701	II-i	19	129	*	*	*	*	15.4	1.8	*	19.0	0.0	19.0	0.07
		19	115	*	*	*	*	16.2	1.9	*	19.8	0.0	19.8	0.10
NGC 0853	III	0	43	48	100	45	4.4	11.0	1.1	0.6	19.3	20.9	23.3	0.07
		0	42	46	100	44	4.3	10.3	1.0	0.6	19.6	21.2	23.7	0.10
NGC 0941	II-CT	5	77	84	120	81	8.6	19.1	2.0	1.4	20.4	18.5	25.0	0.10
		5	76	80	107	77	8.2	19.5	2.1	1.6	20.8	18.0	25.3	0.13
UGC 02081	II-CT	11	48	69	85	53	9.4	21.0	3.7	2.6	21.6	16.1	25.2	0.07
		11	45	74	85	46	8.1	22.3	3.9	2.8	22.2	15.9	25.6	0.10
NGC 1042	II-AB	39	122	122	219	122	10.7	48.0	4.2	1.4	20.9	19.9	23.0	0.08
		39	101	119	212	119	10.4	63.9	5.6	2.2	21.7	19.7	23.4	0.11
NGC 1068	II.o-OLR	105	184	188	362	188	13.9	118.0	8.7	2.0	21.6	19.9	23.4	0.09
		105	183	187	384	189	14.0	128.2	9.5	2.2	22.4	20.4	24.0	0.13
NGC 1084	III	27	91	97	179	95	8.5	18.5	1.7	0.4	18.3	21.4	23.2	0.08
		27	91	100	194	96	8.6	17.9	1.6	0.4	18.7	21.7	23.7	0.11
NGC 1087	III	49	139	142	238	140	14.0	24.5	2.4	0.6	19.0	21.4	24.7	0.10
		49	137	142	231	139	13.9	23.6	2.4	0.6	19.4	22.0	25.4	0.13
NGC 1299	III	22	45	46	75	46	7.0	8.7	1.3	0.7	18.9	20.5	24.5	0.13
		22	47	52	77	49	7.5	8.6	1.3	0.5	19.4	22.5	25.4	0.18
NGC 2543	II-i	34	108	*	*	74	13.3	15.7	2.8	*	19.1	0.0	19.1	0.19
		34	108	*	*	75	13.5	14.3	2.6	*	19.3	0.0	19.3	0.27
NGC 2541	II-CT	48	141	143	216	142	7.2	51.2	2.6	1.6	21.3	19.3	24.5	0.14
		48	143	147	223	145	7.4	55.2	2.8	2.1	21.9	18.6	25.0	0.19
UGC 04393	I	30	125	*	*	*	*	22.4	3.6	*	21.6	0.0	21.6	0.12
		30	114	*	*	*	*	21.7	3.4	*	21.9	0.0	21.9	0.16
NGC 2684	II-CT	4	23	25	42	24	5.1	10.6	2.2	1.9	19.6	17.5	22.1	0.07
		4	23	25	42	24	5.1	10.8	2.3	2.0	20.2	18.0	22.4	0.10
NGC 2701	II-AB + III	16	37	42	71	38	6.7	24.1	4.2	2.9	20.2	16.5	22.1	0.05
		42	71	71	93	73	12.8	8.3	1.4	0.4	16.5	22.4	25.8	0.05
		16	37	41	74	38	6.7	27.8	4.9	3.3	20.7	17.1	21.9	0.07
		41	74	76	102	75	13.1	8.5	1.5	0.4	17.1	22.1	26.1	0.07
NGC 2776	I	29	149	*	*	*	*	19.6	3.8	*	20.0	0.0	20.0	0.04
		29	134	*	*	*	*	20.1	3.9	*	20.5	0.0	20.5	0.05
NGC 2967	III-d	10	59	90	156	73	9.4	16.3	2.1	0.5	19.4	22.0	24.8	0.28
		10	59	90	143	73	9.4	16.9	2.2	0.5	20.1	22.6	25.3	0.38
NGC 3055	II.o-CT	10	53	57	88	54	6.8	17.1	2.1	1.9	19.6	16.3	23.1	0.14
		10	52	56	88	53	6.7	17.5	2.2	2.0	20.1	16.7	23.4	0.20
NGC 3246	II-AB	7	59	64	96	61	9.0	20.2	3.0	2.0	20.8	17.1	24.3	0.10
		7	60	62	93	60	8.9	22.0	3.3	2.2	21.3	17.3	24.5	0.14
NGC 3259	III-d	7	59	64	122	63	8.4	11.4	1.5	0.4	19.4	22.8	24.7	0.04
		7	59	63	138	63	8.4	12.2	1.6	0.4	20.0	23.1	25.0	0.05
NGC 3310	III	10	52	53	172	53	4.4	10.6	0.9	0.3	18.2	21.6	23.2	0.06
		10	52	54	141	53	4.4	10.3	0.9	0.3	18.4	21.7	23.3	0.09
NGC 3359	II-AB	29	183	204	266	184	16.1	51.1	4.5	1.8	20.5	16.9	24.9	0.03
		29	180	192	266	181	15.8	53.0	4.6	1.8	20.9	17.7	25.0	0.04
NGC 3423	II-CT	30	76	93	175	85	6.1	52.2	3.7	2.8	20.9	17.7	22.6	0.08
		30	88	97	160	95	6.8	51.2	3.7	3.2	21.2	17.1	23.1	0.12
NGC 3488	II.o-CT	10	32	52	70	44	9.8	16.8	3.8	2.5	20.3	16.0	23.2	0.04
		10	29	53	72	43	9.6	20.6	4.6	3.0	21.0	16.3	23.3	0.05
NGC 3583	III-d	13	82	84	147	83	13.5	16.3	2.7	0.7	19.0	21.0	24.7	0.04
		13	81	82	138	82	13.3	17.0	2.8	0.7	19.7	21.4	25.7	0.05

Table 3. Results: disk type and exponential disk parameters
(1) Principal name in LEDA, *(2)* profile classification (cf. Sect. 4.1), *(3)* fitting boundaries for the inner and outer exponential disk region, *(4)* break radius in units of arcsec and kpc, *(5)* inner scalelength in units of arcsec and kpc *(6)* inner scalelength in relation to the outer scalelength, *(7)* the central surface brightness of the inner/outer disk, *(8)* the surface brightness at the break radius (estimated at the crossing point of the two exponential fits), *(9)* galactic extinction according to Schlegel et al. (1998) For each

Galaxy	Break type	b_1	b_2	b_3	b_4	$R_{\rm br}$		$h_{\rm in}$		$h_{\rm in}$	$\mu_{0,\rm in}$	$\mu_{0,\rm out}$	$\mu_{\rm br}$	$A_{r'/g'}$
		[″]	[″]	[″]	[″]	[″]	[kpc]	[″]	[kpc]	[$h_{\rm out}$]	[$\frac{\rm mag}{\square''}$]	[$\frac{\rm mag}{\square''}$]	[$\frac{\rm mag}{\square''}$]	[mag]
(1)	(2)	(3)				(4)		(5)		(6)	(7)		(8)	(9)
NGC 3589	II-CT	0	37	38	72	38	5.8	18.6	2.9	1.7	21.1	19.7	23.1	0.03
		0	33	38	84	36	5.5	20.5	3.1	1.8	21.5	20.3	23.0	0.04
UGC 06309	II-i	23	74	*	*	*	*	9.8	2.1	*	18.9	0.0	18.9	0.05
		25	88	*	*	*	*	11.1	2.4	*	19.9	0.0	19.9	0.07
NGC 3631	I	140	233	*	*	*	*	37.8	3.6	*	20.8	0.0	20.8	0.05
		140	226	*	*	*	*	36.7	3.5	*	21.2	0.0	21.2	0.06
NGC 3642	III-d	30	75	79	229	79	10.0	20.9	2.6	0.5	20.3	22.3	24.0	0.03
		30	71	73	236	73	9.3	19.7	2.5	0.4	20.6	22.7	24.3	0.04
UGC 06518	II-i	10	43	*	*	*	*	6.4	1.4	*	19.3	0.0	19.3	0.04
		10	45	*	*	*	*	6.1	1.3	*	19.6	0.0	19.6	0.05
NGC 3756	II.o-CT	11	92	103	154	97	10.2	33.7	3.6	2.0	20.0	16.6	23.2	0.03
		11	78	104	149	100	10.6	38.6	4.1	2.2	20.8	17.7	23.4	0.04
NGC 3888	I	13	81	*	*	*	*	10.1	1.9	*	18.7	0.0	18.7	0.03
		13	84	*	*	*	*	9.9	1.8	*	19.1	0.0	19.1	0.04
NGC 3893	III-d	15	134	134	184	134	11.1	29.1	2.4	0.6	19.2	21.7	24.7	0.06
		15	139	139	184	139	11.5	28.3	2.3	0.5	19.6	22.6	25.5	0.08
UGC 06903	II.o-CT	21	59	72	98	60	8.0	31.8	4.2	3.6	21.6	15.8	23.9	0.06
		21	56	63	92	57	7.6	35.0	4.6	3.6	22.2	17.1	24.2	0.08
NGC 3982	III	13	51	54	91	52	4.9	10.2	1.0	0.7	18.3	19.8	23.8	0.04
		13	49	51	99	50	4.7	10.2	1.0	0.8	18.7	19.8	23.6	0.05
NGC 3992	II.o-OLR	44	133	139	324	137	12.2	84.0	7.5	2.3	20.5	18.1	22.3	0.08
		44	129	133	280	133	11.8	96.4	8.6	2.7	21.3	18.4	22.9	0.12
NGC 4030	III	37	147	164	266	152	15.5	26.2	2.7	0.5	19.2	22.1	25.4	0.08
		37	147	151	230	148	15.1	25.5	2.6	0.6	19.6	22.3	26.0	0.11
NGC 4041	III-d	26	76	80	192	80	8.2	18.6	1.9	0.6	19.7	21.8	24.6	0.05
		26	81	84	186	83	8.5	18.2	1.9	0.5	20.1	22.6	25.2	0.07
NGC 4102	II.o-OLR + III	40	57	57	116	57	4.3	23.3	1.7	1.5	19.1	17.8	21.7	0.06
		57	116	119	165	118	8.8	15.8	1.2	0.6	17.8	20.9	26.0	0.06
		40	59	59	107	59	4.4	21.6	1.6	1.4	19.5	18.4	22.4	0.08
		59	107	109	151	108	8.1	15.7	1.2	0.7	18.4	20.4	26.1	0.08
NGC 4108	II-AB	7	44	46	66	44	8.6	9.1	1.8	1.5	18.9	16.2	24.5	0.05
		7	43	45	68	44	8.6	9.8	1.9	1.6	19.5	16.5	24.5	0.07
NGC 4108B	I	7	67	*	*	*	*	11.4	2.2	*	20.8	0.0	20.8	0.05
		7	71	*	*	*	*	11.0	2.2	*	21.0	0.0	21.0	0.07
NGC 4123	I	20	220	*	*	*	*	35.5	3.4	*	20.6	0.0	20.6	0.06
		20	207	*	*	*	*	36.5	3.5	*	21.2	0.0	21.2	0.08
NGC 4210	II.o-OLR + CT	15	35	37	50	36	7.5	16.3	3.4	1.6	19.9	18.6	22.1	0.05
		37	50	55	76	51	10.6	10.2	2.1	1.5	18.6	15.6	24.1	0.05
		15	32	38	50	37	7.7	19.5	4.1	2.0	20.7	19.0	22.4	0.07
		38	50	52	73	51	10.6	10.0	2.1	1.6	19.0	15.6	24.9	0.07
NGC 4273	II-AB + III	12	43	48	78	47	7.9	24.5	4.1	2.1	19.8	17.6	21.7	0.05
		48	78	79	119	78	13.2	11.5	1.9	0.6	17.6	20.3	25.4	0.05
		12	45	47	84	47	7.9	29.7	5.0	2.6	20.5	17.9	22.1	0.07
		47	84	89	106	84	14.2	11.2	1.9	0.7	17.9	20.0	25.6	0.07
NGC 4480	II.o-CT	8	53	58	90	54	9.3	18.8	3.2	2.3	19.8	15.8	23.0	0.06
		8	54	57	88	54	9.3	21.4	3.7	2.6	20.5	16.1	23.3	0.09
NGC 4517A	II.o-CT + AB	25	76	77	139	77	8.3	53.3	5.8	1.3	22.0	21.4	23.6	0.06
		77	139	159	192	140	15.1	39.7	4.3	2.3	21.4	15.7	25.7	0.06
		25	76	77	139	77	8.3	59.3	6.4	1.4	22.5	21.8	23.9	0.09
		77	139	159	192	140	15.1	41.1	4.4	2.5	21.8	15.5	26.0	0.09
UGC 07700	II.o-CT	12	45	52	94	50	11.2	26.4	5.9	2.2	22.2	20.2	23.8	0.05
		12	49	58	74	50	11.2	29.1	6.5	3.7	22.6	17.5	24.5	0.07
NGC 4545	II.o-CT	7	56	58	97	56	11.6	17.7	3.7	2.0	20.0	16.3	23.8	0.03
		7	49	57	89	55	11.4	19.2	4.0	2.1	20.6	16.7	24.0	0.04
NGC 4653	II-AB	11	102	109	142	103	19.0	23.0	4.2	1.7	20.7	17.1	25.9	0.06
		11	101	107	130	102	18.8	24.5	4.5	1.8	21.2	17.1	26.0	0.09

Table 3. (continued): Results

Galaxy	Break type	b_1 [″]	b_2 [″]	b_3 [″]	b_4 [″]	R_{br} [″]	R_{br} [kpc]	h_{in} [″]	h_{in} [kpc]	h_{in} [h_{out}]	$\mu_{0,in}$ [$\frac{mag}{\square''}$]	$\mu_{0,out}$ [$\frac{mag}{\square''}$]	μ_{br} [$\frac{mag}{\square''}$]	$A_{r'/g'}$ [mag]
(1)	(2)	(3)				(4)		(5)		(6)	(7)		(8)	(9)
NGC 4668	III	0	60	71	110	66	7.6	11.8	1.4	0.5	19.6	22.2	25.5	0.07
		0	65	71	104	68	7.8	11.7	1.3	0.5	20.0	23.2	25.9	0.10
UGC 08041	II.o-CT	14	69	73	148	71	6.8	36.9	3.5	1.4	21.1	20.2	23.1	0.06
		14	69	75	157	70	6.7	39.9	3.8	1.6	21.6	20.5	23.4	0.09
UGC 08084	II.o-OLR	9	38	44	71	42	8.2	29.0	5.7	3.4	22.4	18.8	23.9	0.08
		9	35	45	78	43	8.4	31.3	6.1	3.9	22.8	18.7	24.2	0.11
NGC 4904	II.o-OLR + III	13	38	48	103	39	3.3	27.6	2.3	2.2	20.2	18.2	21.9	0.07
		48	103	116	157	104	8.7	12.5	1.0	0.5	18.2	22.4	26.2	0.07
		13	40	40	99	40	3.4	32.7	2.7	2.6	20.9	18.8	22.2	0.10
		40	99	99	135	99	8.3	12.7	1.1	0.3	18.8	25.1	27.4	0.10
UGC 08237	II.o-OLR	14	25	29	50	26	5.6	14.8	3.2	2.6	20.6	17.8	22.4	0.05
		14	27	31	48	30	6.5	14.0	3.0	2.5	21.1	18.4	23.0	0.06
NGC 5147	II.o-OLR + III	5	29	32	72	30	2.4	20.3	1.6	1.8	19.8	18.3	21.7	0.08
		32	72	77	122	73	5.8	11.0	0.9	0.5	18.3	22.0	25.8	0.08
		5	26	29	75	29	2.3	22.8	1.8	2.2	20.4	18.5	22.0	0.11
		29	75	79	108	76	6.1	10.5	0.8	0.6	18.5	21.6	26.2	0.11
UGC 08658	II-CT	12	57	61	102	61	9.7	22.4	3.5	1.4	21.0	20.0	23.9	0.05
		12	57	61	122	61	9.7	24.4	3.9	1.5	21.6	20.3	24.4	0.06
NGC 5300	II.o-CT	12	80	85	155	83	7.2	37.1	3.2	2.1	20.8	18.2	23.2	0.06
		12	75	82	142	77	6.6	41.8	3.6	2.6	21.4	18.1	23.5	0.09
NGC 5334	II.o-CT	13	80	102	152	92	9.1	40.2	4.0	2.6	21.0	16.7	23.8	0.13
		13	101	103	156	103	10.2	40.3	4.0	2.8	21.5	16.4	24.4	0.18
NGC 5376	II.o-OLR	10	34	35	97	35	5.6	17.0	2.7	1.4	19.4	18.6	21.2	0.04
		10	34	39	95	37	5.9	17.9	2.8	1.7	20.1	18.7	22.2	0.05
NGC 5430	II.o-OLR	10	69	72	105	70	15.7	15.8	3.5	1.4	19.4	17.8	23.9	0.05
		10	69	71	102	69	15.5	16.2	3.6	1.6	20.1	17.6	24.4	0.06
NGC 5480	III-d	9	65	74	129	67	9.8	13.9	2.0	0.5	19.6	22.1	24.9	0.05
		9	67	76	122	68	10.0	13.5	2.0	0.5	20.1	22.6	25.4	0.07
NGC 5584	II.o-CT	14	75	107	165	90	10.6	39.8	4.7	2.0	20.9	18.4	23.3	0.11
		14	68	92	155	84	9.9	45.4	5.4	2.4	21.5	18.7	23.4	0.15
NGC 5624	III	0	46	50	87	48	7.3	9.9	1.5	0.5	20.1	22.6	24.9	0.05
		0	37	47	80	42	6.4	8.9	1.3	0.4	20.3	23.2	25.4	0.07
NGC 5660	II-CT	12	63	70	90	67	12.0	17.8	3.2	1.6	19.9	17.3	24.1	0.06
		12	64	71	105	69	12.4	18.5	3.3	1.7	20.4	17.8	24.2	0.08
NGC 5667	II-i + III	*	*	*	*	*	*	*	*	*	*	*	*	0.03
		28	64	66	96	64	9.8	11.0	1.7	0.6	19.1	21.9	25.7	0.03
		*	*	*	*	*	*	*	*	*	*	*	*	0.04
		28	62	65	111	63	9.7	10.3	1.6	0.4	19.2	23.7	26.4	0.04
NGC 5668	I	20	178	*	*	*	*	26.7	3.1	*	20.6	0.0	20.6	0.10
		20	162	*	*	*	*	24.3	2.8	*	20.7	0.0	20.7	0.14
NGC 5693	II-AB	9	28	50	71	29	5.1	16.7	2.9	2.1	20.9	17.9	23.7	0.10
		9	26	51	71	32	5.6	20.5	3.6	2.2	21.6	19.4	23.5	0.14
NGC 5713	III	8	102	114	164	103	14.0	18.1	2.5	0.7	19.1	21.0	25.6	0.11
		8	112	139	159	112	15.2	18.1	2.5	0.7	19.6	21.5	25.9	0.15
NGC 5768	I	6	95	*	*	*	*	13.1	1.8	*	19.9	0.0	19.9	0.25
		6	98	*	*	*	*	13.2	1.8	*	20.4	0.0	20.4	0.35
IC 1067	II.o-OLR	*	*	40	99	*	*	*	*	*	*	19.8	*	0.14
		*	*	40	80	*	*	*	*	*	*	20.0	*	0.19
NGC 5774	II.o-OLR + III	43	81	86	116	86	9.9	50.2	5.8	2.3	22.1	19.9	23.9	0.12
		86	116	118	182	116	13.3	22.2	2.5	0.7	19.9	21.3	25.1	0.12
		47	74	77	124	77	8.8	60.8	7.0	2.7	22.7	20.5	24.1	0.16
		77	124	125	182	124	14.2	22.9	2.6	0.6	20.5	22.3	25.7	0.16
NGC 5806	III	60	116	118	242	118	11.8	29.9	3.0	0.5	20.3	22.3	24.6	0.14
		60	123	124	257	124	12.4	31.4	3.1	0.5	21.1	23.0	25.3	0.20
NGC 5850	II.o-OLR	96	136	140	233	137	25.0	92.2	16.8	2.7	22.3	19.7	23.8	0.16
		96	133	138	240	138	25.2	127.1	23.2	3.9	23.3	20.0	24.4	0.21

Table 3. (continued): Results

Galaxy	Break type	b_1 [″]	b_2 [″]	b_3 [″]	b_4 [″]	$R_{\rm br}$ [″]	$R_{\rm br}$ [kpc]	$h_{\rm in}$ [″]	$h_{\rm in}$ [kpc]	$h_{\rm in}$ [$h_{\rm out}$]	$\mu_{0,\rm in}$ [$\frac{\rm mag}{\square''}$]	$\mu_{0,\rm out}$ [$\frac{\rm mag}{\square''}$]	$\mu_{\rm br}$ [$\frac{\rm mag}{\square''}$]	$A_{r'/g'}$ [mag]
(1)	(2)	(3)				(4)		(5)		(6)	(7)		(8)	(9)
UGC 09741	III	17	24	29	62	25	4.7	6.8	1.3	0.6	19.8	21.2	23.5	0.06
		17	27	29	62	27	5.1	6.9	1.3	0.7	20.4	21.6	24.0	0.09
UGC 09837	II-CT	8	45	53	69	46	9.4	17.1	3.5	2.4	21.4	16.6	24.6	0.05
		8	44	46	69	46	9.4	18.2	3.7	2.6	21.8	17.0	24.8	0.06
NGC 5937	III	12	62	75	117	63	12.5	12.6	2.5	0.6	19.1	21.1	24.6	0.50
		12	68	70	98	68	13.5	12.8	2.5	0.6	19.8	22.2	25.8	0.69
IC 1125	I	4	77	*	*	*	*	11.4	2.3	*	19.9	0.0	19.9	0.43
		4	68	*	*	*	*	11.6	2.3	*	20.5	0.0	20.5	0.59
IC 1158	II.o-CT	14	53	67	98	65	9.1	30.5	4.3	2.9	21.2	16.9	23.4	0.32
		14	50	67	101	61	8.5	34.8	4.9	3.3	21.9	17.5	23.8	0.44
NGC 6070	II.o-CT	20	87	108	162	97	14.0	37.2	5.4	2.0	20.1	17.3	22.8	0.41
		20	87	108	157	88	12.7	43.4	6.3	2.6	21.0	17.4	23.3	0.56
NGC 6155	II-AB	4	33	36	71	34	6.3	12.2	2.3	1.5	19.4	18.2	21.9	0.04
		4	33	37	63	34	6.3	13.1	2.4	1.8	20.0	17.9	22.7	0.05
UGC 10721	III	16	38	48	80	41	8.9	8.3	1.8	0.5	19.3	21.7	24.6	0.10
		16	38	46	78	41	8.9	7.9	1.7	0.6	19.5	21.8	24.8	0.13
NGC 7437	II-CT	12	39	47	91	43	6.5	26.4	4.0	1.9	21.3	19.7	23.1	0.11
		12	40	43	147	41	6.2	27.1	4.1	1.9	21.8	20.4	23.3	0.15
NGC 7606	II-CT	20	96	113	195	97	14.7	43.4	6.6	1.9	19.6	17.3	22.3	0.10
		20	92	114	187	93	14.1	49.9	7.6	2.2	20.5	17.7	22.9	0.14
UGC 12709	II-CT	5	65	72	102	69	12.8	29.8	5.5	2.2	22.4	19.3	25.1	0.11
		5	64	66	108	66	12.2	33.0	6.1	2.4	23.0	19.8	25.2	0.15

Table 3. (continued): Results

Profile type	Number [#]	Frequency [%]
Type I	9	11 ± 3
Type II	56	66 ± 5
– Type II.i	4 (1)	6 ± 3
– Type II-CT	28 (2)	32 ± 5
– Type II.o-OLR	13 (5)	15 ± 4
– Type II-AB	11 (3)	13 ± 4
Type III	28 (7)	32 ± 5

Table 4. Frequency of disk types: Listed are the number of galaxies per profile type. The values in brackets are those associated to more than one break type (mixed classification). Therefore the last column gives the frequency for each break type and does not add up to 100%.

wise) related to the presence of the bar (Type II.o-OLR), and c) 13% ± 4% (from the full sample) show breaks in their profile (Type II-AB) that could be originated by a lopsided or asymmetric disk, not allowing us to probe for a real, intrinsic break in the stellar light distribution using our azimuthally averaged, fixed ellipse fits.

33% ± 5% of the galaxies show a break with an upbending profile (Type III).

5.2. Parameter distribution

In the following we give all measurement of lengths and ratios as obtained for the r' band and excluding the mixed classifications if not otherwise stated.

No breaks (Type I)

The mean central surface brightness and scalelength of the 9 Type I galaxies are $\mu_0 = 20.2 \pm 0.8\, r'$-mag/$\square''$ and $h = 2.8 \pm 0.8$ kpc respectively, which are typical values for local galaxies (cf. MacArthur et al., 2003; de Jong, 1996). We confidently trace the profiles down to our critical surface brightness of $\mu_{\rm crit} \sim 27.0\ r'$-mag/$\square''$ (see Fig. 2). So, in terms of scalelength we do not find a break down to 6 – 8 times the measured scalelength.

Classical truncations (Type II-CT)

The break in the surface brightness profiles appears at 9.2 ± 2.4 kpc and ranges between 5.1 kpc and 14.7 kpc with a slight trend towards galaxies with higher luminosities having larger break radii (cf. Fig. 7). We do not find a systematic difference between the break radii as measured in the r' or g' band. In relative units the break is at 2.5 ± 0.6 times the inner scalelength with values between 1.4 and 4.2, uncorrelated with rotational velocity and with a weak trend towards higher values for brighter galaxies (cf. Fig. 8). The value found here for the position of the break in terms of radial scalelength is apparently smaller (although compatible within 1σ) to the one quoted for

three galaxies by Pohlen et al. (2002): 3.9 ± 0.7. According to Pohlen et al. (2002), the one galaxy in common (UGC 9837) has a value of 3.1 for $R_{\rm br}/h_{\rm in}$, which is consistent with our ratio of 2.7 obtained from the SDSS image. The two galaxies with high values (4.3 and 4.2) are too distant to be in our sample and both are intrinsically large, having break radii of 14.7 kpc and 21.1 kpc. Fitting the SDSS profile (converted to Johnson R according to Sect. 3.2, see Fig. 3) and using our method for one of them (NGC 5923), we obtain also a consistent value (4.1 compared to 4.3 quoted by Pohlen et al., 2002). Due to the completely different masking of a very close extended companion the comparison for the third galaxy (NGC 5434) is not straightforward (3.2 compared to 4.2). So neither their larger intrinsic size nor a systematic error in determining the ratio ($R_{\rm br}/h_{\rm in}$) is responsible for the apparent mismatch of the mean values for the two samples, suggesting that its origin is due to small number statistics.

However, our mean value of 2.5 ± 0.6 is significantly lower compared to the 4.5 ± 1.0 value obtained for 16 face-on galaxies by van der Kruit (1988). This large offset is almost certainly due to the different definition (break versus cut-off) and method used to mark the truncation. We determine the truncation at the position of the measured break in the profile (so quite far in), whereas van der Kruit was looking for a sharp outer boundary estimated from isophote maps. Our value is supported by Bosma & Freeman (1993) who stated that for 7 galaxies (with breaks in their surface brightness profiles), of the 21 reported by Wevers (1984) (so virtually the same dataset van der Kruit (1988) used), the mean value of the break to scalelength is 2.8 ± 0.4, so very close to our mean value.

The mean scalelength of the inner disk $h_{\rm in}$ in our sample is 3.8 ± 1.2 kpc and ranges between 2.0 kpc and 6.6 kpc, which is typical for local galaxies (cf. MacArthur et al., 2003; de Jong, 1996).

The central surface brightness (extrapolated from the fitted inner exponential, corrected for galactic extinction, but uncorrected for inclination) ranges between $\mu_{0,\rm in} = 18.5\,r'$-mag/$\square''$ and $\mu_{0,\rm in} = 22.3\,r'$-mag/$\square''$ ($18.9 - 22.8\,g'$-mag/$\square''$) with a clear trend towards galaxies with fainter luminosities having a fainter central surface brightness (cf. Fig. 9) as seen by MacArthur et al. (2004) or de Jong (1996).

However, the surface brightness at the break radius only weakly correlates with absolute magnitude (cf. Fig. 9) and peaks (cf. Fig. 10) at a mean value of $\mu_{\rm br} = 23.5 \pm 0.8\,r'$-mag/$\square''$ ($\mu_{\rm br} = 23.8 \pm 0.8\,g'$-mag/$\square''$). The mean ratio of inner to outer scalelength is $h_{\rm in}/h_{\rm out} = 2.1 \pm 0.5$ with a mildly peaked distribution ranging between $h_{\rm in}/h_{\rm out} = 1.3 - 3.6$.

OLR breaks (Type II.o-OLR)

The break radii for the Type II.o-OLR breaks span a wider range, compared to Type II-CT breaks, between 2.4 kpc and 25.0 kpc (mean: 9.5 ± 6.5 kpc) again with a clear trend towards galaxies with higher luminosities having larger break radii (cf. Fig. 7). In terms of inner scalelength almost all breaks appear in the small range between 1.4 – 2.4 times $h_{\rm in}$ (with a mean at $1.7h_{\rm in}$), except for one galaxy (NGC 5430) where the break is at $4.4h_{\rm in}$ but which could be also classified as Type I with bumps shaped by the prominent bar (cf. Appendix A). The surface brightness at the break radius is $\mu_{\rm br} = 22.6 \pm 1.0\,r'$-mag/$\square''$. Although on the lower end compared to the distribution for $R_{\rm br}/h_{\rm in}$ and $\mu_{\rm br}$, neither of these parameters works out as a clear discriminatory property for the two different downbending break types Type II-CT and Type II.o-OLR.

Upbending profiles (Type III)

In relative units the Type III break appears further out, compared to Type II-CT or Type II.o-OLR breaks, at 4.9 ± 0.6 times the inner scalelength with values between 3.7 and 5.8 (excluding the seven galaxies with mixed classifications where an inner scalelength is not well defined). However, in absolute units they span the same range. The break appears at 9.3 ± 3.3 kpc and ranges between 4.4 kpc and 15.5 kpc having the same trend with luminosity (cf. Fig. 7). The inner scalelength is on average smaller with 1.9 ± 0.6 kpc ranging only between 0.9 kpc and 3.0 kpc. The central surface brightness (extrapolated from the fitted inner exponential and corrected for galactic extinction) ranges only between $\mu_{0,\rm in} = 18.1\,r'$-mag/$\square''$ and $\mu_{0,\rm in} = 20.3\,r'$-mag/$\square''$ (mean: $19.2 \pm 0.6\,r'$-mag/$\square''$) without showing the clear trend with luminosity as for the Type II-CT breaks. The mean value for the surface brightness at the break radius, $\mu_{\rm br} = 24.7 \pm 0.8\,r'$-mag/$\square''$ ($\mu_{\rm br} = 25.6 \pm 0.4\,r'$-mag/$\square''$ for the seven galaxies with additional downbending breaks inside), is clearly fainter compared to the Type II-CT breaks (see Fig. 10).

5.3. Correlations

Plotting the frequency of break types versus the Hubble types (grouped in three bins: Sb–Sbc, Sc–Scd, and Sd–Sdm) reveals a clear correlation (cf. Fig. 11). Whereas the few Type I galaxies are evenly distributed with Hubble type, the frequency of Type III breaks decreases, and that of the Type II-CT increases, with later Hubble type. The Type II.o-OLR breaks appear to have a minimum for the Sc–Scd galaxies which might be related to a minimum in the overall RC3 strong bar frequency for Sc galaxies as mentioned by e.g. Lütticke (1999). We know that the Hubble type T correlates with absolute magnitude $M_{\rm abs}$ (cf. Sect. 2.1), but marking the different break types in such a plot shows that the correlation of break type is more pronounced with the Hubble type compared to $M_{\rm abs}$.

For the classical truncations (Type II-CT) the position of the break at 2.5 ± 0.6 times the inner scalelength shows a trend with Hubble type (cf. Fig. 8) in the sense of later types being *earlier* truncated. However, it seems to be almost uncorrelated with total mass (either measured with $M_{\rm abs}$ or $\mathcal{M}_{\rm dyn}$, see Fig. 7).

5.4. Environment

We find for some of our Type III galaxies indication for a recent interaction (cf. Appendix A) such as close physical companions, streams, or shells. However, using the number of neighbours (as determined in Sect. 2.2), to characterise the environment, we do not find a clear correlation with the profile type.

Although it looks like the Type III galaxies tend to have more neighbours within a 1 Mpc volume (59% have 3 or more neighbours while for the Type II-CT the fraction is only 35%), such a correlation is far from being clear-cut. There are still many classical truncations among the galaxies having three or more (even up to nine) neighbours as well as Type III galaxies without any companion. However, we have the problem that criteria for environment are often too crude and lead even to controversial results. For example, our prototypical classical truncation, NGC 5300, has five neighbours in the SDSS database, which is clearly in a denser region according to our environment criterion. Using the CfA catalogue and applying a different criterion Varela et al. (2004) list it as being part of their *truly isolated* galaxy sample.

6. Discussion

As reported by Pohlen et al. (2004) we also do not find any galaxy with a sharp cut-off in the radial light distribution. This means that the so-called *truncated* galaxies are best described by a broken exponential. This seems to be now the intrinsic structure associated to the inferred sharp cut-offs proposed by van der Kruit (1979). A similar result is found, using a completely independent approach, by Ferguson et al. (2006) mapping the prototypical truncated galaxy M 33. They traced the profile down to $\mu_{\rm lim} \sim 30$ I-mag/$\square''$ (transformed to surface brightness) using star-counts.

In general, the shape of the transition regions we found (measured in terms of the boundary difference $b_3 - b_2$) is no longer as sharp as measured by Pohlen et al. (2002). Only very few cases (e.g. NGC 5300 or NGC 7437) exhibit a very sharp transition between the inner and outer disk region. Most often the Type II-CT breaks appear with a more gradual transition zone up to an almost exponential region of size ~ 4 kpc in between.

Since the discrimination between Type II.o-OLR and Type II-CT is solely based on bar size measurements one could argue that there are some undetected Type II.o-OLR breaks among the galaxies classified as Type II-CT. However, we carefully use either bar sizes from the literature or in most cases estimated them from the image to make sure the Type II-CT is as good as possible separated from the Type II.o-OLR breaks.

In total, without specifying the origin, most of the galaxies ($\gtrsim 60\%$) exhibit a break followed by a downbending profile almost consistent with the edge-on results by Kregel, van der Kruit, & de Grijs (2002), although they probably would have excluded the Type II-AB galaxies from their initial sample.

We do not find truncation breaks beyond ~ 25.2 r'-mag/$\square''$ (cf. Fig. 10). We have explored whether this could be an observational bias caused by the difficulty of detecting breaks at faint levels. To do that we simulated 2D galaxies with breaks in their surface brightness distribution at different surface brightness levels. These galaxies are added to the real sky background and we measured the breaks as for real galaxies. From this we estimate our limit for detecting breaks of ~ 26.0 r'-mag/$\square''$. This limit leaves a range of ~ 1mag to reach our critical surface brightness of $\mu_{\rm crit} \sim 27.0$ r'-mag/$\square''$ (down to which the slope of the outer profile could be traced confidently, see Fig. 2). So we expect to detect all truncations in the region $25.2 - 26.0$ r'-mag/$\square''$ if they do exist. Consequently, the decline observed in Fig.10 seems to be real. In addition, in terms of scalelength the largest break we find is at $R_{\rm br}/h_{\rm in} = 4.2$, but we are able to trace the profiles of our Type I galaxies down to $\sim 6-8$ radial scalelength. So we think that we do not miss any truncation breaks due to the limiting depth of the SDSS data and our Type I galaxies are indeed *untruncated*. This is consistent with measurements on individual galaxies being intrinsically untruncated down to ~ 10 scalelength (e.g. Weiner et al., 2001; Bland-Hawthorn et al., 2005). One of the key questions is now to find why some galaxies show truncations and (the minority) does not.

The strong increase for the Type III frequency towards earlier Hubble types (Sb–Sbc) could be used to argue against the Type III feature being really related to the disk itself, by explaining the rise in the profile as a traditional $R^{1/4}$ bulge component taking over from the exponential disk in the outer parts. However, Erwin (2005) already showed that this is only true for about $\sim 1/3$ of the earliest types (SB0-SBb, having the highest chances of being bulge dominated). We see that $\sim$ 40% of our Type III late-type galaxies exhibit clear signs for spiral arms in the outer disk excluding any spheroidal (pressure supported) nature of the outer structure. For another $\sim$ 23% of the Type III galaxies we do not find a significant decrease in ellipticity (expected if produced by a spheroidal component) while fitting free ellipses across the break. So we conclude that in most ($>$ 63%) of our Type III galaxies the outer region is indeed related to the disk. This results fits nicely to the extended outer (star-forming) disks (e.g. NGC 4625) which have been recently reported by the GALEX team (Thilker et al., 2005; Gil de Paz et al., 2005) as being significantly more frequent than thought before. Unfortunately, we do not have any galaxy classified as Type III on our SDSS images in common with those reported by the GALEX team. However, the profile shown by Swaters & Balcells (2002) of NGC 4625 clearly suggests a Type III classification.

7. Summary

The main goal of our study is to provide a census of the radial disk structure of local ($v_{\rm vir} < 3250$ km/s) late-type galaxies. Using the LEDA catalogue we selected a complete sample of 655 galaxies down to $M_{\rm abs} = -18.4$ B-mag. 98 (85 with useful images) of them are part of the SDSS Second Data Release (DR2) which provides the imaging data used here. After careful sky subtraction we obtained our radial surface brightness profiles from fixed ellipse fits. We classified the resulting profiles searching for clear breaks either of the *downbending* (steeper outer region) or *upbending* kind (shallower outer region) (following Erwin et al., 2006) and derived scalelength and central surface brightness values for exponential fits to the individual regions.

The main conclusions are as follows:

1. We are able to reliably trace azimuthally averaged, fixed ellipse profiles of face-on to intermediate inclined galax-

ies down to a critical surface brightness of $\sim$ 27.0 r'-mag/$\square''$ using SDSS imaging data. We have taken extreme care in determining the background *(sky)* around our objects. Our surface brightness limit value is supported by finding similar sky values with different methods. In addition, our profiles match those from available deeper photometry and we are able to recover simulated profiles added to empty SDSS sky fields down to the above surface brightness limit.

2. 90% of our galaxies could be classified into one of the following classes –Type I (no break), Type II (downbending break), and Type III (upbending break)– extending Freemans original classification. The remaining 10% of the sample could be well described being a mix from two individual classes. We introduced two main sub-classifications for the Type II class connecting the observed break with possible different physical origins: Type II-CT, *classical truncations*, probably associated with a global, radial star-formation threshold (cf. Sect. 1), and exclusively for barred galaxies, Type II.o-OLR *OLR breaks*, observed at around twice the bar radius and probably associated with the outer Lindblad resonance of the bar (see Erwin et al., 2006).
3. Surprisingly only $\lesssim$15% of all galaxies have a *normal* purely exponential disk down to our noise limit. A good deal more (33% of each) have profiles with an upbending break (Type III) or a classical truncation (Type II-CT).
4. We find a correlation of break type with morphological type. Classical truncations (Type II-CT) are more frequent in later types while the fraction of upbending breaks rise towards earlier types.
5. Our Type I galaxies seem to be *genuinely* untruncated. The exponential profiles extend reliably down to a surface brightness of $\sim$27.0 r'-mag/$\square''$ (equivalent to $\sim 6-8$ times the scalelength).
6. We do not find any galaxy with a sharp (or complete) cut-off in the radial light distribution. This means *truncated* galaxies are in fact best described by a broken exponential with a shallow inner and a steeper outer exponential region separated at a more or less well defined break radius.
7. For Type II-CT galaxies the break happens already at 2.5 ± 0.6 times the inner scalelength at a typical surface brightness of $\mu_{\rm br} = 23.5 \pm 0.8\, r'$-mag/$\square''$. The position of the break (in kpc) seems to be correlated with absolute magnitude: the more *luminous* the *larger* the inner disk of the galaxy.
8. For Type III galaxies the break happens typically further out at 4.9 ± 0.6 times the inner scalelength, and at a lower surface brightness of $\mu_{\rm br} = 24.7 \pm 0.8\, r'$-mag/$\square''$. For more than 60% of these galaxies we find good indication that the outer upbending part is a disk-like structure (e.g. by finding spiral arms). Close physical neighbours and slightly disturbed morphology suggest in several cases interaction as a possible origin.

Acknowledgements. We would like to thank Peter Erwin and John Beckman for their stimulating discussions and useful suggestions during this work and especially Peter Erwin for helping with the ellipse task and for carefully reading parts of this paper. Thanks also to Reynier Peletier for reading the paper and for suggesting to use the derivative method for objectively quantifying the break radius. We also thank Marco Barden for very stimulating discussions and we would like to thank the anonymous referee for detailed comments which helped us to improve the quality of the manuscript. Part of this work was supported by a Marie Curie Intra-European Fellowship within the 6th European Community Framework Programme. This research has made use the Lyon/Meudon Extragalactic Database (LEDA, `http://leda.univ-lyon1.fr`) and the NASA/IPAC Extragalactic Database (NED) which is operated by the Jet Propulsion Laboratory, California Institute of Technology, under contract with the National Aeronautics and Space Administration. This research has made use of NASA's Astrophysics Data System Bibliographic Services. Funding for the creation and distribution of the SDSS Archive has been provided by the Alfred P. Sloan Foundation, the Participating Institutions, the National Aeronautics and Space Administration, the National Science Foundation, the U.S. Department of Energy, the Japanese Monbukagakusho, and the Max Planck Society. The SDSS Web site is `http://www.sdss.org/`. The SDSS is managed by the Astrophysical Research Consortium (ARC) for the Participating Institutions. The Participating Institutions are The University of Chicago, Fermilab, the Institute for Advanced Study, the Japan Participation Group, The Johns Hopkins University, the Korean Scientist Group, Los Alamos National Laboratory, the Max-Planck-Institute for Astronomy (MPIA), the Max-Planck-Institute for Astrophysics (MPA), New Mexico State University, University of Pittsburgh, University of Portsmouth, Princeton University, the United States Naval Observatory, and the University of Washington.

References

Abazajian, K., Adelman, J., Agueros, M., et al. 2004, AJ, 128, 502
Abazajian, K., , Adelman, J., Agueros, M., et al. 2005, AJ, 129, 1755
Arp, H. 1966, ApJS, 14, 1
Barteldrees, A., & Dettmar, R.-J. 1994, A&AS, 103, 475
Barton, I.J., & Thompson, L.A. 1997, AJ, 114, 655
Baryshev, Y. V., & Paturel, G. 2001, A&A, 371, 378
Binggeli, B., Sandage, A., & Tammann, G. A. 1985, AJ, 90, 1681
Bland-Hawthorn, J., Vlajić, M., Freeman, K. C., & Draine, B. T. 2005, ApJ, 629, 239
Bosma, A., & Freeman, K. C. 1993, AJ, 106, 1394
Chernin, A. D. 1999, MNRAS, 308, 321
Conselice, C. J., Gallagher, J. S., Calzetti, D., Homeier, N., & Kinney, A. 2000, AJ, 119, 79
Courteau, S. 1996, ApJS, 103, 363
Cuillandre, J.-C., Lequeux, J., Allen, R. J., Mellier, Y., & Bertin, E. 2001, ApJ, 554, 190
Debattista, V. P., Mayer, L., Carollo, C. M., Moore, B., Wadsley, J., & Quinn, T. 2005, ApJ sub., astro-ph/0509310
de Grijs, R., Kregel, M., & Wesson, K. H. 2001, MNRAS, 324, 1074
de Jong, R. S., & van der Kruit, P. C. 1994, A&AS, 106, 451
de Jong, R. S. 1996, A&A 313, 45
de Vaucouleurs, G. 1959, Handbuch der Physik, 53, 311
de Vaucouleurs, G., de Vaucouleurs, A., Corwin, H.G., Buta, R.J., Paturel, G., & Fouque, J.B. 1991, Third reference catalogue of bright galaxies, Springer-Verlag New York

Elmegreen, B. G., & Hunter, D. A. 2006, ApJ, 636, 712
Erwin, P. 2004, A&A, 415, 941
Erwin, P. 2005, MNRAS, 364, 283
Erwin, P., Beckman, J.E., & Pohlen, M. 2005, ApJ, 626, 81
Erwin, P., Pohlen, M., & Beckman, J.E. 2006, in prep.
Ferguson, A.M.N., Irwin, M., Chapman, S. et al. 2006. To appear in the proceedings of the conference "Island Universes: Structure and Evolution of Disk Galaxies", ed. R. de Jong (Springer: Dordrecht), astro-ph/0601121
Ferguson, A.M.N., Wyse, R.F.G., Gallagher, J.S., & Hunter, D.A. 1998, ApJ, 506, L19
Florido, E., Battaner, E., Guijarro, A., Garzón, F., & Jiménez-Vicente, J. 2001, A&A, 378, 82
Freeman K.C. 1970, ApJ, 160, 811
Fukugita, M., Ichikawa, T., Gunn, J.E., Doi, M., Shimasaku, K., & Schneider, D.P. 1996, AJ, 111, 1748
Gil de Paz, A., Madore, B. F., Boissier, S., et al. 2005, ApJ, 627, L29
Giuricin, G., Marinoni, C., Ceriani, L., & Pisani, A. 2000, ApJ, 543, 178
Graham, A. W. 2001, AJ, 121, 820
Gunn, J.E., Carr, M.A., Rockosi, C.M., Sekiguchi, M., et al. 1998, AJ, 116, 3040
Hunter, D. A., & Elmegreen, B. G. 2005, ApJS, in press, astro-ph/0509189
Jansen, R. A., Franx, M., Fabricant, D., & Caldwell, N. 2000, ApJS, 126, 271
Jansen, R. A., & Kannappan, S. J. 2001, Ap&SS, 276, 1151
Jogee, S., Knapen, J. H., Laine, S., Shlosman, I., Scoville, N. Z., & Englmaier, P. 2002, ApJ, 570, L55
Karachentsev, I. D. 1972, Astrofizicheskie Issledovaniia Izvestiya Spetsial'noj Astrofizicheskoj Observatorii, 7, 3
Kennicutt, R.C., 1989, ApJ, 344, 685
Kregel, M., van der Kruit, P. C., & de Grijs, R. 2002, MNRAS, 334, 646
Lütticke, R. 2001, PhD Thesis, Ruhr-University Bochum, Germany
MacArthur, L. A., Courteau, S., & Holtzman, J. A. 2003, ApJ, 582, 689
MacArthur, L. A., Courteau, S., Bell, E., & Holtzman, J. A. 2004, ApJS, 152, 175
Möllenhoff, C. 2004, A&A, 415, 63
Nordgren, T. E., Chengalur, J. N., Salpeter, E. E., & Terzian, Y. 1997, AJ, 114, 77
Patterson, F. S. 1940, Harvard College Observatory Bulletin, 914, 9
Pérez, I. 2004, A&A, 427, L17
Pisano, D. J., & Wilcots, E. M. 1999, AJ, 117, 2168
Pohlen, M., Dettmar, R.-J., & Lütticke, R. 2000a, A&A, 357, L1
Pohlen, M., 2001, Ph. D. Thesis, Ruhr-University Bochum, Germany
Pohlen, M., Dettmar, R.-J., Lütticke, R., & Aronica, G. 2002, A&A, 392, 807
Pohlen, M., Beckman, J. E., Hüttemeister, S. H., Knapen, J. H., Erwin, P., & Dettmar, R.-J. 2004b. In Penetrating Bars through Masks of Cosmic Dust: The Hubble Tuning Fork Strikes a New Note, ed. D. L. Block, I. Puerari, K. C. Freeman, R. Groess, & E. K. Block (Dordrecht: Springer), 713
Prada, F., Vitvitska, M., Klypin, A. et al. 2003, ApJ, 598, 260
Sandage, A., & Bedke, J. 1994, The Carnegie atlas of galaxies, Washington, DC: Carnegie Institution, 1994
Schaye, J. 2004, ApJ 609, 669
Schlegel, D. J., Finkbeiner, D. P., & Davis, M. 1998, ApJ, 500, 525
Schinnerer, E., Eckart, A., Tacconi, L. J., Genzel, R., & Downes, D. 2000, ApJ, 533, 850
Smith, J.A., Tucker, D.L., Kent, S.M., et al. 2002, AJ, 123, 2121
Swaters, R. A., & Balcells, M. 2002, A&A, 390, 863
Takase, B., & Miyauchi-Isobe, N. 1984, Annals of the Tokyo Astronomical Observatory, 19, 595
Thilker, D. A., Bianchi, L., Boissier, S. et al. 2005, ApJ, 619, L79
Trujillo, I., et al. 2002, MNRAS, 333, 510
Trujillo, I., & Pohlen, M. 2005, ApJ, 630, L17
Tully, R.B. 1988, *Nearby Galaxies Catalog* (Cambridge: Cambrige University Press)
Tully, R. B., Verheijen, M. A. W., Pierce, M. J., Huang, J., & Wainscoat, R. J. 1996, AJ, 112, 2471
van der Kruit, P. C., 1979, A&AS 38, 15
van der Kruit, P. C. 1988, A&A, 192, 117
van der Kruit, P. C. 1987, A&A, 173, 59
Varela, J., Moles, M., Márquez, I., Galletta, G., Masegosa, J., & Bettoni, D. 2004, A&A, 420, 873
Weiner, B. J., Williams, T. B., van Gorkom, J. H., & Sellwood, J. A. 2001, ApJ, 546, 916
Wevers, B.M.H.R., 1984, Ph. D. Thesis, Groningen University, The Netherlands
York, D.G., Adelman, J., Anderson, J.E., et al. 2000, AJ, 120, 1579
Zaritsky, D., Smith, R., Frenk, C., & White, S. D. M. 1993, ApJ, 405, 464

Appendix A: Galaxy Atlas

The atlas presented here contain the 85 (from 98) galaxies with useful images in the SDSS Second Data Release (DR2) as described in Sect. 2.1. The data for every two galaxies is presented on a single page. On the left side we give detailed comments on the individual galaxies concerning the applied classification and global characteristics (such as distinct morphological features or environment). The headline gives the name and classification type. Below we reproduce the main parameters: Position (`J2000`), RC3 Hubble-type, coded LEDA Hubble parameter `T`, absolute B band magnitude $\mathtt{M_{abs}}$ `[B-mag]`, apparent diameter `[']`, virgocentric radial velocity $\mathtt{v_{vir}}$ $[\mathtt{km\,s^{-1}}]$. On the right side we reproduce the JPEG 800x600 colour mosaics obtained with the SDSS 'Finding Chart' tool[6]. Overlayed are a N-S, E-W grid through the center, a 1′ scale bar, and the outline of the individual SDSS fields. In addition we show azimuthally averaged, radial surface brightness profiles in the g' *(triangles)* and r' *(circles)* band obtained from fixed ellipse fits. The r'-band is overlayed by the best exponential fits (cf. Sect. 4.2) to the individual regions: single disk, inner and outer disk, or three fits in the case of a mixed classification. The boundaries (b_{1-4}) used for the fit are marked with the short *vertical, dashed lines* on the abscissa. Following Courteau (1996) we also chose not to show error bars on all the profiles to avoid overcrowding of the plots. Instead, we show for the g'-band *(horizontal, dashed line)* and for the r'-band *(horizontal, dotted line)* the critical surface brightness ($\mu_{\rm crit}$) down to which the profile is reliable. This limit is placed where profiles obtained by using $\pm 1\sigma$*sky* deviate by more than 0.2 mag from the one with our mean sky value (cf. Sect. 3.3). In the upper right corner of the surface brightness profiles we note the galaxy name, the Hubble type according to RC3 (for galaxies without or uncertain (S?) classification from LEDA), and the profile type.

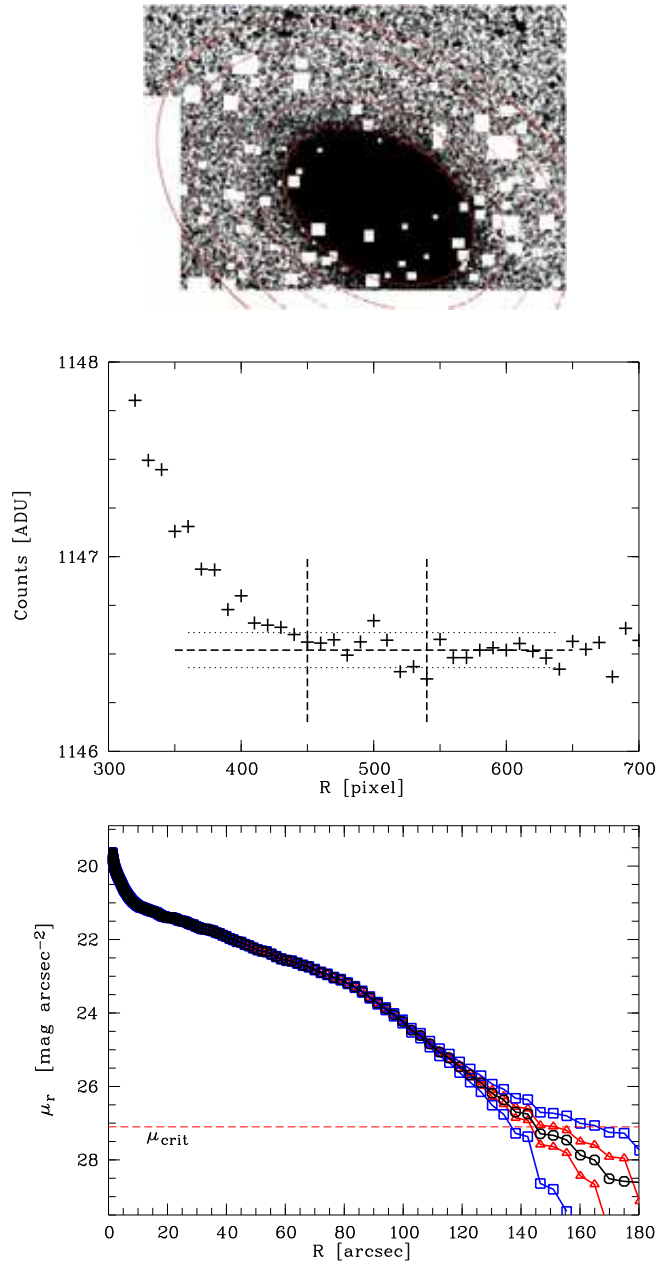

Fig. 2. Sky obtained by ellipse fitting: *Upper panel:* r'-band image of NGC 5300 exemplary overlayed by eight fixed ellipses at every 100 pixels in the range 300-700 pixels. The white rectangular regions are masked areas. *Middle panel:* mean isophotal intensity (in counts) of the fixed ellipses fitted every 10 pixels. The region between the vertical dashed lines is used to determine the sky value (1146.52 ± 0.09), which is indicated as a horizontal dashed line together with the two dotted lines at $\pm 1\sigma$. *Lower panel:* Final surface brightness profile *(circles)* overlayed by the four profiles obtained by either over- or undersubtracting the sky by $\pm 1\sigma$ *(triangles)* or by $\pm 3\sigma$ *(squares)*. The horizontal dashed line gives the critical surface brightness ($\mu_{\rm crit}$) up to where we trust the profile i.e. where the $\pm 1\sigma$ profiles deviate by more than 0.2 mag.

[6] `http://cas.sdss.org/dr4/en/tools/chart/chart.asp`

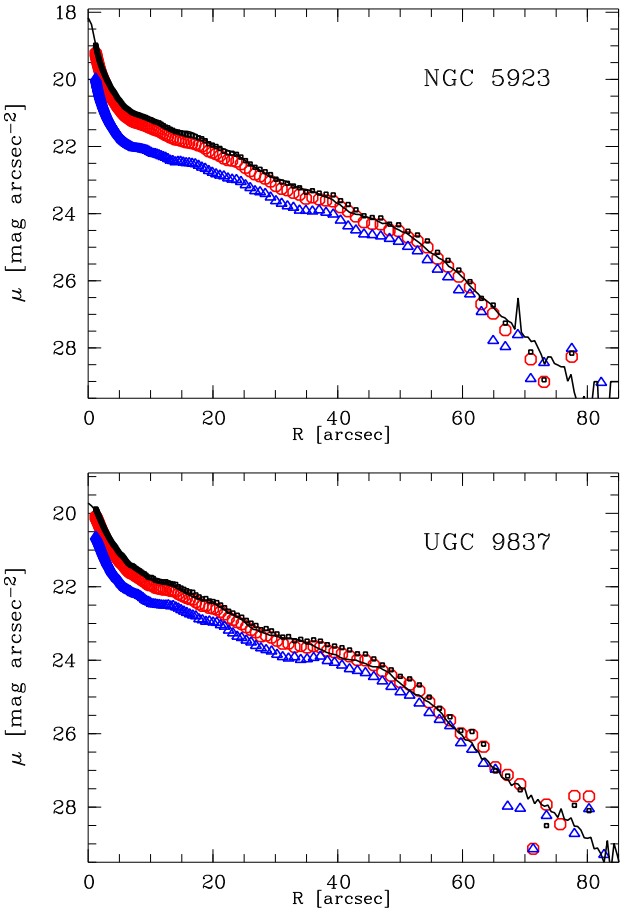

Fig. 3. SDSS quality check: Azimuthally averaged, radial surface brightness profiles obtained from SDSS images *(r′ band with big circles; g′ band with big triangles))* are compared with much deeper imaging *(thin, continuous line)* presented in Pohlen et al. (2002). The *small squares* are obtained by using the transformation to convert SDSS *g′* and *r′* into standard Johnson *R* band (used by Pohlen et al., 2002) following Smith et al. (2002).

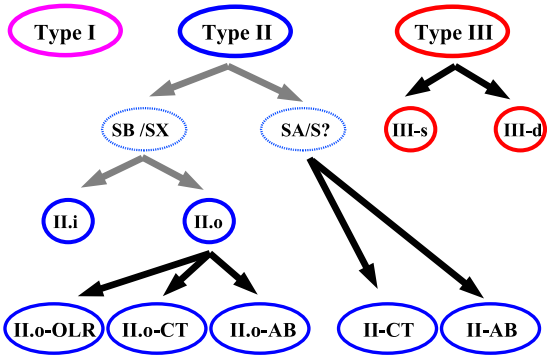

Fig. 4. Classification schema (following Erwin et al., 2006): The three main disk types according to break features in their surface brightness profiles are Type I (no break), Type II (*downbending* break), and Type III (*upbending* break). In case the galaxy is barred (SB/SX) the *downbending* breaks (Type II) are subdivided according to the position of the break in respect to the bar: Type II.i (inside) or Type II.o (outside). An additional level of subclassification is applied for this class trying to relate the observed break to a physical origin. These are Type II.o-AB, Type II.o-OLR, and Type II.o-CT (see text). For apparently unbarred galaxies (SA/S?) we use only Type II-CT or Type II-AB. The *upbending* breaks (Type III) are subdivided according to the possible nature of the outer region: *(d)*isk- or *(s)*pheroid-like. Some galaxies are better described with two breaks, each of which could be associated to one of the individual types. They are assigned a mixed classification (e.g. Type II-CT + III).

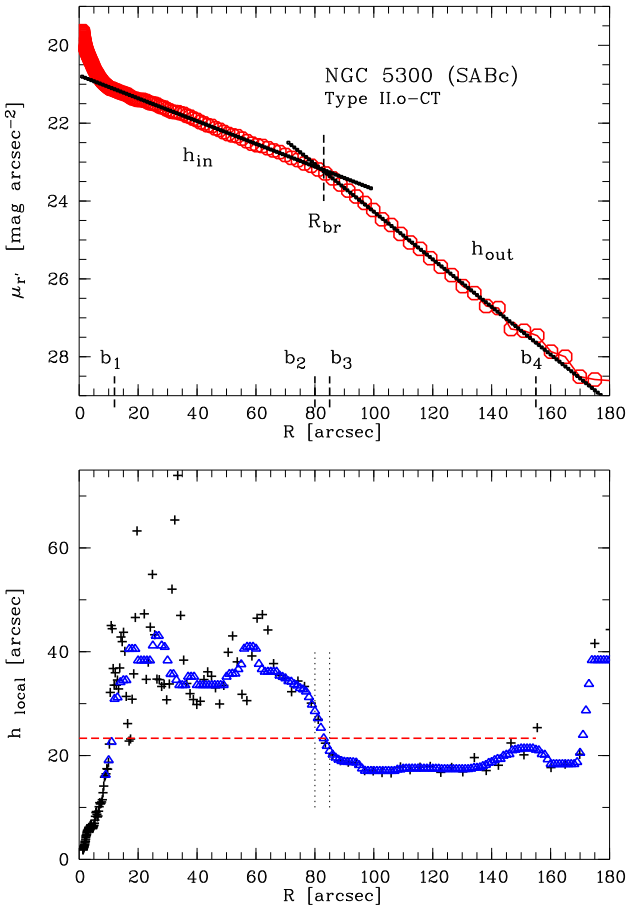

Fig. 6. Example of how to establish the break radius, the break region and the associated scalelengths: *(Upper panel):* Azimuthally averaged, surface brightness profile, overlayed by the best fitting exponentials (with scalelengths $h_{\rm in}$ and $h_{\rm out}$) marking the position of the boundaries (b_{1-4}) and the break radius $R_{\rm br}$. *(Lower panel):* Approximated derivative *(crosses)* of the profile providing a local scalelength ($h_{\rm local}$) together with the rebinned and smoothed version *(triangles)*. The *horizontal dashed line* marks our characteristic (or mean) value which is the median of the $1/h_{\rm local}$ distribution. The *vertical dotted lines* mark the inner and outer boundary of the break region.

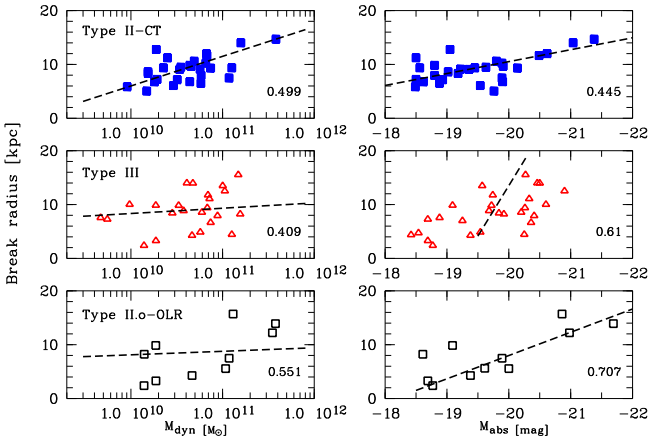

Fig. 7. Break radius ($R_{\rm br}$) in absolute units (kpc) versus dynamical mass ($\mathcal{M}_{\rm dyn} = 2.326 \cdot 10^5 \frac{D_{25}}{2} v_{\rm rot}{}^2$) and absolute magnitude ($M_{\rm abs}$) in the B-band according to LEDA for the different break types: Type II-CT *(upper row)*, Type III *(middle row)*, and Type II.o-OLR *(bottom row)*. Overplotted are robust linear fits *(dashed lines)* to guide the eye and in the lower right corner of each plot the Spearman rank correlation coefficient. The break radius correlates in all three cases with absolute magnitude. With the exception of the Type II-CT, the relation of the position of the break with the dynamical mass is less tight.

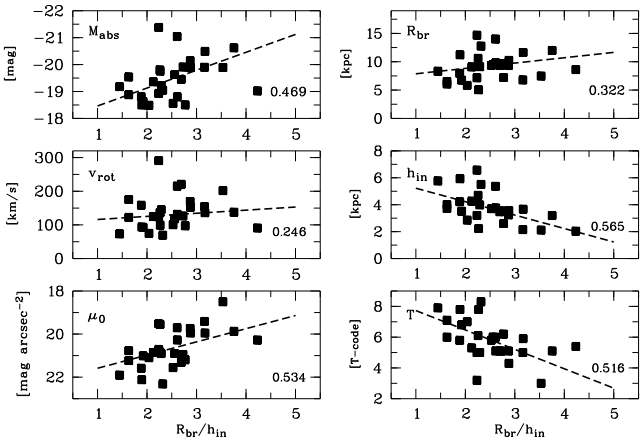

Fig. 8. Classical truncations (Type II-CT): Break radius in units of inner scalelength versus absolute magnitude ($M_{\rm abs}$) *(left, upper panel)*, rotational velocity ($v_{\rm rot}$) *(left, middle panel)*, extinction corrected central surface brightness of the inner disk ($\mu_{0,\rm in}$) *(left, lower panel)*, break radius in linear unit ($R_{\rm br}$) *(right, upper panel)*, inner scalelength in linear unit ($h_{\rm in}$) *(right, middle panel)*, and Hubble type (T) *(right, lower panel)*. Overplotted are robust linear fits *(dashed lines)* to guide the eye and in the lower right corner of each plot the Spearman rank correlation coefficient.

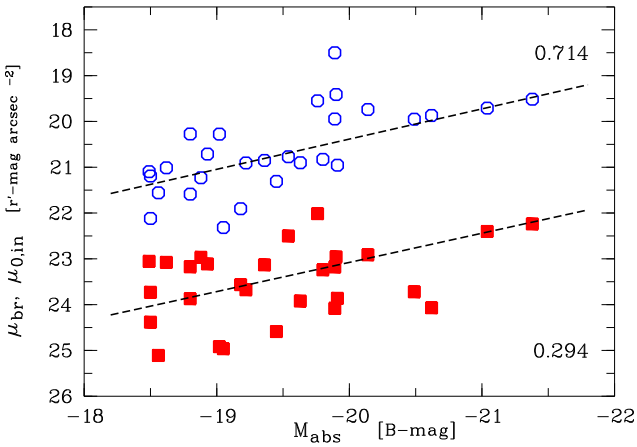

Fig. 9. Classical truncations (Type II-CT): Extrapolated central surface brightness μ_0 *(open circles)* and surface brightness at the break radius μ_{br} *(filled squares)* in the r' band versus absolute magnitude (M_{abs}) in B according to LEDA. Overplotted are robust linear fits *(dashed lines)* to guide the eye and in the lower and upper right corner the Spearman rank correlation coefficient for each data set.

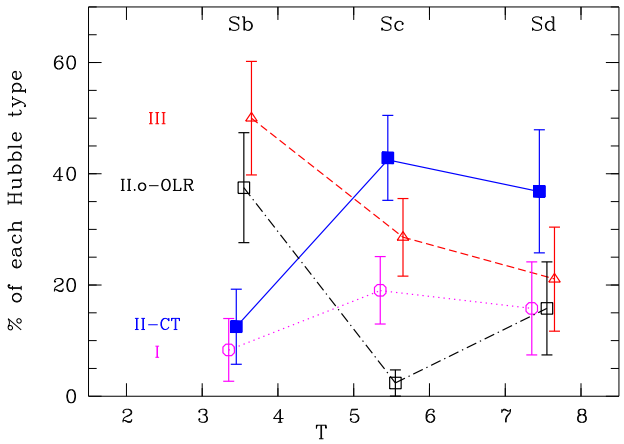

Fig. 11. Frequency of profile types Type I *(open circles)*, Type II-CT *(filled squares)*, Type III *(open triangles)*, and Type II.o-OLR *(open squares)* in relation to the Hubble type. The galaxies are merged in three morphological bins (T between 2.5 – 4.4, 4.5 – 6.4, and 6.5 – 8.4). The associated points are connected with lines and slightly shifted in T to be able to separate them.

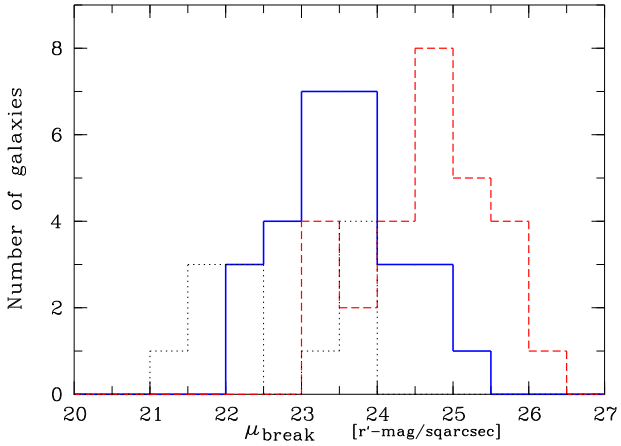

Fig. 10. Histogram of the surface brightness (in the r' band) at the break radius for the galaxies of Type II-CT *(solid line)*, Type III *(dashed line)*, and Type II.o-OLR *(dotted line)*.

IC 1067 : Type II.o-OLR (possible Type I)
`J145305.2+031954 .SBS3. 3.0 -18.97 2.0 1665`

Galaxy close to the border of the SDSS field but almost complete with a nearby, physical companion (IC 1066, v = 1577km s^{-1}) only 2.2′ away, which slightly influences the background estimation (together with two nearby bright stars). The strong peak at ∼ 20″ in the final profile is related to the ring around the prominent bar and the dip at ∼ 35″to the inter-arm region of the two symmetric spiral arms peaking at ∼ 40″. Although possible to fit (at least for the r' band profile) with a single exponential (Type I), we classify the galaxy as Type II.o-OLR, with a break around twice the bar radius at ∼ 40″, having an inner disk region too small to be detected with our automatic break searching routine. This is consistent with the classification and profile by Erwin et al. (2006). The region inside ∼ 40″ is excluded for the fit of the outer scalelength.

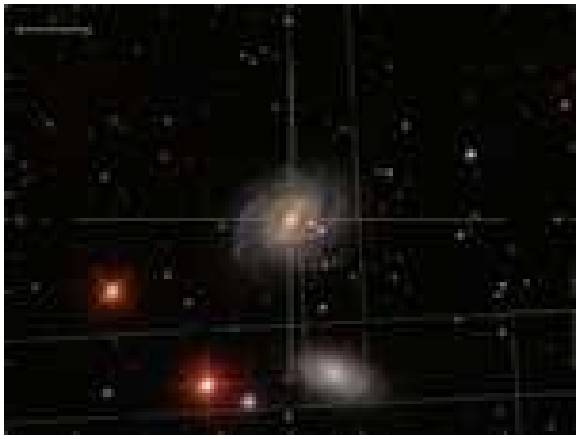

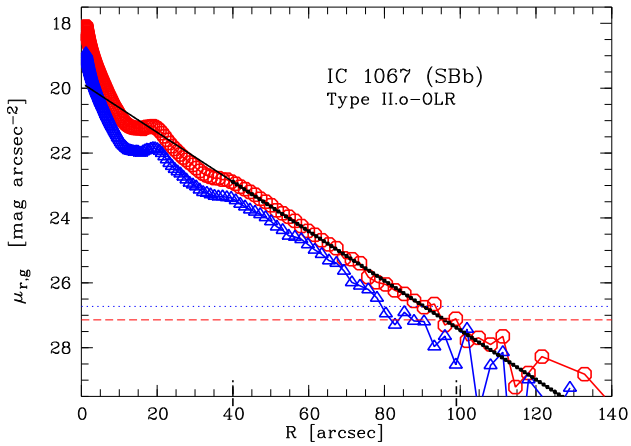

IC 1125 : Type I
`J153305.6-013742 .S..8* 7.7 -20.05 1.7 2868`

According to the coordinates in NED the companion (KPG 467A) in Karachentsev's Isolated Pairs of Galaxies Catalogue Karachentsev (1972) corresponds only to a faint starlike object about 11″ away. The small bump in the radial profile at ∼ 40″ corresponds to an outer spiral arms. Otherwise we see no obvious deviation from a single exponential and therefore the galaxy is classified as Type I.

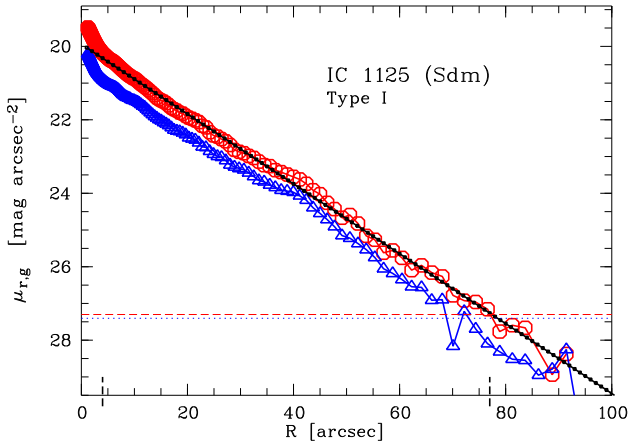

IC 1158 : Type II.o-CT
`J160134.1+014228 .SXR5* 5.3 -19.36 2.2 2018`

Galaxy shows clearly a truncated profile with an extended break region, starting approximately at the end of the spiral arms. The center looks like a secondary bar with a small ring embedded in larger bar of size roughly $\lesssim 22''$ (without any noticeable feature in the final profile). So the break with downbending profile at $\sim 60''$ is well beyond a typical Type II.o-OLR break.

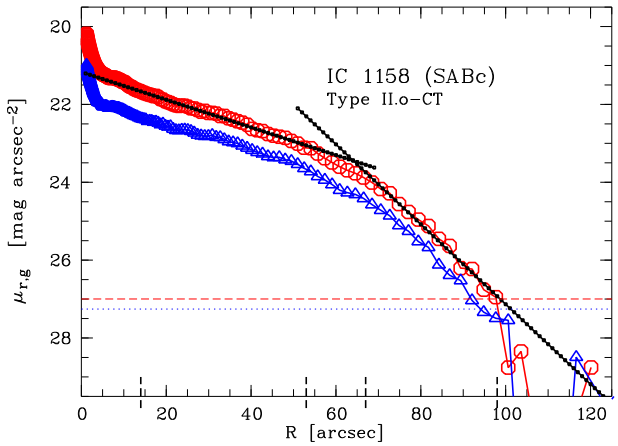

NGC 0450 : Type II.o-CT
`J011530.8-005138 .SXS6* 6.0 -19.63 3.0 1712`

A background galaxy (UGC 00807, 11587km s^{-1}) is superimposed. The mean ellipticity of the outer disk is difficult to determine. The inner disk looks fairly round whereas the outer disk looks rather elliptical. The size of the slightly more elliptical inner part, associated to be the bar (although without any noticeable feature in the final profile), is roughly $\sim 8''$, so the break with the downbending profile at $\sim 84''$ is well beyond a typical Type II.o-OLR break and roughly outside the spiral arm region.

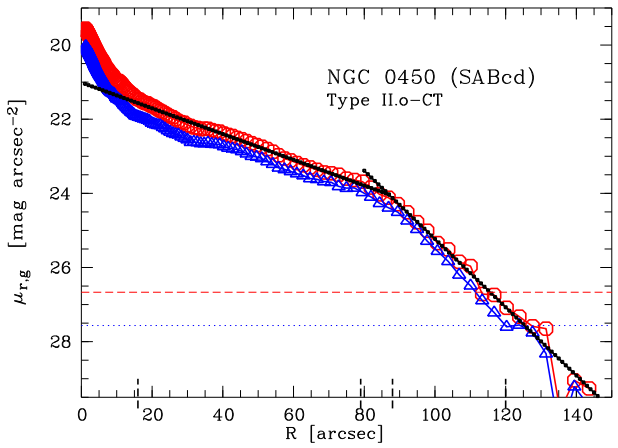

NGC 0701 : Type II.i (possible Type I)
`J015103.8-094209 .SBT5. 5.1 -19.74 2.5 1729`

Galaxy is in a multiple system together with NGC 0681 and NGC 4594 (where PGC 006667 (see below) is also part of) with an additional small physical companion (IC 1738, $v = 1750\,\mathrm{km\,s^{-1}}$) about 6′ away. Galaxy close to our high axis ratio limit so the dust may have some influence. The inner region shows no nucleus, so the centering is done from the outer isophotes. The extend of the bar is unknown, but the visible bump at 45″ is probably not related to a bar. It is possible to construct a break at 45″ (which would be more pronounced in the g' band), but the inner drop could be also due to the higher inclination with dust and/or patchy star formation affecting the profile.

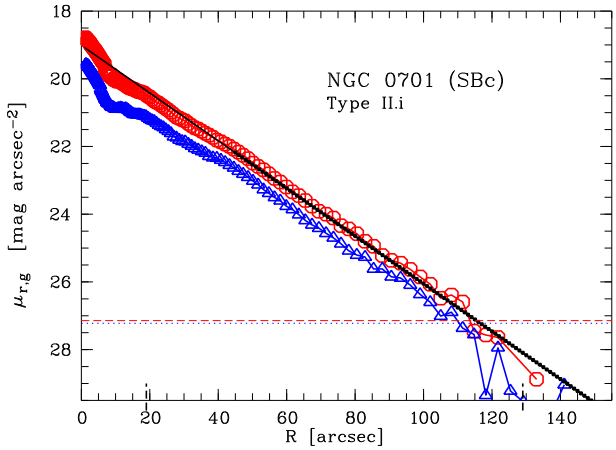

NGC 0853 : Type III
`J021141.5-091817 .S..9P 8.3 -18.42 1.5 1405`

The inner region shows no clear nucleus but many H II regions, so the centering is done from the outer isophotes. The inner disk is slightly asymmetric with an additional light patch in the western part, therefore mean ellipticity and PA difficult to fix. Almost continuously upbending profile beyond the peak at 15″, which includes all H II regions, getting flat at ∼ 42″. The inner profile is rather curved and not well approximated with a single exponential. The apparent outer break at ∼ 100″ is only due to the improper fixed ellipse fit in the outer parts.

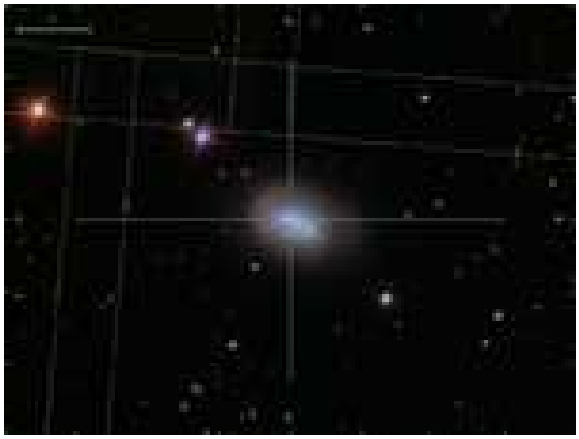

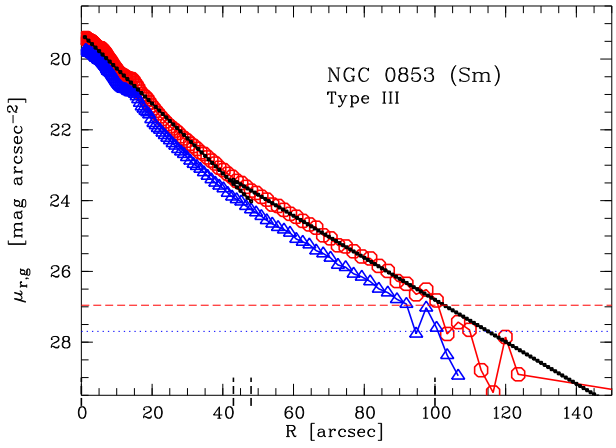

NGC 0941 : Type II-CT
`J022827.9-010906 .SXT5. 5.4 -19.02 2.5 1535`

Galaxy shows only a very small, point-like nucleus and is in a small group of galaxies (including NGC 936 and NGC 955). The small dip at $\sim 40''$ is associated with the inner spiral arm region. Although classified as SAB no real bar visible on image or in the profile thus the downbending break is classified as Type II-CT.

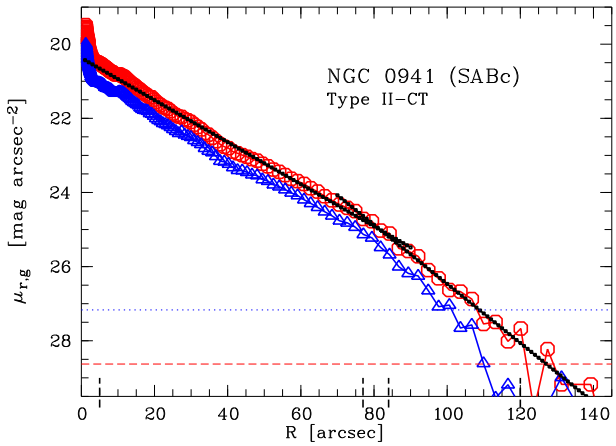

NGC 1042 : Type II-AB
`J024023.9-082558 .SXT6. 6.1 -19.83 4.4 1264`

A large scale gradient (from top to bottom) in the background of the r' and g' band image is removed with a linear fit. Only partly fitted since $\lesssim 1/3$ of galaxy is beyond SDSS field. Galaxy shows an asymmetric (frayed) extension towards the south-east and a sharper edge towards the north-west, which makes it not really lopsided but looking rather like being affected by moving in a dense IGM. The extended (frayed) spiral arms build the outer disk, so ellipticity and PA very difficult to fix. The inner bump in the profile at $\sim 90''$ is due to spiral arms. The inner profile is below the inward extrapolation of the outer disk, but due to the asymmetric shape of the disk we call this galaxy only Type II-AB.

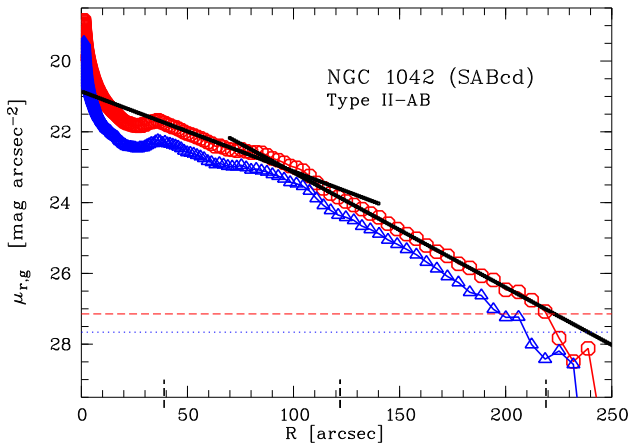

NGC 1068 ≡ M 77 : Type II.o-OLR
`J024240.8-000048 RSAT3. 3.0 -21.69 7.6 1068`

Only partly fitted since $\lesssim 1/3$ of galaxy is beyond the SDSS field. Galaxy appears to have an inner disk, elongated into a bar-like structure sitting in an outer disk with clearly different PA and with indication for an additional outer ring at $\sim 200''$. According to Erwin (2004) it is a double-barred galaxy with an inner bar of size $\sim 15 - -20''$ and an outer bar which is very oval (not very strong) and very large (extending out to $\lesssim 100''$; as seen by e.g. Schinnerer et al. (2000)). The galaxy looks in this sense similar to NGC 5248 (Jogee et al., 2002). This peculiar shape makes its very difficult to decide on a mean ellipticity and PA of the outer disk from the photometry. The position of the outer ring corresponds to the downbending break at $\sim 190''$ and is therefore roughly twice the bar radius. This suggests the Type II.o-OLR classification, although the profile looks at first glance more like a Type III with a break at $\sim 100''$.

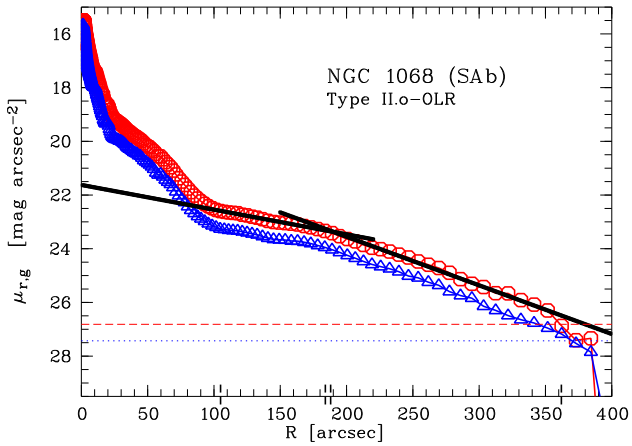

NGC 1084 : Type III
`J024559.7-073437 .SAS5. 5.1 -20.20 3.2 1299`

A large scale gradient (from top to bottom) in the background of the r' band image is removed with a linear fit. Slightly inclined galaxy sitting clearly in a more roundish outer envelope, beyond which some stream-like remnants of a possible recent interaction are visible. Small edge-on galaxy along the stream path is confirmed to be only a background galaxy. According to SDSS spectroscopy there is another object inside the disk (RA: 02 46 00.3, DEC −07 34 17) with similar velocity and associated to a visible light concentration. The peculiar shape of the outer disk region makes it very difficult to decide on a mean ellipticity and PA from the photometry. The resulting profile inside the break at $\sim 90''$ is rather curved towards the center with additional kinks ($\sim 25''$ and $\sim 50''$), so it is not clear what the galaxy might be inside the Type III envelope.

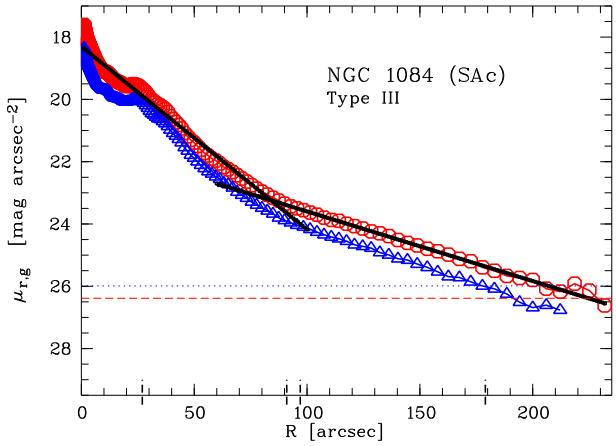

NGC 1087 : Type III
`J024625.2-002955 .SXT5. 5.3 -20.46 3.7 1443`

An apparent faint low surface brightness (center-less) structure towards the North is only scattered light from a nearby star. The galaxy center is not well defined, it shows only a small bar-like structure with a double nucleus, so we used the slightly lopsided (but symmetric) outer disk for centering, which accounts for the central drop inside $\sim 50''$ in the final profile. There is no spiral structure visible in the outer disk. The transition seems to be rather sharp, but the inner profile is almost curved, so it is not clear what its break type is inside the Type III envelope.

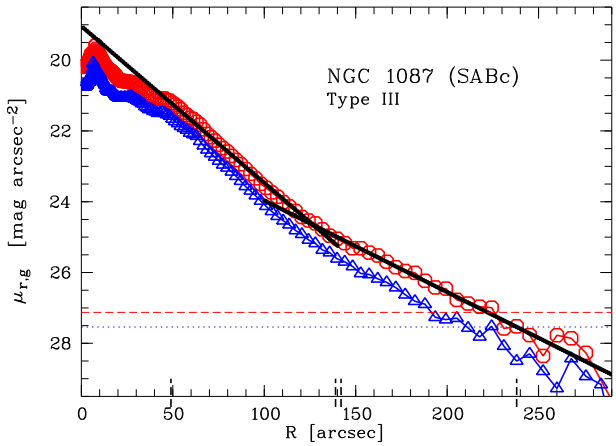

NGC 1299 : Type III
`J032009.4-061550 .SBT3? 3.2 -19.25 1.2 2197`

Galaxy is small and close to our high axis ratio limit. The background exhibits a gradient but the galaxy is small enough to avoid fitting it. SDSS spectroscopy detects an object 0.2′away from center with similar velocity. The rather symmetric outer disk shows no spiral structure but has slightly different ellipticity and PA compared to the inner part. The shoulder in the profile at $\sim 15''$is related to the inner (bar-like) region with changing PA.

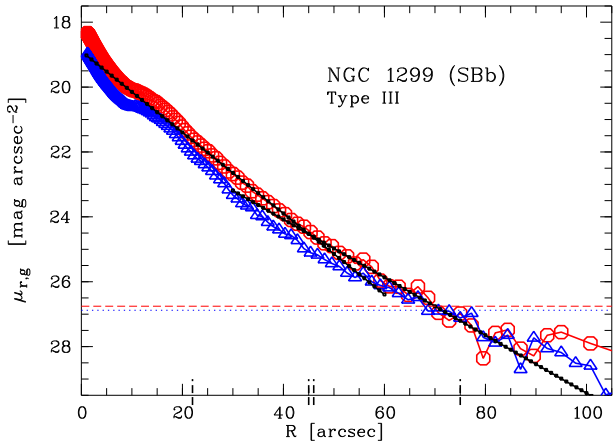

NGC 2541 : Type II-CT
`J081440.1+490341 .SAS6. 6.2 -18.50 5.8 734`

Galaxy with low surface brightness disk, having many patchy SF knots and an asymmetric (not well described with an ellipse), lopsided outer disk, which makes the chosen ellipticity and PA of the disk uncertain. The central peak is off by $\sim 8''$ compared to the outer disk where the centering is done, which causes the dip in the final profile close to the center. The downbending break at $\sim 140''$ is still inside the nearly symmetric part of the disk, thus classified as Type II-CT but this should be taken with some caution. This galaxy was classified as SB in our original LEDA catalogue but has been recently reclassified being now SAB. However, NED lists this galaxy as SA, using the RC3 classification, which is consistent with no bar being visible on the image or in the profile, so the downbending break is not a Type II.o-OLR break.

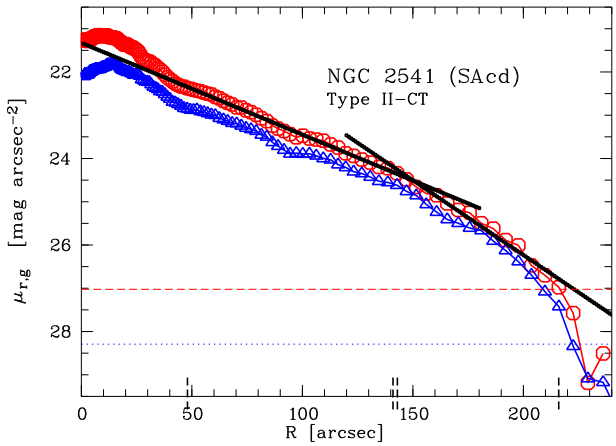

NGC 2543 : Type II.i
`J081258.0+361516 .SBS3. 3.1 -20.66 2.5 2590`

According to NED there is a dwarf elliptical galaxy (KUG 0809+363) at a similar distance. On the SDSS image (confirmed with DSS) there is an additional, low surface brightness structure visible at RA 08 13 08.5 and DEC +36 16 35, which is possibly another dwarf companion with an unknown distance. The galaxy is clearly double barred with a $R \sim 9''$ long secondary bar. Two bright, s-shaped spiral arms dominate the inner disk. The extended spiral arm towards the north-east is responsible for a slightly asymmetric outer disk. This structure makes the photometric measurement of the inclination (ellipticity) and PA very difficult. The bar and pseudo-ring build by the inner spiral arms are responsible for the prominent bump at $\sim 35''$ in the profile, followed by a dip inside, which leads to the Type II.i classification.

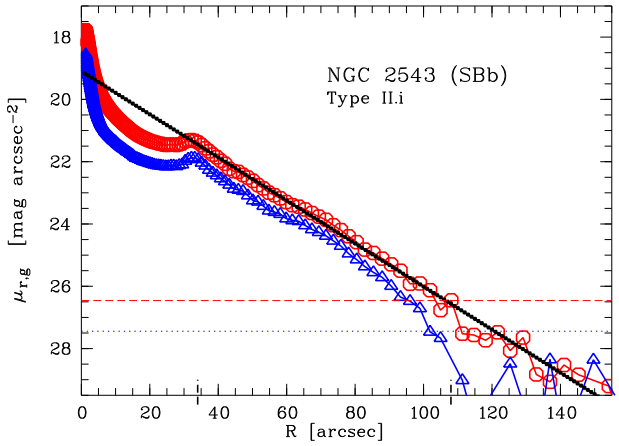

NGC 2684 : Type II-CT
`J085454.1+490937 .S?... 7.8 -19.76 1.0 3043`

The rich cluster in background, with significantly redder colour, forces a large background mask covering a small part of the galaxy. Slightly asymmetric disk with bright center and no coherent spiral arms makes ellipticity and PA uncertain. Bump at $\sim 12''$ in profile is due to an inner ring-like structure, without an associated obvious bar structure. The break at $\sim 25''$ is not related to a morphological feature in the disk and, although at about twice the ring radius, classified as Type II-CT. The upbending profile starting at $\sim 42''$ is most probably due to an improper sky subtraction caused by extended light from the background cluster.

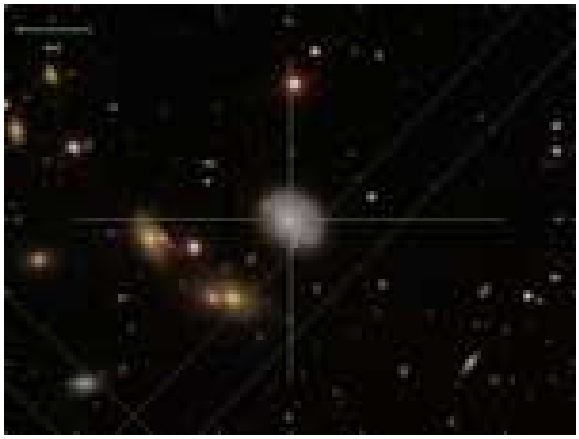

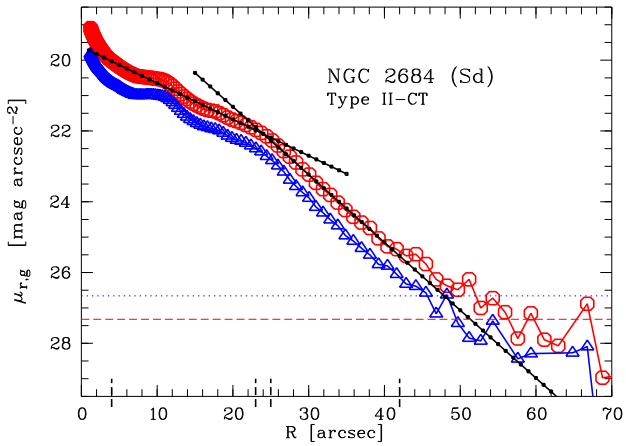

NGC 2701 : Type II-AB + III
`J085905.9+534616 .SXT5* 5.1 -20.36 2.1 2528`

According to NED there is a small companion (with similar velocity) superimposed on the galaxy disk towards the South at the end of a spiral arm which is masked here in addition to the bright star on the disk towards the West. The galaxy has a lopsided disk with the bar being offcenterd compared to the outer isophotes, where the centering is done. This is responsible for the dip in the center an possibly for the break at $\sim 42''$, which is therefore called Type II-AB. The region beyond the second break at $\sim 70''$ corresponds to some faint, almost symmetric light around the galaxy with some large extension towards north-east, adding the classification Type III. This is possibly triggered by interaction with the dwarf companion at the other side.

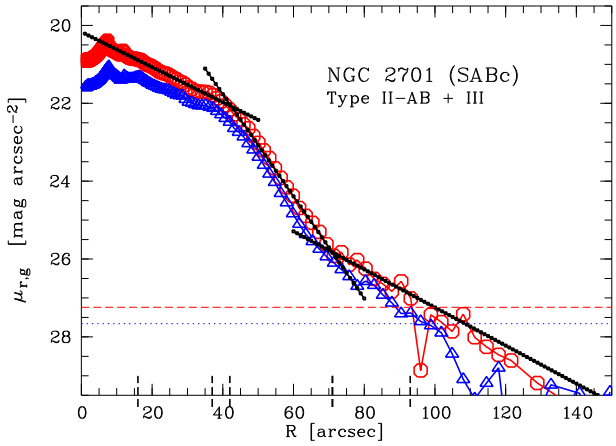

NGC 2776 : Type I
`J091214.3+445717 .SXT5. 5.1 -21.04 2.9 2796`

The galaxy is classified as SAB but a bar is not obvious on the image. The background estimate is uncertain due to a nearby (off-field), extremely bright star. For the final profile we used a round ellipticity instead of the usual value at 1σ (cf. Sect. 3.5) which gives an almost prototypical Type I profile with some minor wiggles, a bump at $\sim 25''$ due to the inner spiral arms, and some outer bumps due to some very weak spiral arm structures in the outer disk.

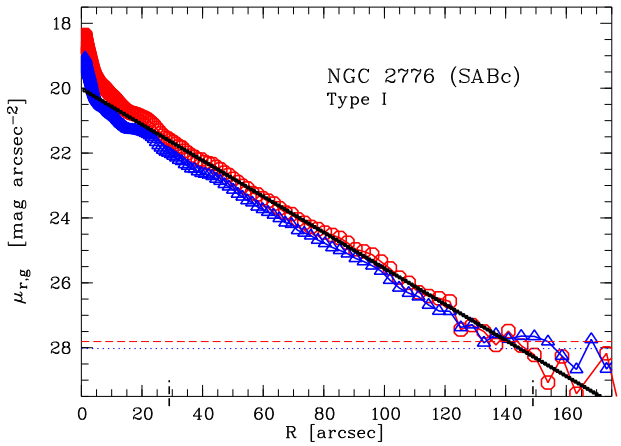

NGC 2967 : Type III-d
`J094203.3+002011 .SAS5. 4.8 -20.26 2.6 1858`

The galaxy is close to the edge of the SDSS field in an area with an increased background which is masked. Very faint, extended, but symmetric spiral arms inside the outer disk at $\sim 100''$ are visible, which do not continue inwards but start beyond the bump in the transition region at $\sim 75''$. The exact break radius is therefore uncertain.

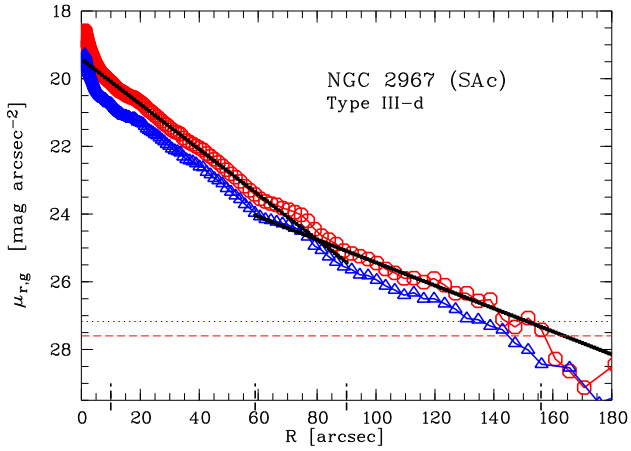

NGC 3055 : Type II.o-CT
`J095517.9+041611 .SXS5. 5.0 -19.90 2.1 1816`

Galaxy is classified as SAB and shows a narrow, thin bar, with the spiral arm structure wrapped around, which is responsible for the bump in the final profile at ∼18″. The break with a downbending profile at ∼55″ is well beyond a typical Type II.o-OLR break.

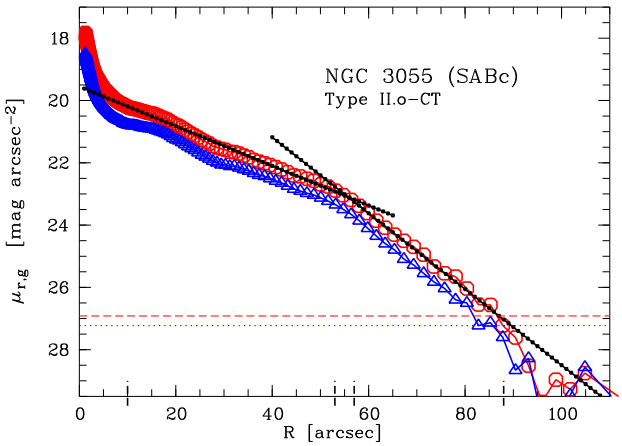

NGC 3246 : Type II-AB
`J102641.8+035143 .SX.8. 8.0 -18.91 2.2 2138`

Galaxy is selected from the NGC catalogue Tully (1988) by (Pisano & Wilcots, 1999) as being isolated. Their H I measurements show a lopsided disk which resembles the one on the present SDSS image. The central bar region is clearly offcenterd compared to the outer isophote, which is used for the centering. The downbending break in the final profile and the downbending at the very center is therefore most probably only an apparent break due to the fixed ellipse fitting. Thus the galaxy is classified as Type II-AB. The background is rather disturbed by a bright star, but the galaxy is small enough not to be significantly influenced.

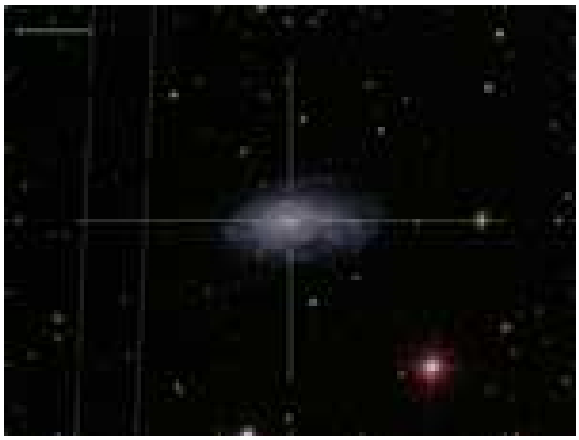

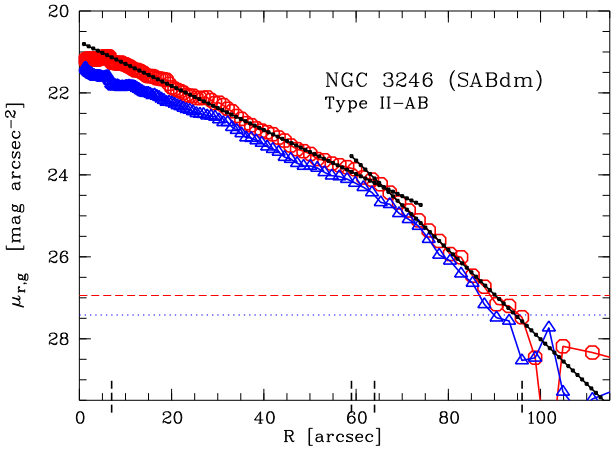

NGC 3259 : Type III-d
`J103234.8+650228 .SXT4* 4.0 -19.84 2.1 1929`

The background is rather disturbed by a bright star, but the galaxy is small enough not to be significantly influenced. Galaxy is isolated according to Prada et al. (2003), but has one SDSS-detected dwarf companion ($\sim 18.0\ g'$-mag) about $10'$away with similar velocity ($v = 1744\mathrm{km\,s^{-1}}$) and another possible, dwarf companion (or large H II region) projected on the south part of the disk (no counterpart in NED), which is partly covered by a foreground star, but also clearly present on the DSS image. The break region of the upbending profile at $\sim 55''$ is fairly extended and curved. The inner profile shows wiggles at $\sim 15''$ and $\sim 30''$, but the resolution is too low to identify a bar or ring. The spiral structure apparently extends into the outer disk well beyond the break, with two, thin symmetric spiral arms (plus more fluffy ones) starting at the defined break radius. However, it is not clear if they are really the continuation of the inner arms. The upbending characteristic is confirmed by a profile shown in Courteau (1996) (see UGC 05717).

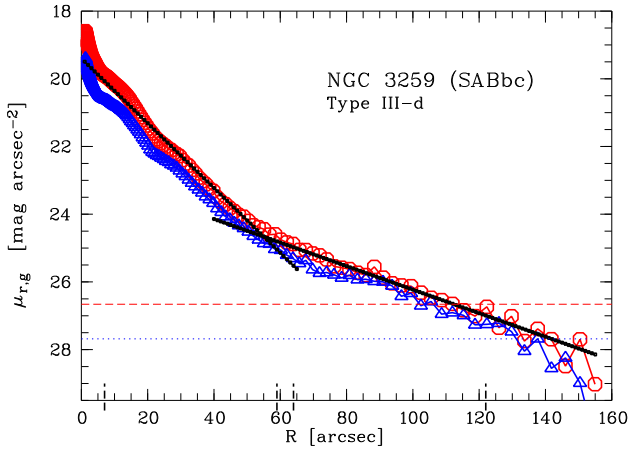

NGC 3310 : Type III
`J103845.8+533012 .SXR4P 4.0 -20.25 2.8 1208`

The galaxy is clearly disturbed with a shell-like structure in the outer disk, which is probably the result of a recent merger with a smaller galaxy (Conselice et al., 2000, cf.). The inner region is also slightly asymmetric, but still used for centering. The inner region, corresponding to a high surface brightness, tightly wound spiral, inside the break at $\sim 50''$, is curved starting at $\sim 20''$. The wiggles in the outer disk are due to the shells. An additional upbending beyond $\sim 150''$ is due to a prominent outer shell. The very outer parts are in addition influenced by an inhomogeneous sky and a large mask.

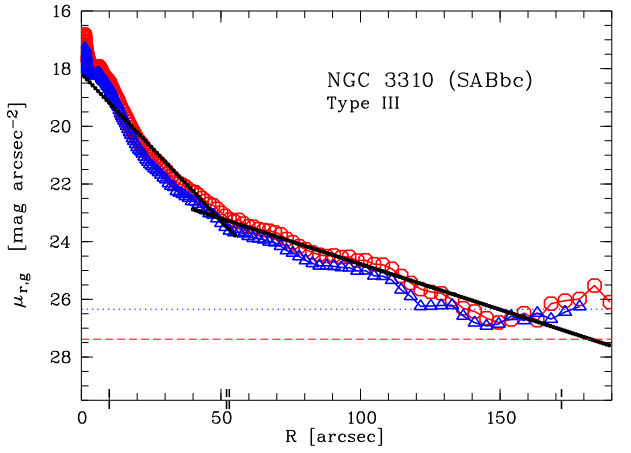

NGC 3359 : Type II-AB
`J104636.3+631328 .SBT5. 5.0 -20.42 7.2 1262`

The inner disk shows an extended bar (roughly $R \sim 45''$), which is not visible in the final profile, and two bright spiral arms. The broad extension of this arms build the outer disk, so there is no clear elliptical outer structure visible which makes the photometric inclination (ellipticity) and PA measurements highly uncertain. The outer slope is influenced by a rather uncertain sky estimate in both bands, but the apparent downbending break at $\sim 200''$is not due to a sky error, but coincides with the region where the two outer arms dominate. Thus the galaxy is classified as Type II-AB.

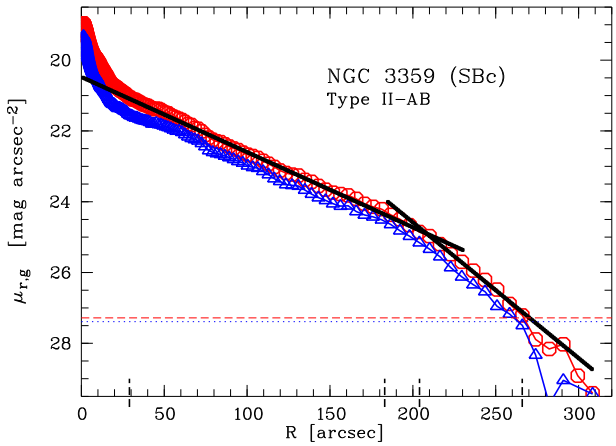

NGC 3423 : Type II-CT
`J105114.3+055024 .SAS6. 6.0 -19.54 3.9 1032`

Bulge-like inner region ($\lesssim 30''$) coincides with inner high surface brightness disk with spiral structure. Final profile is clearly downbending but the exact break radius is difficult to place due to an extended feature around $\sim 70''$ corresponding to an aligned spiral arm (with a possible straight structural element towards the north-east, called (Chernin, 1999) spiral-arm row).

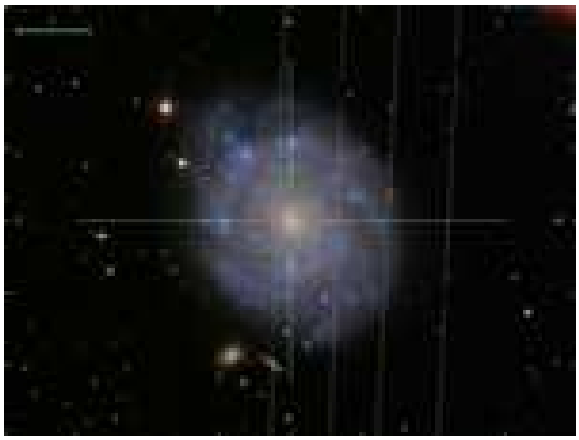

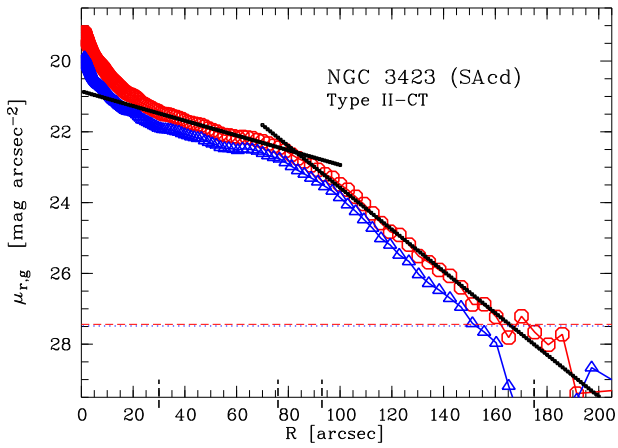

NGC 3488 : Type II.o-CT
`J110123.6+574039 .SBS5* 5.1 -18.80 1.6 3226`

Galaxy is isolated according to Prada et al. (2003). A bright star covering part of the outer disk needs an extended mask. A small bar of roughly $R \sim 6''$ size is visible as an elongated isophote on the image. The final profile is clearly downbending, but the exact break radius is difficult to place. The extended break region resembles in this case again a straight line, thus one could also define two break radii at $\sim 32''$ and $\sim 58''$. This could be caused by the extended mask, whereas the spiral structure extending to $\sim 40''$ seems not to be responsible for this behaviour. The bar is to small for its OLR to be associated with the first break, thus the galaxy is classified Type II.o-CT. The light beyond $\sim 58''$ is still symmetric and not affected by sky errors. The peak at $\sim 20''$ corresponds to the inner two arms.

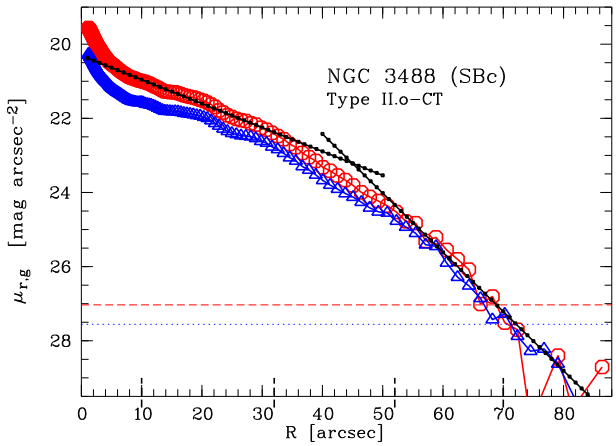

NGC 3583 : Type III-d
`J111411.0+481906 .SBS3. 3.2 -19.57 2.3 2347`

The apparent companion, a spiral galaxy (NGC 3577) towards the south-west is non-physical with $v = 5336\,\mathrm{km\,s^{-1}}$. The galaxy shows a stream-like arm extending towards the north-west outside of the galaxy connected to a small superimposed E0 satellite at 0.9′ north (not in NED). Due to this structure the outer disk seems to have a slightly different ellipticity and PA. The bump at $\sim 30''$in the final profile is due to the end of the bar and beginning of spiral arms. The inner profile with an extended wiggle at $\sim 55''$ (corresponding to the spiral arms) makes it difficult to characterise the break region (starting at $\sim 85''$ with an upbending profile) as being curved or sharp.

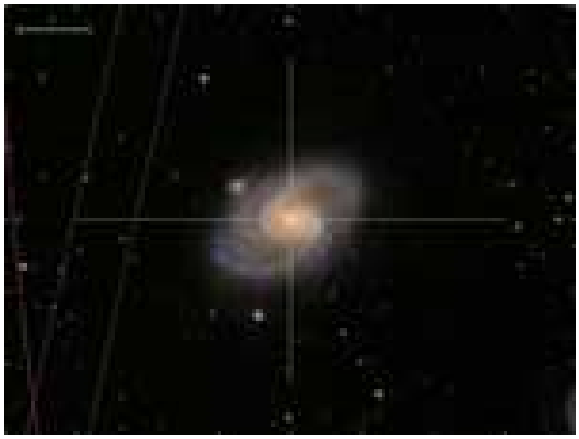

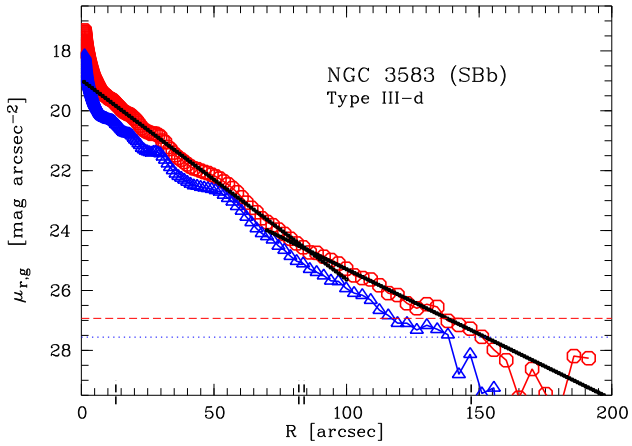

NGC 3589 : Type II-CT
`J111513.2+604201 .S..7* 7.0 -18.49 1.5 2217`

Due to the higher inclination and extended elongated structure the size of the bar is not well defined. The center is also not well defined, but centering on the outer isophote coincides roughly with the brightest pixel. The sky estimate is rather uncertain due to the bright star in the FOV. The final profile shows a downbending break at $\sim 40''$, classified as Type II-CT but also consistent with being Type II.o-OLR allowing the bar to be of size $\sim 20''$ which is consistent with the image. The small bump $\sim 22''$ in the profile just corresponds to some aligned H II regions.

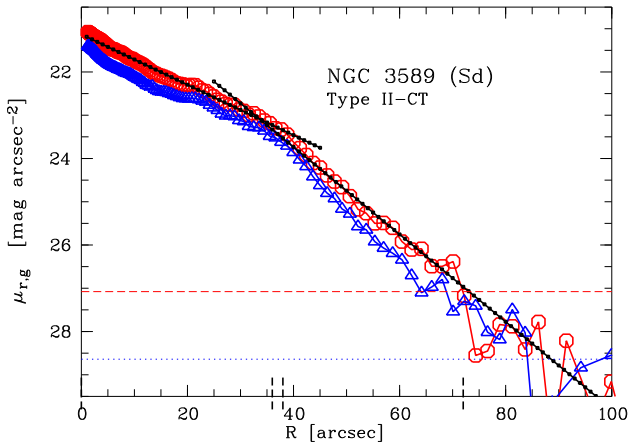

NGC 3631 : Type I
`J112102.4+531008 .SAS5. 5.1 -20.62 4.9 1388`

The galaxy forms a nearby group together with NGC 3178, NGC 3898, NGC 3953 and NGC 3992 (also part of our sample) in the Ursa Major cluster and shows plenty of substructure. It has two prominent spiral arms with different pitch angles, one of them turns nearly straight, classified by Arp (1966) as a spiral galaxy with one heavy arm. In addition, it has a faint extended spiral arm (or maybe stream-like structure) in the far outer disk towards North, therefore the outer disk is slightly asymmetric and the mean ellipticity and PA are difficult to fix. There is an extended light patch on the image visible towards south-west. Although there is no bright star nearby which could create such an artefact it is unlikely a dwarf companion, since it is not visible on the DSS. The final radial light profile is quite unusual and cumbersome to classify, since it exhibits an extended bump between $\sim 50-140''$, which corresponds to the begin of the two spirals to the end of the inner (undisturbed) disk. Beyond $\sim 140''$ the extended, slightly offcenterd outer disk with the spiral arm structure (or stream) starts. If we do not exclude the bump from the fit, one can argue for a downbending break at $\sim 75''$, or a Type I profile with an extreme wiggle (this would be a Type II.i if the galaxy would be barred). We decided to exclude the bump and the inner region from the fit ($R \gtrsim 140''$) which gives also a Type I profile where the region around $\sim 35''$ is also roughly fitted. Due to this problems the classification should be taken with caution.

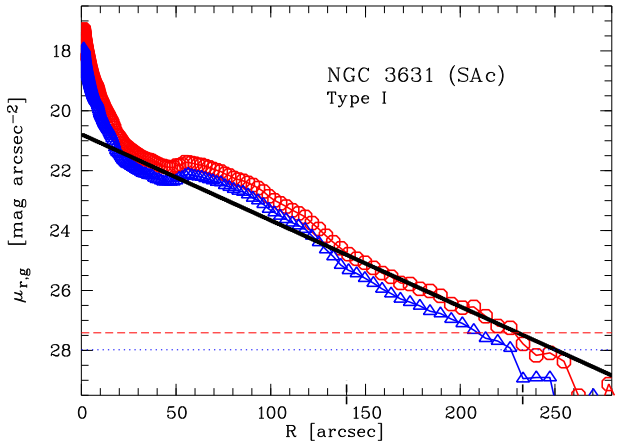

NGC 3642 : Type III-d
`J112218.0+590427 .SAR4* 4.0 -20.60 5.5 1831`

The background is slightly inhomogeneous and the galaxy is rather extended. From the nearly round inner disk a single, star forming, spiral arm starts towards the outer disk with slightly more than one revolution, forming the strongly asymmetric, lopsided outer disk. Therefore the ellipticity and PA is determined further inside. The final profile looks fairly curved and with extended wiggles in the outer disk at $\sim 100''$ and $\sim 155''$due to the outer spiral arm passing the ellipse. There is a steeper inner exponential part visible between $\sim 25-75''$ followed outwards by an upbending profile, which is roughly at the position where the extended spiral arm starts to unwrap, which leads to the Type III classification. Inwards of $\sim 25''$ there is again another steeper exponential part visible together with a possible bulge component.

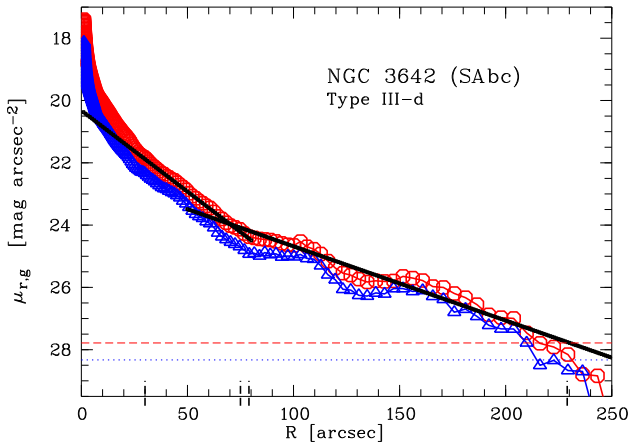

NGC 3756 : Type II.o-CT
`J113648.3+541737 .SXT4. 4.3 -19.89 3.8 1525`

Only partly fitted since $\lesssim 1/4$ of galaxy is beyond field. Known three armed spiral galaxy which shows one wide spiral arm starting at $\sim 60''$ extending roughly towards the downbending break at $\sim 100''$. The extended bump $\sim 45''$ is due to the three inner tightly wound spiral arms and makes it, similar to NGC 3631, difficult to fit the inner region. However, since the bump is less strong we decided to include it. The galaxy is classified as SAB (RC3) but the bar is not obvious on the image and its maximum size would be $R \lesssim 25''$ thus the break is well outside the range for typical Type II.o-OLR breaks and is classified as Type II.o-CT.

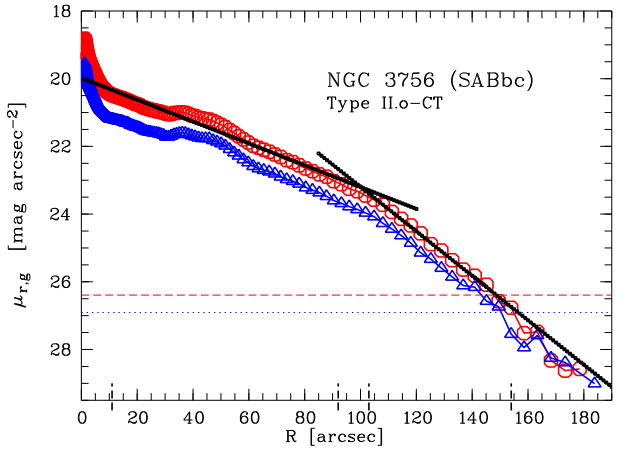

NGC 3888 : Type I
`J114734.7+555800 .SXT5. 5.3 -20.43 1.8 2648`

The background on the image shows a large gradient due to a bright star off the field, but the galaxy is small enough to be not affected. The galaxy has one 'malformed' (kinked) spiral arm across the disk. There is a possible dwarf, irregular companion visible towards the south-west, but without any distance information. The final profile exhibits an extended wiggle (with an unusual integral sign shape) at $\sim 33''$, looking like two shifted exponential regions, but there is no point in placing a break there. The peak at $\sim 22''$ is related to an aligned spiral arm, whereas the peak at $\sim 12''$ could be due to the end of a possible bar or inner ring (no obvious on the image). Therefore the galaxy is classified as Type I and not as Type II.i, although the dip in the profile is clearly visible. It could be explained by dust lanes close to the center, which also explains the dip being more prominent in the g' band.

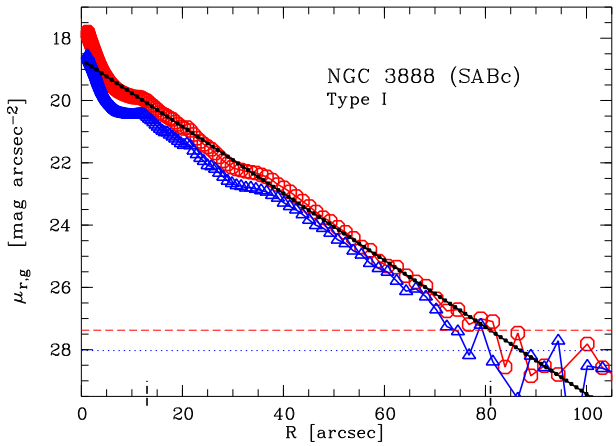

NGC 3893 : Type III-d
`J114838.4+484234 .SXT5* 4.8 -20.33 4.1 1193`

The background around the galaxy is affected by a nearby, bright star and a close (3.7′away, with similar velocity $v = 905\,\mathrm{km\,s^{-1}}$, SB0/a:pec), smaller, companion galaxy (NGC 3896), both members of the Ursa Major Cluster. Galaxy exhibits a wide, extended spiral arm like structure towards the east, which could also be a stream or tidal feature. Due to this structure it is not possible to derive the ellipticity and PA from the outer disk, so their values are more uncertain. The final profile clearly shows an Type III upbending profile starting at $\sim 150''$ corresponding to the beginning of the extended structure to one side and some more symmetric faint light on the other side. The inner disk shows a prominent wiggle $\sim 90''$ which is associated to a pseudoring of wrapped spiral arms.

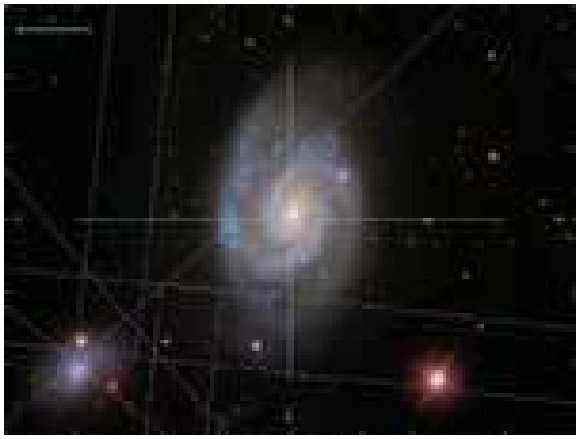

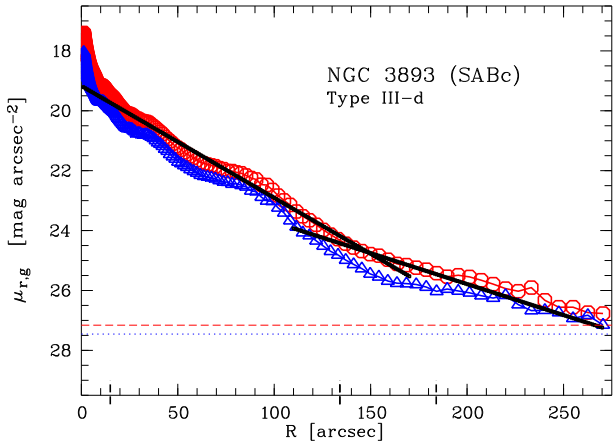

NGC 3982 : Type III
`J115628.3+550729 .SXR3* 3.2 -19.54 2.3 1351`

Close to Ursa Major Cluster but membership questionable (Tully et al., 1996). Galaxy exhibits a detached, narrow, star-forming spiral arm embedded into the very outer, symmetric disk towards south-west. The final profile beyond the central part is smooth and straight down to $\sim 55''$ where it clearly starts upbending, classified as Type III, which is consistent with the profile by (Tully et al., 1996). The break corresponds to the end of the inner disk, excluding the faint outer arm, which produces the bump at $\sim 75''$ (more pronounced in the g' band). The transition zone is rather sharp. Dip-peak structure between $\sim 5-12''$ corresponds to the inner bar/ring region. The exact size of the bar is not well determined on the SDSS image. Erwin (2005), using HST images, gives $5''$and classifies the galaxy therefore as Type II.o-OLR + III (with an 'extreme' OLR break). We exclude the inner $R \lesssim 13''$ from our fit and leave it with a Type III classification.

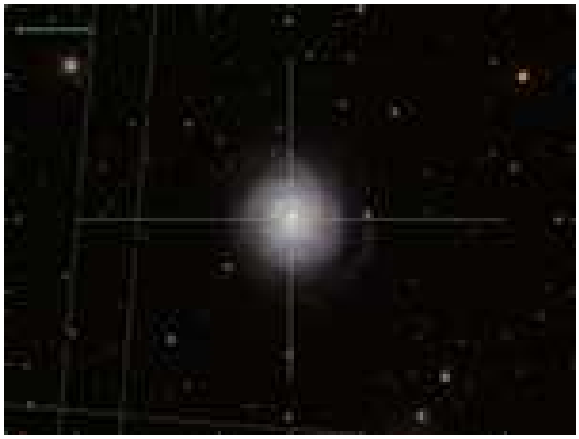

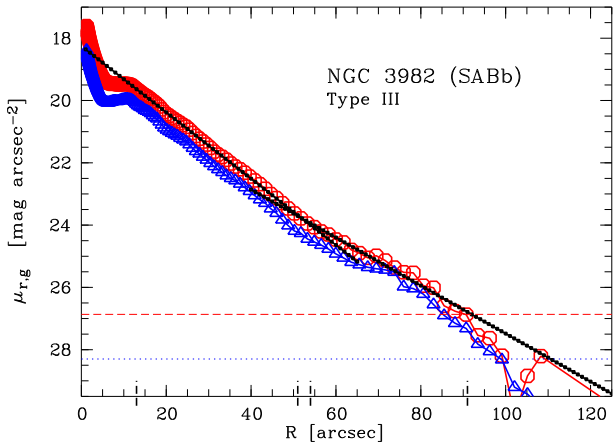

NGC 3992 ≡ M 109: Type II.o-OLR
`J115735.9+532235 .SBT4. 3.8 -20.98 6.9 1286`

Large galaxy with a small part off the SDSS field. Member of Ursa Major Cluster (Tully et al., 1996). Embedded in the large bar of size roughly $R \sim 70''$ (as measured on the image) is possibly a secondary bar half the size. Unusual very faint extension visible in both bands (more pronounced in g' band) towards north-east, which is possibly but unlikely stray-light from a nearby bright, red star. The one-sigma ellipse is therefore not representative so the mean ellipticity and PA are determined further inside. Final profile shows a clear downbending break at $\sim 140''$at about twice the bar radius corresponding roughly to a pseudoring of the spiral arms, therefore classified as Type II.o-OLR. Bump at $\sim 200''$ does not coincide with a spiral arm.

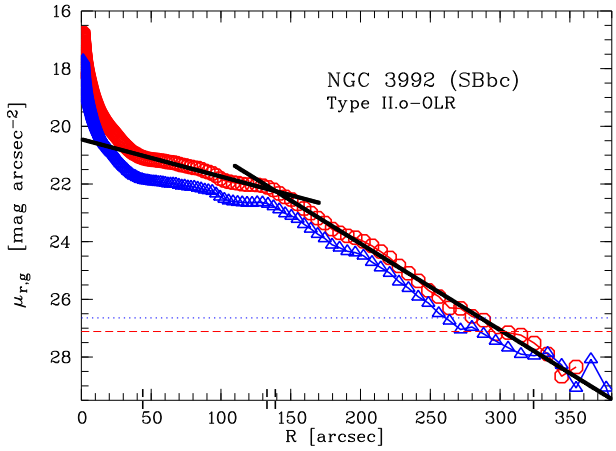

NGC 4030 : Type III
`J120023.4-010603 .SAS4. 4.1 -20.27 3.9 1476`

Two superimposed bright stars are masked. According to Zaritsky et al. (1993) it is an isolated galaxy with a satellite system (largest UGC 06970, SB(s)m, with $M_{\rm abs} = -17.7$). The galaxy shows two prominent spiral arms beyond a more flocculent center starting at $\sim 30''$, followed by a single arm extending slightly further out towards south-west. Final profile shows a Type III break at $\sim 150''$ where the transition zone is rather sharp, followed by a fairly symmetric outer region without spiral structure. The bump at $\sim 80''$ corresponds to the end of inner spiral arms.

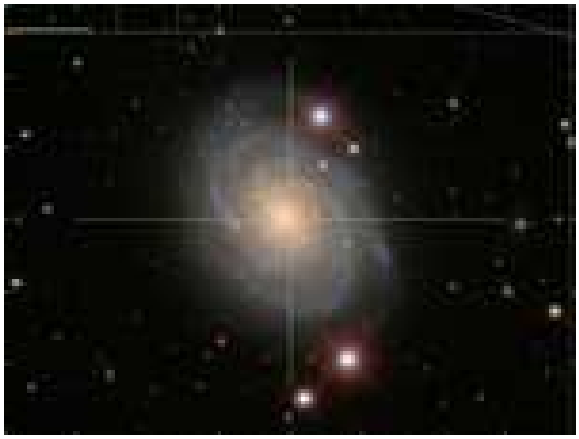

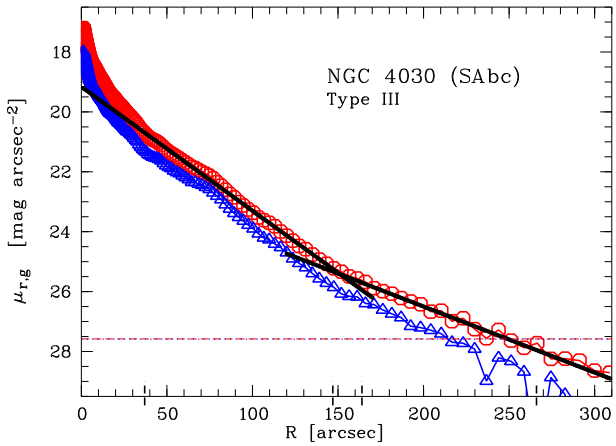

NGC 4041 : Type III-d
`J120212.2+620814 .SAT4* 4.3 -19.92 2.7 1486`

According to Sandage & Bedke (1994) this galaxy forms a kinematic triplet with NGC 4036 and UGC 7009 and is probably member of the Ursa Major Cluster. However, Tully et al. (1996) does not list any of these as members. Galaxy shows a detached, extended, star-forming spiral arm structure in the outer, asymmetric disk, similar to NGC 2967, but smaller and only one-sided, which makes the photometric inclination (ellipticity) and PA uncertain. In the final profile the disk inside the Type III break at $\sim 75''$ corresponds roughly to the region with the spiral arms, which are also responsible for the extended bump between $\sim 30 - 75''$ (more pronounced in g' band). The very inner region looks bar-like, but is probably only the spiral structure continuing into the center.

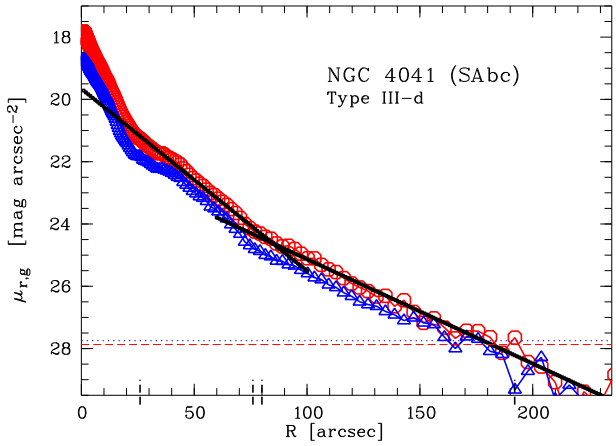

NGC 4102 : Type II.o-OLR + III
`J120623.1+524239 .SXS3$ 3.0 -19.38 3.1 1082`

Galaxy belongs to the Ursa Major Cluster Tully et al. (1996). On the image an elongated inner bar region inside a star-forming ring is visible which is responsible for the dip and bump structure between $\sim 25-35''$ in the final profile. Erwin (2005) measures the size of the bar to $\sim 15''$ and the outer ring to $\sim 35''$, so the apparent break at $\gtrsim 40''$ (although measured from outside, it starts only at $\sim 58''$) is classified as a Type II.o-OLR. The apparent upbending at $\sim 120''$ is unlikely a sky error, visible around the whole galaxy and confirmed by the profile in Courteau (1996) (see UGC 07096) and also visible in Erwin et al. (2006). This adds the Type III classification.

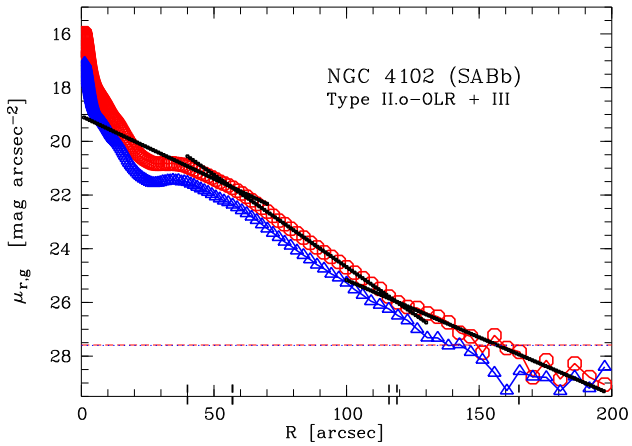

NGC 4108 : Type II-AB
`J120644.0+670944 PSA.5* 5.0 -20.13 1.7 2828`

Galaxy in a triple system with NGC 4108A (v = 2256km s^{-1}) and NGC 4108B (v = 2673km s^{-1}), the latter is also part of the present sample. According to Nordgren et al. (1997) NGC 4108 and NGC 4108B appear to be possibly joined by an H I bridge. Very inner center $\lesssim 5''$ looks like small bar, or the spiral structure starts from the very center. The outer disk is asymmetric with one side rather sharp and the other more shallow with indication for a single spiral arm. The disk is lopsided, so the outer contour is used for centering (center $\sim 4''$ off the brightest pixel, causing the central dip in the profile), which implies that the photometric inclination (ellipticity) and PA are not well defined. The apparent break at $\sim 44''$ is related to the transition between the symmetric outer disk going inwards to the offcenterd inner disk and therefore most probably not intrinsic but a Type II-AB break.

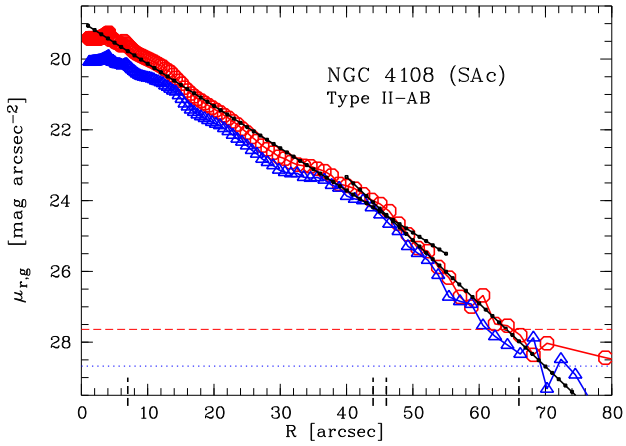

NGC 4108B : Type I
`J120711.3+671410 .SXS7P 7.0 -18.46 1.3 2840`

Companion to NGC 4108 (see above). Galaxy exhibits an offcentered bar ($\sim 5''$ off compared to the center derived from the outer isophote). Very outer disk slightly asymmetric towards north-east (outer spiral arm?). In the final profile the central dip and inner wiggle are due to the the offcentered bar, the peak at $\sim 22''$ corresponds to an aligned spiral arm-like region. Although a downbending break at $\sim 32''$ with low scalelength contrast is possible, Type II-AB, the galaxy is consistent and classified as Type I due to the wiggles in the center.

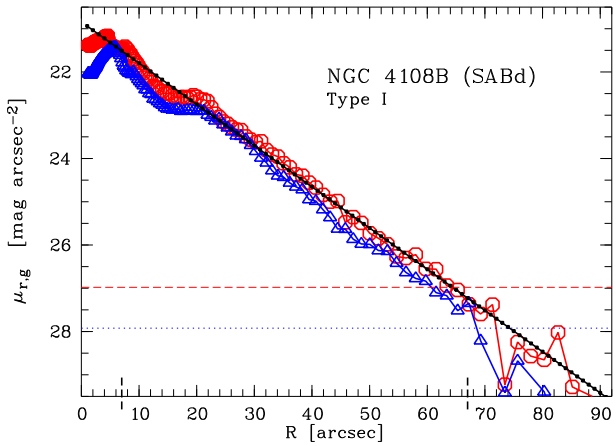

NGC 4123 : Type I
`J120811.1+025242 .SBR5. 4.8 -19.55 4.1 1364`

Galaxy with extended bar ($R \sim 55''$) studied in detail by Weiner et al. (2001) using a surface brightness profile which is consistent with the SDSS one. The outer disk is slightly asymmetric, more rectangular than elliptical, with an extended starforming spiral arm structure towards south-west, which makes the photometric inclination (ellipticity) and PA uncertain. The final profile exhibits extended wiggles. The bar and associated spiral arms are visible between $\sim 30-110''$ and the bump at $\sim 170''$ corresponds to a starforming outer spiral arm. Although being far from a prototypical Type I we used this classification, since the profile shows too many changes to reasonably argue for any other type.

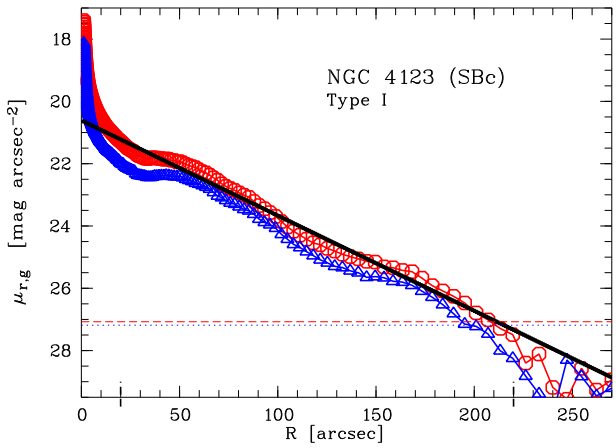

NGC 4210 : Type II.o-OLR + II.o-CT
`J121515.9+655908 .SBR3. 3.0 -19.89 2.0 3000`

Companion galaxy (CGCG 315-030, $m = 15.5$) 13′away with similar velocity ($v = 2679\,\mathrm{km\,s^{-1}}$). Gradient in the background due to a very bright star (off field), but galaxy small enough to be not significantly influenced. The final profile shows an inner bump at ∼ 15″ corresponding to a pseudoring of wrapped spiral arms (slightly further out than the bar). The apparent dip ∼ 8″ is due to the bar orientation being perpendicular to the major axis of the galaxy. Similar to NGC 3488 the profile shows a clear downbending. However, the break radius is uncertain due to the extended break region, which resembles in this case again a straight line. Thus one could also define two break radii at ∼ 33″, corresponding roughly to end of inner spiral arm structure, and ∼55″, not related to sky errors and symmetric around the disk. In contrast to NGC 3488 the bar is here large enough to argue for a combination of a Type II.o-OLR and a Type II.o-CT break, this should be confirmed with a more detailed study on the bar size of NGC 4210.

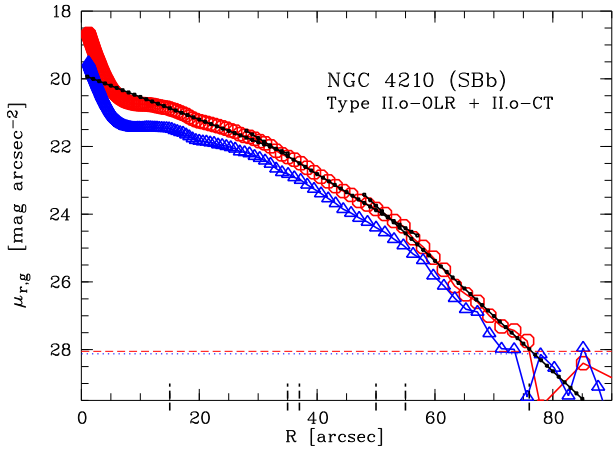

NGC 4273 : Type II-AB + III
`J121956.2+052036 .SBS5. 5.1 -20.41 2.1 2435`

Galaxy in south-western corner of the Virgo Cluster with three similar sized neighbours, NGC 4268, NGC 4281, and closest and slightly overlapping at the very outer disk NGC 4277. The disk is lopsided with one side sharp edged and the other side with a wide spiral arm feature towards south-east (embedded in the outer disk), similar to NGC 4108. Centering on the outer disk causes the dip at ∼ 10″ and hides the very bright nucleus sitting in a bar-like structure which is offcentered by ∼ 16″. The break at ∼45″ in the final profile is clearly related to the lopsided disk and therefore classified as Type II-AB. In addition, there is an Type III break with an upbending profile visible beyond ∼80″ due to the influence of the companion (possibly intrinsic and not just projected).

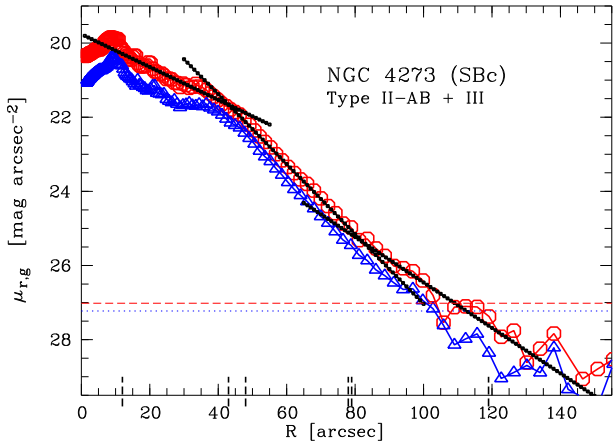

NGC 4480 : Type II.o-CT
`J123026.8+041447 .SXS5. 5.1 -20.14 2.1 2494`

The galaxy is small, rather inclined, and classified as SAB with bar size of roughly $R \sim 10''$ (measured from the image). The final profile shows a clear downbending break at $\sim 55''$, significantly further out compared to a typical Type II.o-OLR break thus classified as Type II.o-CT, corresponding roughly to the end of the spiral arms. The inner profile exhibits an extended bump at $\sim 35''$ (more pronounced in the g' and less in the i' band) most probably related to the star formation in the spiral arms and not to a possible Type II.o-OLR + II.o-CT as for NGC 4210, which shows the same structure in both bands.

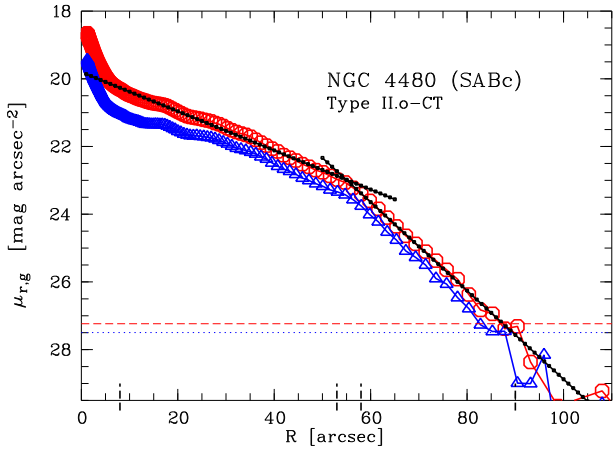

NGC 4517A : Type II.o-CT + II.o-AB
`J123228.1+002325 .SBT8* 7.9 -19.18 3.8 1562`

This low surface brightness galaxy has an elongated, barred center, of size $R \sim 30''$, with a foreground star very close and a slightly asymmetric, lopsided outer disk. The final profile exhibits a sharp break at $\sim 150''$due to the asymmetric outer disk, which is not well described with the mean ellipticity and PA used, thus classified as Type II-AB. There is an additional feature (bump or break) visible around $\sim 80''$, which is not obviously related to an aligned spiral arm and could be explained by a weak downbending break. Since the bar appears to be only weak and the break at more than twice the bar radius it is classified as Type II.o-CT, which should be taken with caution.

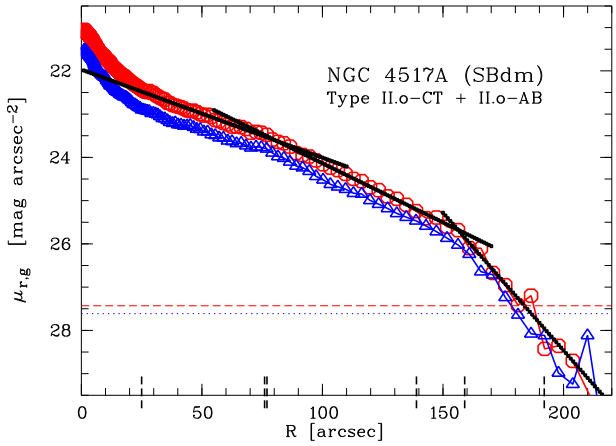

NGC 4545 : Type II.o-CT
`J123434.2+633130 .SBS6* 5.9 -20.49 2.5 3000`

Small galaxy with an s-shaped inner region of size ∼ 12″ (associated to be the bar) leading to two (or three) tightly wrapped, spiral arms. Final profile exhibits a break at ∼58″, being too far out for a typical Type II.o-OLR thus classified as Type II.o-CT. The dip at ∼ 8″ corresponds to the region where the spiral arms start from the bar-structure which is nearly perpendicular to the ellipse major axis.

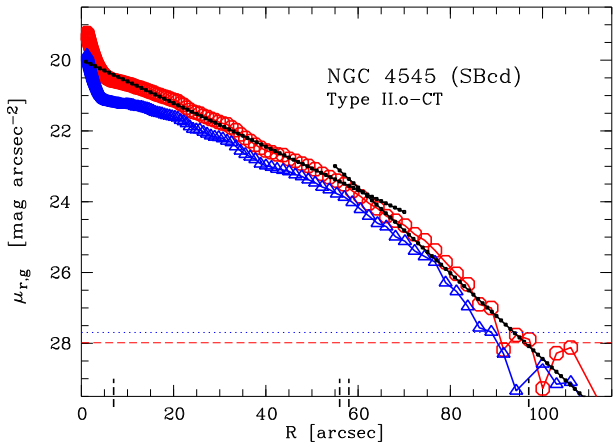

NGC 4653 : Type II-AB
`J124350.9-003341 .SXT6. 6.1 -20.37 3.0 2658`

Paired galaxy with NGC 4642 (v = 2471km s^{-1}, ∼ 10′ away) while apparent dwarf companion on the image towards south-east is a confirmed background galaxy (v = 7843km s^{-1}). Extended mask used to avoid straylight by bright stars. Mean ellipticity and PA difficult to determine, since it is different for the inner disk (used for centering) with two, very regular spiral arms inside ≲30″, compared to the outer disk with more frayed spiral fragments, starting to be asymmetric on larger scales at ≲80″ (mainly towards south-west). This asymmetry causes also the apparent break at ∼105″ thus the galaxy is classified as Type II-AB.

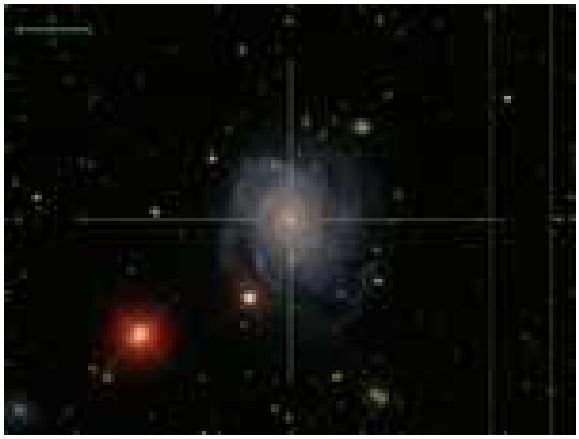

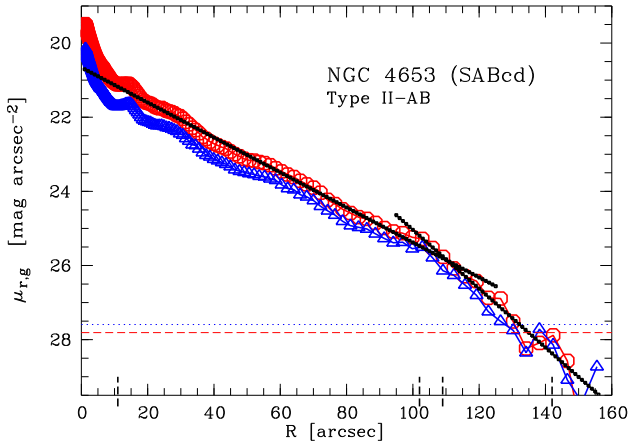

NGC 4668 : Type III
`J124532.0-003209 .SBS7* 7.1 -18.88 1.5 1654`

Small galaxy close to our high axis ratio limit, which forms a close pair with NGC 4666 (v = 1474km s^{-1}) about 7′ away and also has a wider association with NGC 4632 (v = 1557km s^{-1}) according to Sandage & Bedke (1994). The final profile exhibits a break at ∼ 70″ followed by an upbending profile corresponding to a slightly asymmetric, faint outer disk and although close to, most probably not related to a sky error, thus classified as Type III. The full extend of the bar is uncertain, although the bump around ∼ 20″ is certainly related to the bar and a possible spiral arm. The whole inner region is included in the inner disk fit.

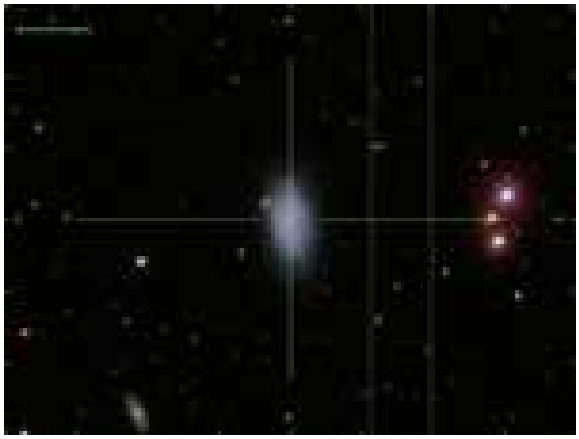

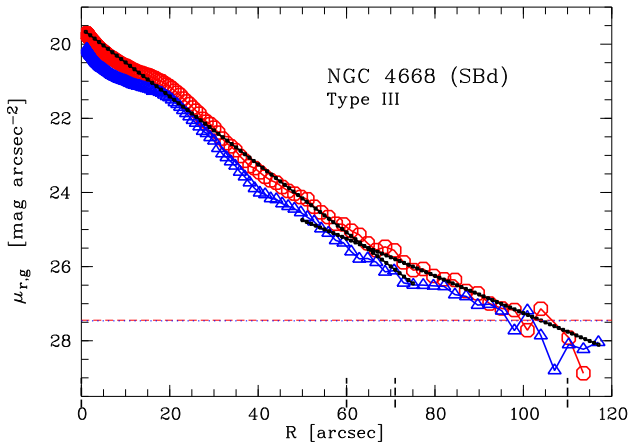

NGC 4904 : Type II.o-OLR + III
`J130058.6-000138 .SBS6. 5.7 -18.69 2.1 1213`

Only partly fitted since $\lesssim 1/5$ of galaxy is beyond field. The galaxy has a dominating, thick bar of size $R \gtrsim 20''$whereas the center along the bar is not well defined (centering on brightest pixel). It has an unusual spiral arm structure with one extending nearly straight towards south-west forming more droplet shaped isophotes. The image shows indication for an additional, extremely faint, extended patch of light outside the disk towards south-west. Final profile shows a clear downbending break at ∼ 40″, associated on one side with a ring-like structure which is about twice the bar radius, thus classified as Type II.o-OLR. The apparent upbending at ∼ 90″ is almost certainly produced by the additional patch of light unrelated to any artificial source, thus adding the Type III classification.

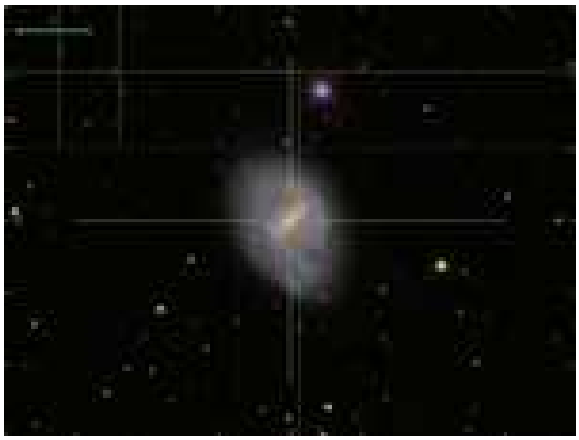

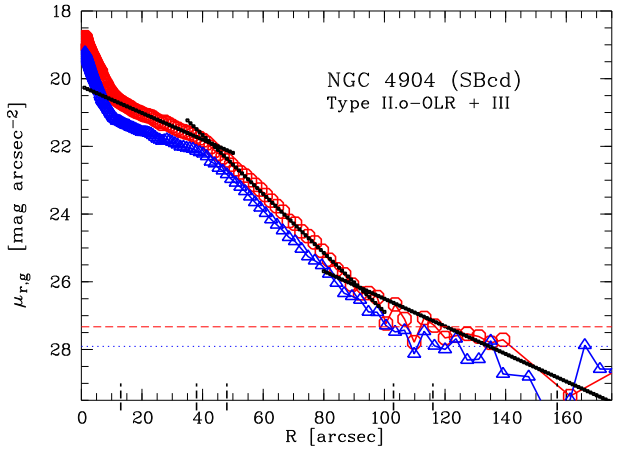

NGC 5147 : Type II.o-OLR + III
`J132619.2+020604 .SBS8. 7.9 -18.77 1.8 1154`

The medium-sized star superimposed on the galaxy close to its center is masked. The bar size is uncertain but could be associated to an elliptical region of size $R \lesssim 15''$ on the image not reflected in the final profile. The extended bump between $\sim 25 - 45''$ is associated to the inner disk containing the spiral arms with some ring-like, distributed SF regions. Excluding the full region allows for a crude Type I classification. However, using a break at $\sim 30''$ (about twice the bar radius thus classified as Type II.o-OLR) followed by a downbending profile with another break at $\sim 75''$ leading to an upbending profile (therefore classified as Type III) seems more reasonable, even so the upbending is very close to our detection limit. The disk beyond the ring-like structure is slightly asymmetric with a single, wide, and faint spiral arm-like structure towards north-east just inside the outer break. The outermost isophote is again nearly round and symmetric.

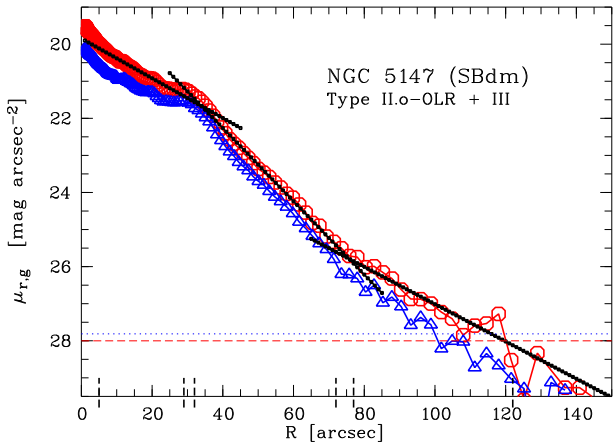

NGC 5300 : Type II.o-CT
`J134816.1+035703 .SXR5. 5.0 -18.93 3.5 1246`

Galaxy close to border of SDSS field but almost complete. The size of the weak bar is about $R \sim 12''$ (measured from the image). The final profile shows the prototypical Type II.o-CT behaviour. A sharp break at $\sim 85''$ followed by a downbending profile. The break is way to far out for a normal Type II.o-OLR break given the small bar size, and corresponds roughly to the end of the visible spiral arm structure.

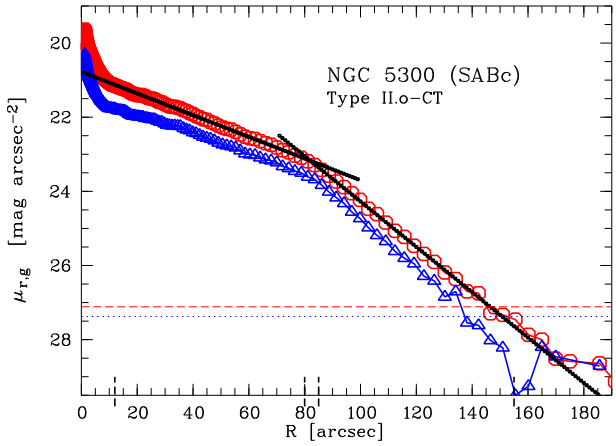

NGC 5334 : Type II.o-CT
`J135254.4-010651 .SBT5* 5.0 -19.22 3.9 1433`

Galaxy has a bar with a visible dust lane of size $R \lesssim 20''$as measured from the image. The final profile is clearly downbending, but the exact position of the break is difficult to place. The extended break region resembles in this case again a straight line, so that one could also define two break radii at $\sim 85''$ and $\sim 125''$. However, since the first one is not even close to twice the bar radius and no other particular feature is responsible for the second break, the galaxy is classified Type II.o-CT with a single break at $\gtrsim 90''$.

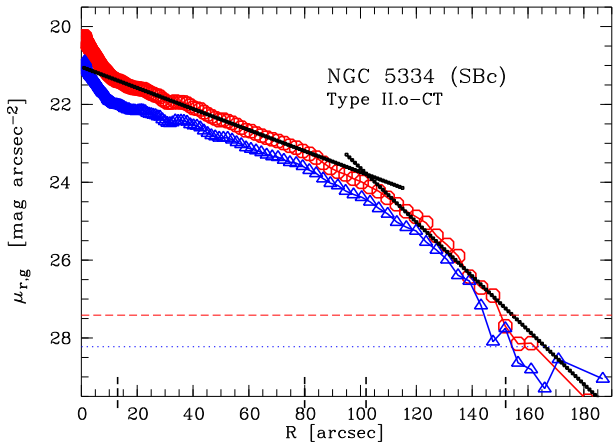

NGC 5376 : Type II.o-OLR
`J135516.1+593024 .SXR3$ 3.0 -20.00 2.1 2293`

Galaxy close to the border of the SDSS field but almost complete. It has a known, similar-sized companion (UGC 08859, $v = 1610\,\mathrm{km\,s^{-1}}$) about 7.4′ away and there is another possible, much fainter dwarf companion (3.5′ away towards north-west) visible on the image. The final profile shows a weak break at $\sim 35''$ coinciding with the end of some very faint spiral arms. The dip at $\sim 14''$and the peak at $\sim 18''$ are related to a pseudoring structure (mentioned also in RC1) around a possible bar. Although the exact size of the bar is difficult to fix, assuming it is there, the break is close to twice the inner ring radius and therefore classified as Type II.o-OLR.

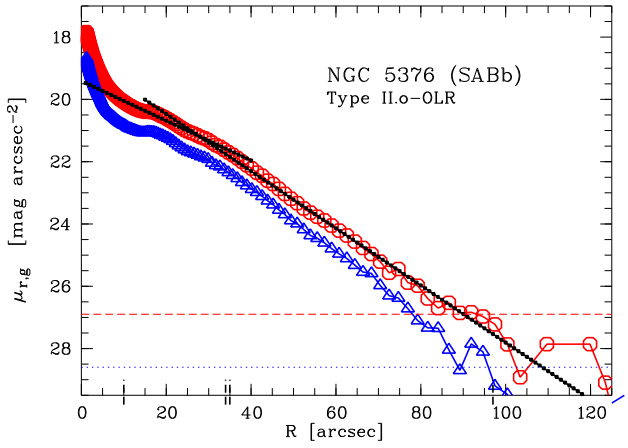

NGC 5430 : Type II.o-OLR
`J140045.8+591943 .SBS3. 3.1 -20.86 2.2 3238`

Galaxy is isolated according to Prada et al. (2003). The center is dominated by a strong bar with dustlanes of size $R \sim 35''$, followed by two wrapped spiral arms. The very center is slightly elongated, looking twofold (effect of dust lane?), thus the centering is uncertain. The extended bump at $\sim 45''$ in the final profile is associated with the wrapped spiral arms. We have included the bump and bar for fitting the inner scalelength, because it does not change the result much. It is in principle possible to fit the full profile with a single exponential (Type I), allowing for this extended bump. However, we chose to fit a break at $\sim 70''$. This reduces the deviation from the model and since it is about twice the bar radius the galaxy is classified as Type II.o-OLR.

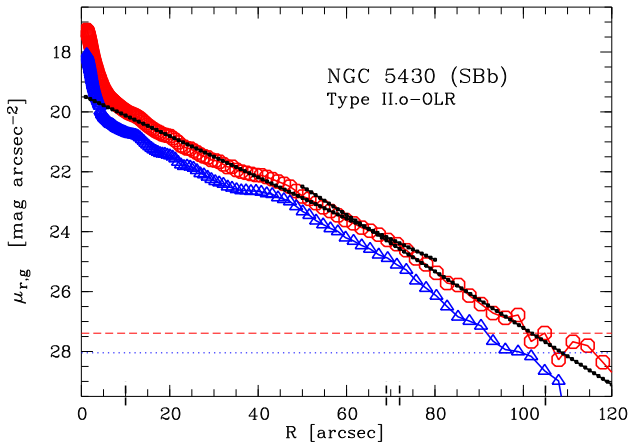

NGC 5480 : Type III-d
`J140621.5+504332 .SAS5* 5.0 -19.72 1.7 2119`

A large scale gradient (from top to bottom) in the background of the r' band image is removed with a linear fit. Galaxy forms a close pair with NGC 5481 ($v = 2143$km s^{-1}) only 3.1′ away with the very outer isophotes starting to overlap. Galaxy appears to consist of two regions. An inner disk with the bright center and the spiral arms of size $R \sim 40''$with a common ellipticity and PA, sitting in a more diffuse outer disk having a different ellipticity and a nearly orthogonal PA. The systems looks like an extended bar in an underlying disk, similar to NGC 1068 and the photometric inclination (ellipticity) and PA is difficult to determine and therefore uncertain. The final profile exhibits a break with an upbending profile at $R \sim 75''$, thus classified as Type III, which is consistent with the profile shown by Courteau (1996) (cf. UGC 09026). Between the inner disk and the break there is indication for two symmetric, thick spiral arms emerging from the inner bar-like disk.

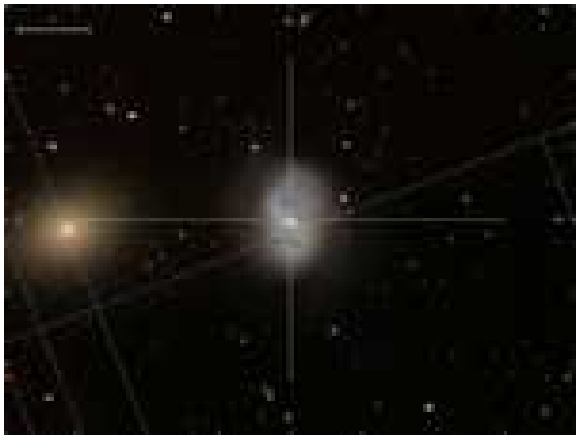

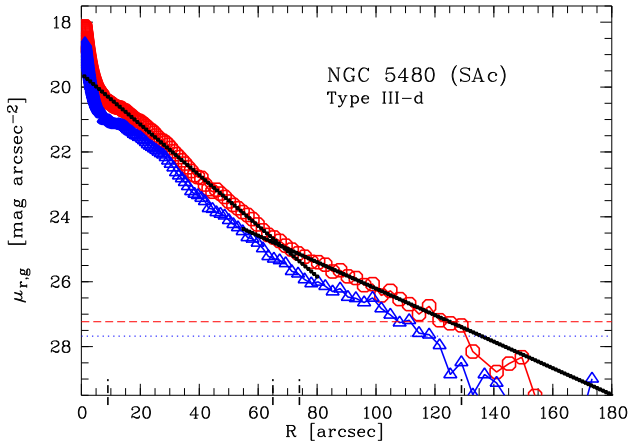

NGC 5584 : Type II.o-CT
`J142223.8-002315 .SXT6. 6.1 -19.80 3.2 1702`

Bright foreground star nearby but the influence is small. Two additional brighter stars in the outer disk force extended masking. The inner disk is dominated by two prominent spiral arms plus some more asymmetric ones with many star-forming patches. The galaxy is classified as SAB, but the bar size ($R \sim 10''$) is difficult to determine, since the spiral arms seem to continue towards the center. Similar to NGC 3488 the profile shows a clear downbending, however, with uncertain break radius due to the extended break region which resembles in this case again a nearly straight line, so that one could also define two break radii at $\sim 60''$ and $\sim 110''$. Since the bar is too small to be responsible for the inner break we use a single break at $\sim 90''$ enclosing roughly the inner spiral structure followed by a slightly asymmetric outer disk (one side with a clearly more diffuse appearance).

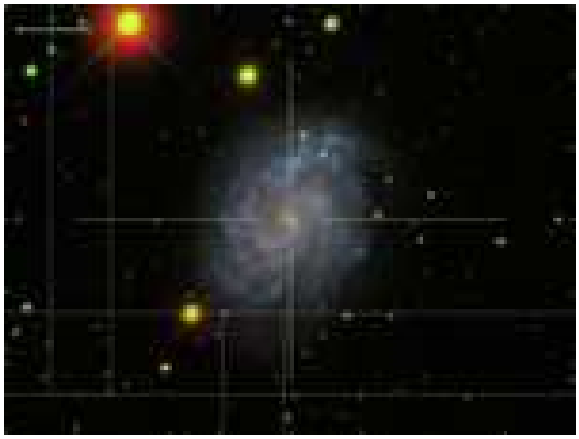

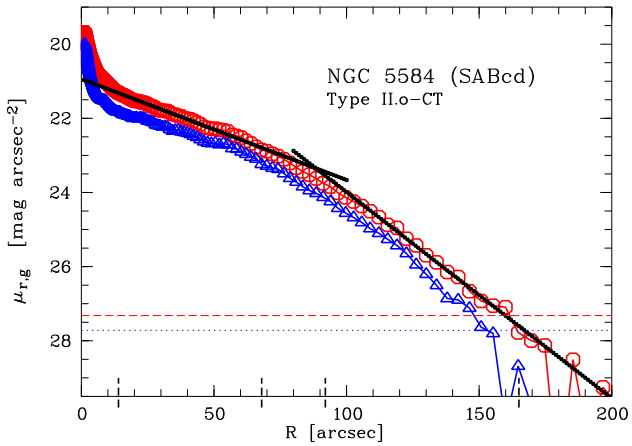

NGC 5624 : Type III
`J142635.3+513503 .S?... 5.0 -18.69 1.1 2186`

Large scale gradient (from top to bottom) in the background of the r' band image is removed with a linear fit. Very small galaxy which is most probably of noticeably later type than classified (Sc). Inner region dominated by an offcenterd (compared to the outer isophote used for centering) narrow bar, or rim-like structure of size $\sim 10''$ which is responsible for the central dip in the profile. The PA of the outermost region is twisted compared to the inner, bar-like structure. The final profile exhibits a straight line starting from $\sim 20''$ (enclosing the central region including the bar having the same PA) down to a break at ~ 45 followed by an upbending profile (classified as Type III) into the more symmetric, diffuse outer disk without visible substructure.

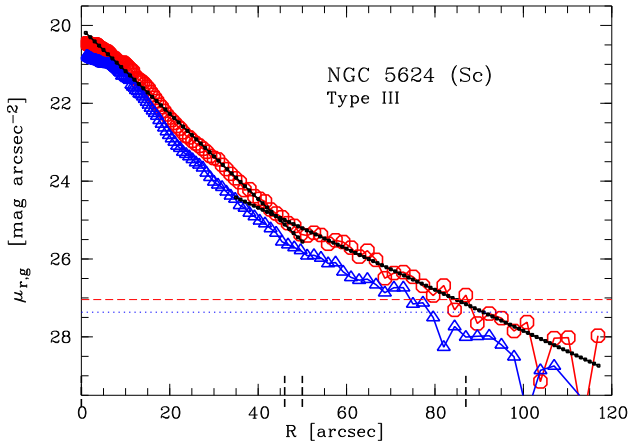

NGC 5660 : Type II-CT
`J142949.8+493722 .SXT5. 5.1 -20.62 2.8 2585`

Galaxy close to the edge of the SDSS field but almost complete sitting in a strip with higher background. According to Sandage & Bedke (1994) it has a small companion nearby ("a likely dwarf Im companion of unknown redshift"), however this could be associated with UGC 09325 (v = 3730km s^{-1}) being clearly a background galaxy. Galaxy shows two, slightly asymmetric inner spiral arms plus an additional one extending towards the outer disk. Although classified as SAB there is no bar-like structure visible except for a possible ring-like structure of size $R \sim 5''$. The final profile is not well described with a single exponential (Type I), already excluding the region beyond $R \sim 90''$ which is most probably affected by an incorrect sky subtraction. Unaffected of this it is better described as having a break at $\sim 70''$, corresponding to the end of the single extended spiral arm, with a following downbending profile, which is too far out to be related to the possible bar and therefore classified as Type II-CT. The bump at $\sim 40''$ is related to the end of the inner spiral arms and beginning of the outer extended one. NIR imaging of the underlying old disk population should give clarification to the classification.

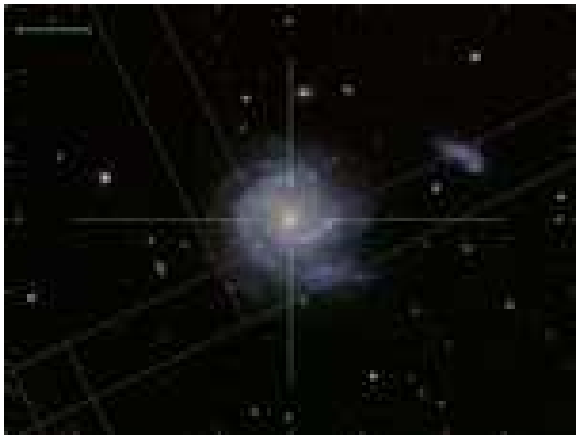

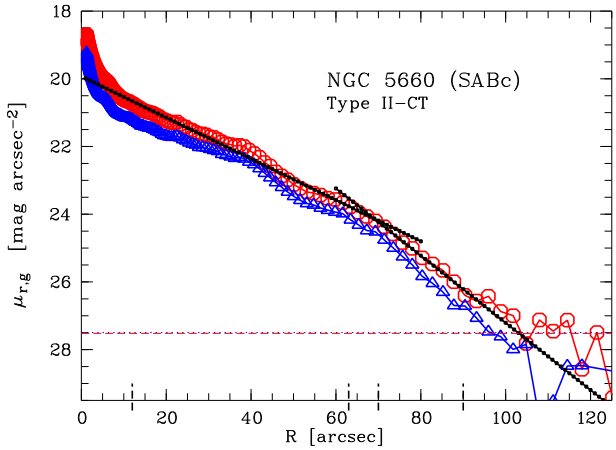

NGC 5667 : Type II.i + III
`J143022.9+592811 .S..6* 5.8 -19.69 1.7 2222`

Galaxy small and close to the edge of the SDSS field but almost complete with an untypical appearance. The inner region ($R \lesssim 30''$) looks like an extended bar with dustlanes and a possible additional, tilted, secondary inner bar of size $R \lesssim 7''$. Outside this region there are two asymmetric narrow spiral arms visible towards north-west followed by an outer, slightly asymmetric, envelope, which makes the photometric inclination (ellipticity) and PA uncertain. The final profile shows a downbending break at $\sim 25''$, related to (and inside) the extended bar structure, therefore classified as Type II.i, followed by an exponential down to another break at $\sim 65''$ where an additional upbending starts adding the Type III classification. The outer profile is uncertain due to a higher error in the sky. A still justifiable sky value could create a continuous outer slope, but this is unlikely, since it will not create the asymmetric shape of the outer isophotes.

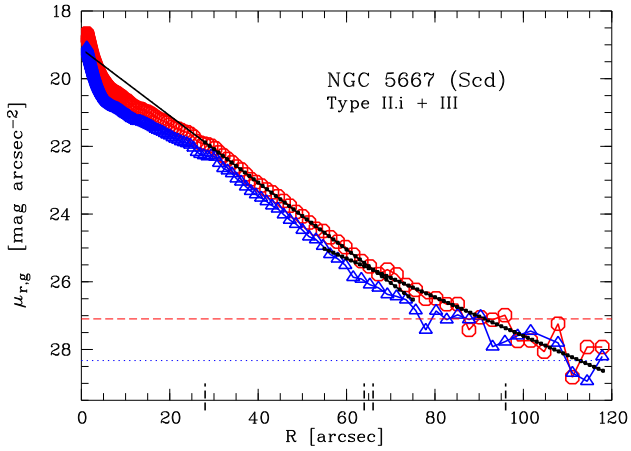

NGC 5668 : Type I
`J143324.4+042702 .SAS7. 6.7 -19.65 2.8 1672`

Galaxy close to the edge of the SDSS field but almost complete. Although classified as SA there is a weak bar or oval inner structure of size $R \sim 12''$ visible on the image, reflected by a small shoulder in the final profile. The outer disk (beyond $R \sim 100''$) is slightly asymmetric and more extended towards the North. The bump at $\sim 70''$ in the final profile is related to brighter spiral arms in this region. There is a possible upbending break visible at $\sim 100''$(associated to the asymmetric outer disk) or $\sim 140''$ but the scalelength contrast is too low and it is too close to the sky error to argue for a Type III classification.

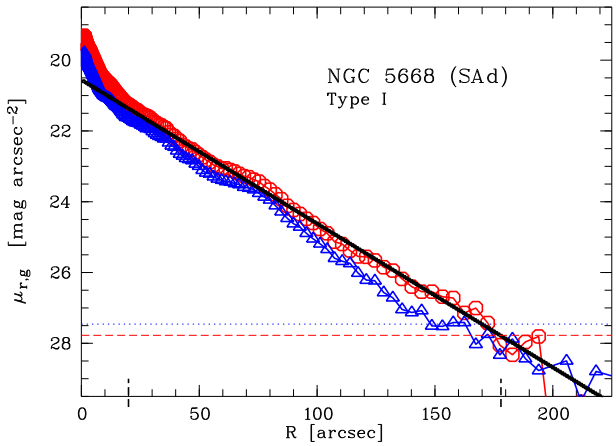

NGC 5693 : Type II-AB
`J143611.2+483504 .SBT7. 6.8 -18.64 1.9 2537`

Small galaxy with unusual appearance, showing an inner extended bar-like structure of size $R \sim 15''$, apparently with two central peaks, probably caused by a superimposed foreground star. The brightest pixel in the bar structure does not correspond to the center obtained from the outer isophotes and is off by $\sim 7''$ causing the inner dip in the final profile. The bar-like structure is followed by a single spiral arm extending towards the outer (quite roundish and symmetric) disk, which is used to obtain the ellipticity and PA. The final profile cannot be well fitted with a single exponential (Type I) but rather shows a downbending behaviour albeit with an uncertain break radius due to the extended break region which resembles again a nearly straight line, so that one could also define two break radii at $\sim 30''$ and $\sim 50''$. Although the first break is at twice the bar radius, we classify this galaxy as Type II-AB since this whole region is clearly lopsided with an significantly offcentered bar.

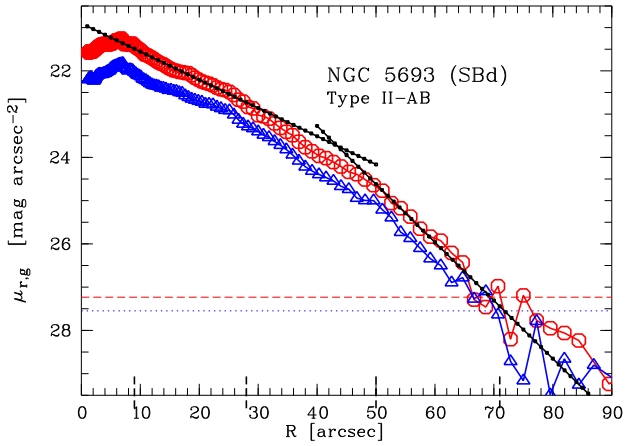

NGC 5713 : Type III
`J144011.4-001725 .SXT4P 4.1 -20.50 2.8 1958`

According to Sandage & Bedke (1994) in a group of late-type spirals with four members in a region smaller than the Local Group. No bright nucleus in the bar-like structure so the centering is done from the outer isophotes. In addition to a more chaotic inner region with spiral structure (producing the bump between $R \sim 10 - 35''$ in the final profile) there is clear substructure in the outer disk visible. Towards the South (1.5′ from the center) we see a very diffuse additional patch of light (size $R \lesssim 20''$and masked), in addition to a more elongated feature ($\approx 1'$ from the center, unmasked) towards north-east. The profile shows a break at $\sim 115''$ with an upbending profile associated with a rather symmetric featureless outer part. The break is not caused by a possible sky error thus classified as Type III.

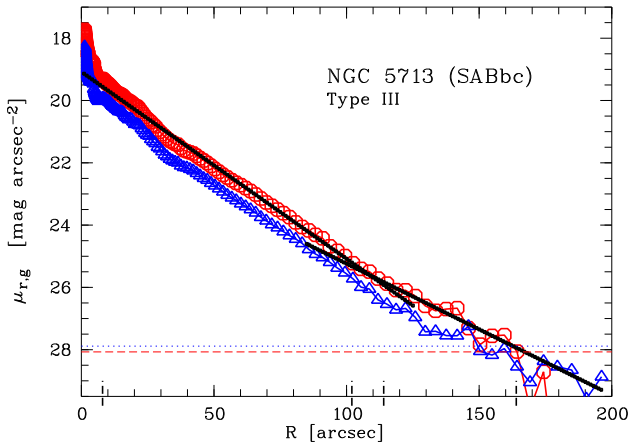

NGC 5768 : Type I
`J145207.9-023147 .SAT5* 5.0 -19.24 1.6 2018`

Bright star superimposed so using an extended mask. Photometric inclination (ellipticity) at 1σ in the free ellipse fit does not match the outer parts well, therefore we used the outermost ellipse which leaves the ellipticity and PA uncertain. Similar to NGC 3888 the final profile exhibits an extended wiggle (with an unusual integral sign shape) at $\sim 50''$ (without being a break) corresponding to a set of spiral arms in the outer disk which do not start at the center. The inner break at $\sim 18''$ is associated with the inner spiral arms and the bar-like center. Although showing extended wiggles the galaxy is classified as Type I since there is no better fitting alternative.

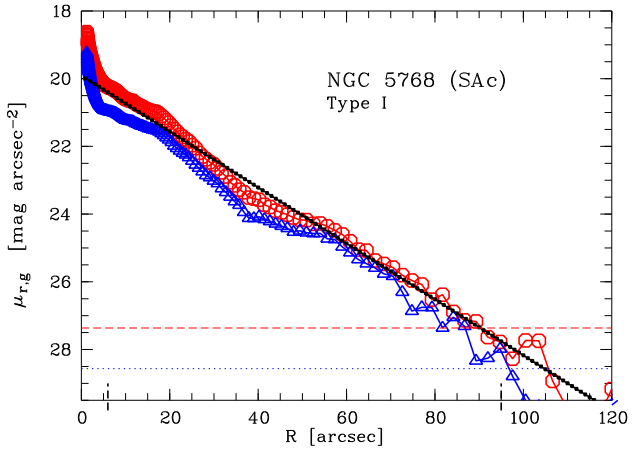

NGC 5774 : Type II.o-OLR + III
`J145342.6+033500 .SXT7. 6.9 -19.09 2.8 1655`

Galaxy has a close physical, edge-on, companion (NGC 5775, SBc?, $v = 1681\,\mathrm{km\,s^{-1}}$) and exhibits an outer, extended spiral arm pointing towards NGC 5775 (similar to the M 51/NGC 5159 system but having a more similar sized mass) producing an asymmetric outer disk where the very outer isophotes already overlap. The center is obtained from outer ellipse fits (different from brightest pixel) since the inner elongated, narrow, bar-like region $R \sim 10''$ is without an obvious nucleus. The shoulder in the final profile at $\gtrsim 35''$ corresponds to the end of the more extended bar-like structure enclosing the inner bar having a different PA. The break at $\sim 80''$ with the downbending profile being at about twice the extended bar radius is therefore classified Type II.o-OLR. The upbending profile (classified as Type III) beyond a break at $\sim 120''$ is due to the asymmetric outer disk with extended spiral arms. Fitting the profile with a single exponential (Type I) leaves three extended wiggles which are better explained by a Type II.o-OLR + III break combination.

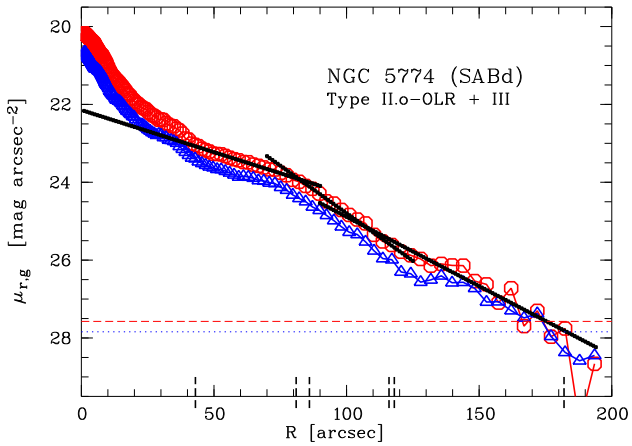

NGC 5806 : Type III
`J150000.4+015329 .SXS3. 3.3 -19.74 3.0 1440`

Galaxy close to our high axis ratio limit (dust lane visible?) and close to the edge of the SDSS field but almost complete. From the inner disk there is an additional patch of diffuse light visible towards the south-east (not masked) extending into the asymmetric outer disk, which makes the photometric inclination (ellipticity) and PA uncertain since obtained further in. The final profile shows a shoulder at $\sim 40''$ related to the inner bar-like center with the beginning of the spiral arms and a break at $\sim 120''$. The break is close to the position of the extra patch of light followed by an upbending profile (classified as Type III) extending into the outer asymmetric disk without spiral structure. Our classification agrees well with Erwin et al. (2006) and the Type III profile is also visible in Courteau (1996) (cf. UGC 09645).

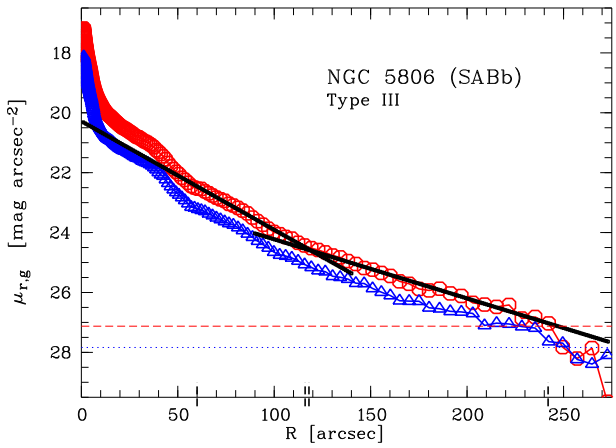

NGC 5850 : Type II.o-OLR
`J150707.7+013240 .SBR3. 3.0 -21.43 4.3 2637`

Bright star nearby needs extended mask. The r' band background is slightly inhomogeneous. Galaxy is dominated by an extended bar of size $R \sim 55''$ enclosed by an inner ring out to $R \sim 75''$ having a secondary, inner bar of size $R \sim 7''$ with clearly different ellipticity and PA. There is an additional, faint outer ring (or pseudo-ring, since looking similar to some wrapped spiral arms) visible on the image related to the break at $\sim 130''$ in the final profile, thus obviously classified as Type II.o-OLR. Since the outer ring is used to determine the photometric inclination (ellipticity) and PA they are rather uncertain.

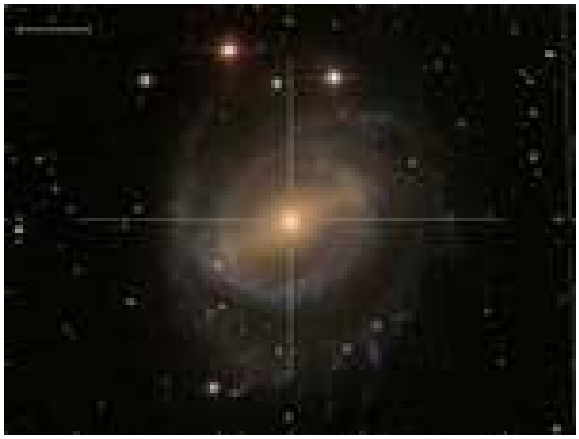

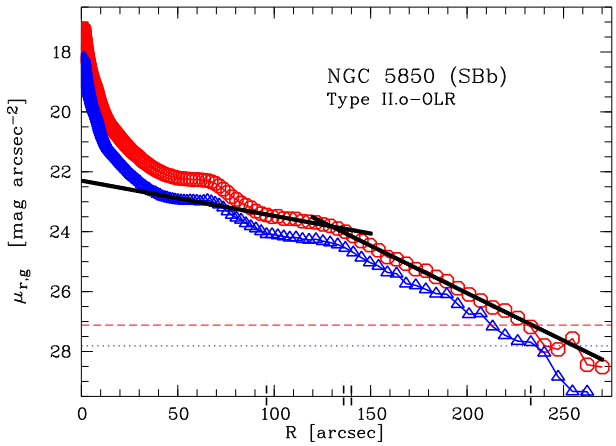

NGC 5937 : Type III
`J153046.1-024946 PSXT3P 3.2 -20.90 1.9 2870`

Bright stars nearby need extended mask without really covering the outer disk. There is a possible, small dwarf companion (not in NED) visible about 1.5′ away towards the northwest. The outer disk is slightly asymmetric with continuously changing ellipticity and PA, so the values applied for the final profile are rather uncertain. The break at $\sim 70''$ with an upbending profile (classified as Type III) is most probably related to the changing ellipticity and should be taken with caution.

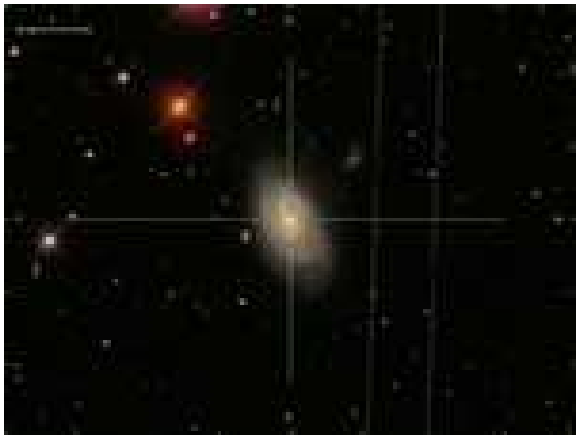

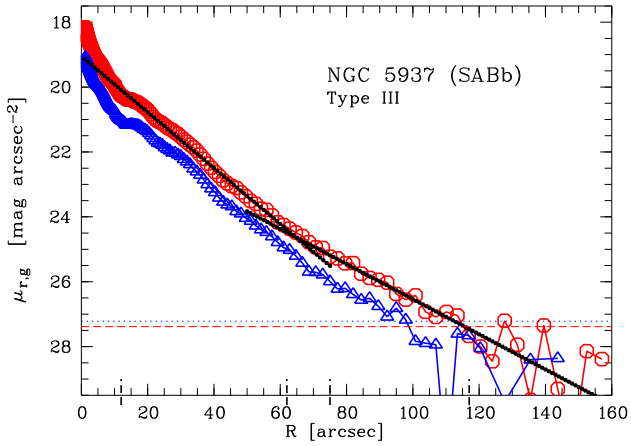

NGC 6070 : Type II.o-CT
`J160958.9+004234 .SAS6. 6.0 -21.04 3.4 2085`

Galaxy close to our high axis ratio limit having a very bright star (with an extended halo) in the FOV which is still small enough to avoid significant influence. Only partly fitted since $\lesssim 1/5$ of galaxy is beyond SDSS field. The outer isophotes are slightly asymmetric, with one sharp and one more fluffy side, so the ellipticity and PA are uncertain. The final profile exhibits a clear downbending with a more extended break region around $R \sim 95''$ corresponding to the end of the spiral arm structure and classified as Type II.o-CT. Although the galaxy is classified as SA there is an elliptical central bar-like structure of size $\lesssim 10''$ visible which would be however too small to argue for a Type II.o-OLR break. The small dip at $\sim 30''$ is produced by spiral arm contrast.

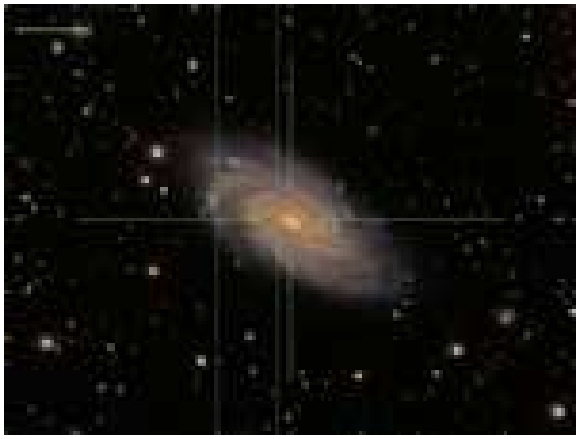

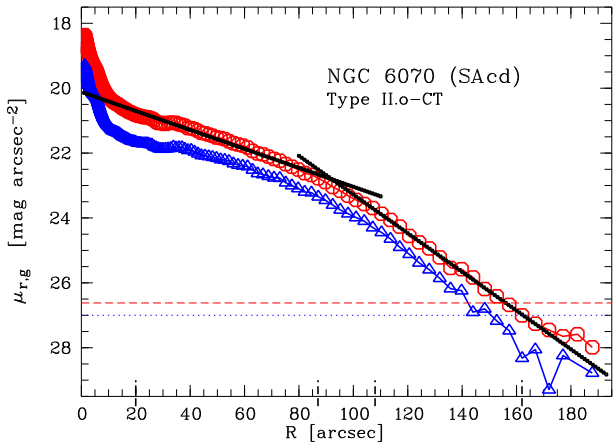

NGC 6155 : Type II-AB
`J162608.3+482201 .S?... 7.8 -19.45 1.3 2684`

Small galaxy with an extended mask reaching into the outer disk to cover a very bright star close by. Lopsided disk with centering done from the outer isophotes. The center is $\sim 3''$ off the brightest pixel associated to a small bar-like central structure of size $R \sim 5''$ followed by a thin, star-forming, blue spiral arm feature towards north-east. The final profile shows a downbending break at $\sim 35''$ corresponding to the inner lopsided disk thus classified as a Type II-AB break, although this is just at the radius of an outer ring (best visible in the colour image).

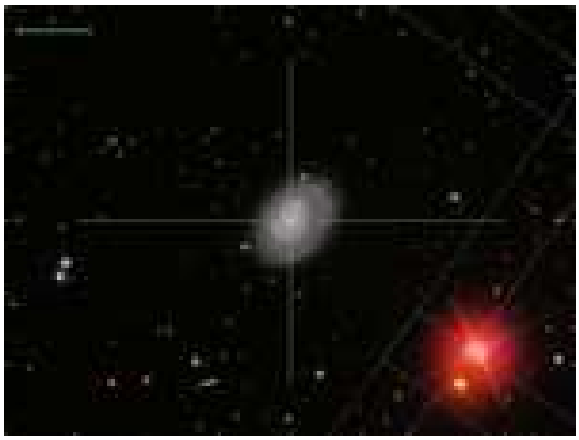

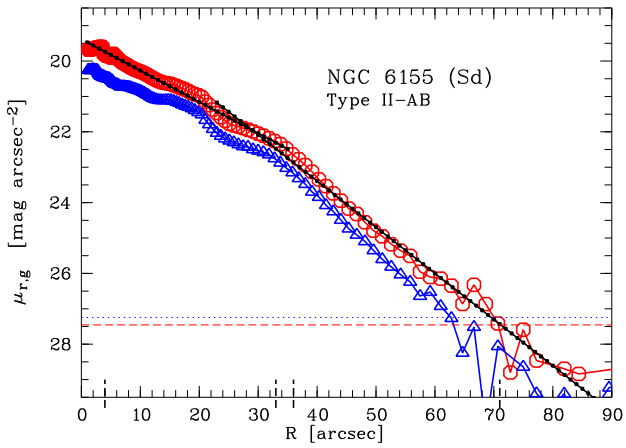

NGC 7437 : Type II-CT
`J225810.0+141832 .SXT7. 7.1 -18.88 1.8 2190`

Small galaxy close to the edge of the SDSS field but almost complete. Similar to NGC 5300 the final profile shows the prototypical Type II.o-CT behaviour. A sharp break at $\sim 40''$, corresponding roughly to the end of the apparent flocculent spiral arm structure, followed by a downbending profile. Although classified as SAB there is no obvious structure visible which could be identified with a bar. Using the beginning spiral arms as an upper limit ($R \lesssim 8''$) the break is still too far out for a normal Type II.o-OLR break.

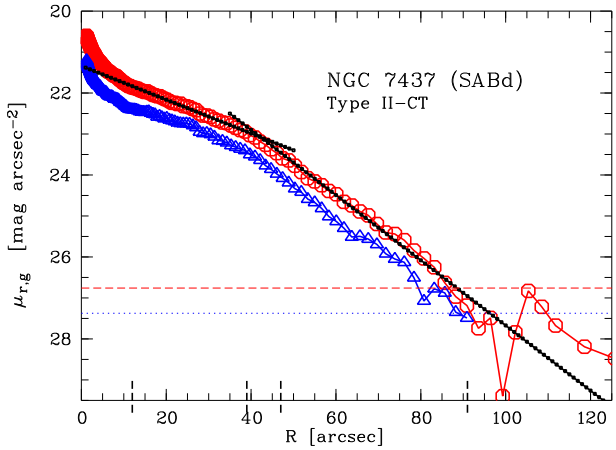

NGC 7606 : Type II-CT
`J231904.8-082906 .SAS3. 3.2 -21.38 4.3 2187`

Galaxy with multiple thin spiral arms. The final profile exhibits clearly a break at $\sim 110''$corresponding roughly to the end of the visible spiral arm structure, following part of the ring enclosing an apparent hole (enhanced dust extinction?) in the disk towards the north-west. Since the galaxy is classified as SA and no bar structure visible the break is a Type II-CT. The apparent upbending of the profile beyond $\sim 190''$is not related to a sky error but due to a changing ellipticity in the very outer disk (maybe due to a warp?).

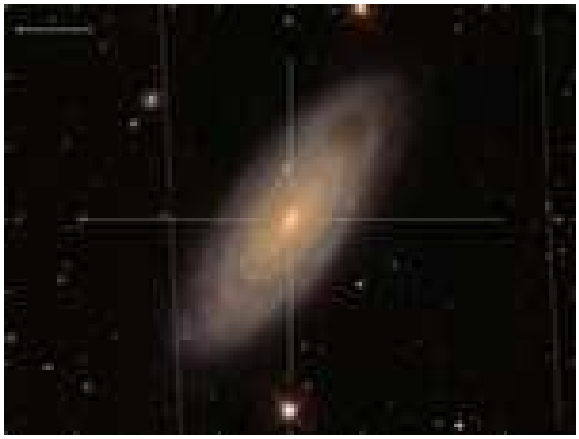

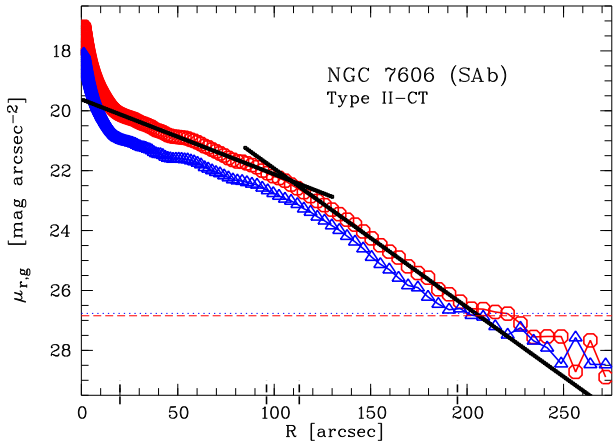

PGC 006667 ≡ UGCA 021 : Type II-AB
`J014910.2-100345 .SBS7. 7.1 -18.77 2.9 1887`

A large scale gradient (from top to bottom) in the background of the r' band image is removed with linear fit. Galaxy in NGC 701 group (see above). Final profile shows a bump at $\sim 20''$ due to the spiral arms starting from the bar-like center. The clear downbending break at $\sim 75''$ corresponds to a transition from the inner more symmetric to an asymmetric, extended outer disk region and is therefore classified as Type II-AB.

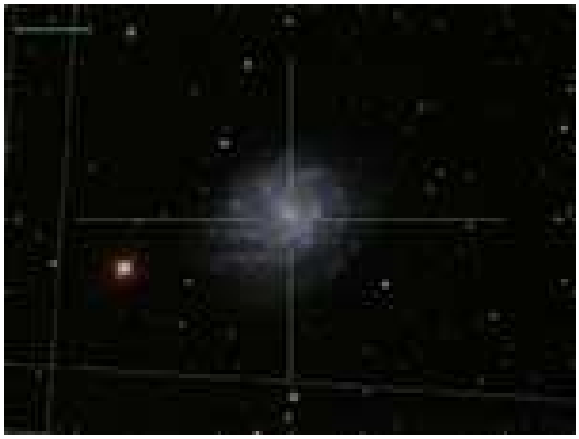

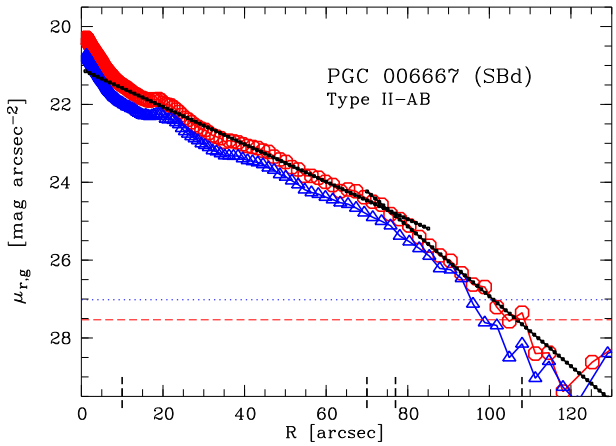

UGC 02081 : Type II-CT
`J023600.9+002512 .SXS6. 5.8 -18.56 1.8 2549`

Galaxy close to the edge of the SDSS field but almost complete. The final profile shows a downbending break starting around $\sim 55''$ (clearly at $\sim 70''$) with a very faint, but symmetric light distribution beyond. Although classified as SAB the bar is not obvious from the image but the spiral arms allow to estimate an upper limit of $R \lesssim 7''$. Therefore the break (which is not produced by a sky error) is classified Type II-CT. The profile published in de Jong & van der Kruit (1994) is not deep enough to confirm the downbending.

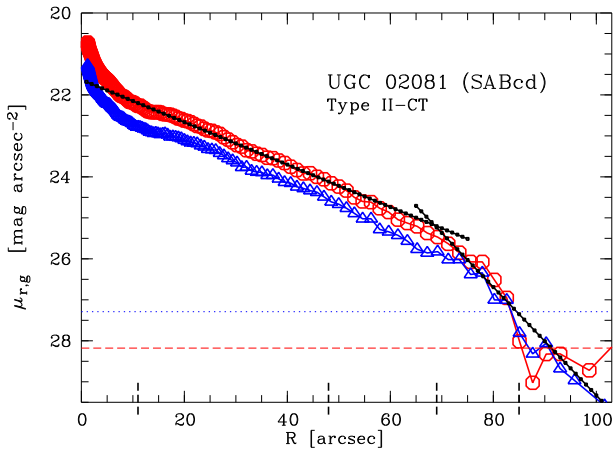

UGC 04393 : Type I
`J082604.3+455803 .SB?.. 5.5 -19.49 2.2 2290`

Galaxy is classified as SB and the inner region is dominated by an elongated bar-like structure of size $R \sim 30''$. Therefore this region is excluded from the fit. The extended bar, having a kind of double nucleus, is slightly offcenter (central dip in profile) compared to the center obtained from the outer isophotes and is followed by a single, narrow spiral arm like structure extending south-west. In the outer disk there is an additional, faint spiral arm visible towards the south-east. There is also a very faint shell or stream-like structure detected, detached from the galaxy about $2'$ away to the north-west. The inclination (ellipticity) and PA are rather uncertain since they are continuously changing towards the outer disk. The final profile, beyond the inner bar region, is classified as Type I, due to the uncertain ellipticity and the asymmetric outer disk with the spiral arm, although there are two possible breaks visible at $\sim 60''$ and $\sim 80''$, of which the first could correspond to a Type II.o-OLR break and the latter to a Type III.

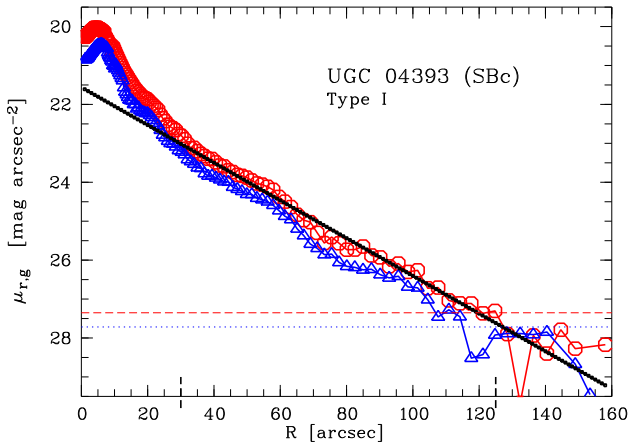

UGC 06309 : Type II.i
`J111746.4+512836 .SB?.. 5.0 -19.63 1.3 3097`

There is a small BCG (MRK 1445) about $3.5'$ away at roughly the same distance ($v = 2863\,\mathrm{km\,s^{-1}}$). Galaxy exhibits very unusual, disturbed shape. The inner disk is dominated by a narrow bar of size $R \lesssim 20''$ followed by two asymmetric spiral arms (one highly wrapped, forming an inner ring, the other almost extending straight). The disk beyond the spiral arms is also highly asymmetric and more egg-shaped with a region of low emission (high extinction?) towards the south-east, which makes the bar appear to be offcentered. However, the center from the very outer isophotes coincides again with the nucleus inside the bar. The extended dip and peak structure around $15-20''$ in the final profile corresponds to the inter-arm region, respectively the pseudoring build by the arms, so the break around this radius is classified as Type II.i. This should be used with caution, since alternatively one can argue for a break at $\sim 35''$, at about twice the bar radius thus a Type II.o-OLR break, while excluding the region between $15 - 30''$.

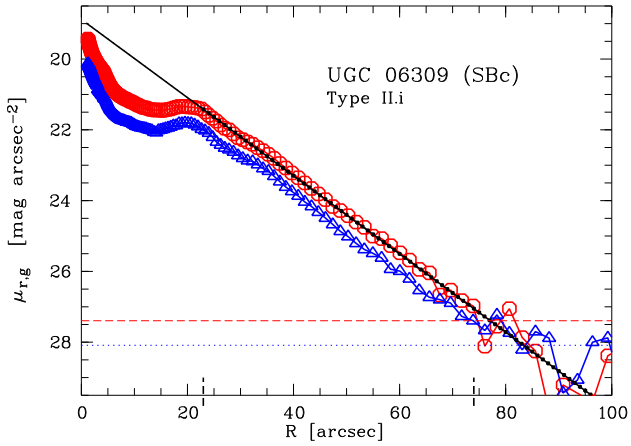

UGC 06518 : Type II.i
`J113220.4+535417 ..... 4.3 -18.94 1.0 3044`

Small galaxy where, although not classified as barred in NED or LEDA, there is clearly a bar of size $R \sim 10''$ visible, with indication for a ring-like structure around, already reported by Takase & Miyauchi-Isobe (1984). Despite the possibility to argue for a break at $\sim 15''$ in the final profile we classify the galaxy as Type II.i excluding the region inside $R = 10''$ from the fit.

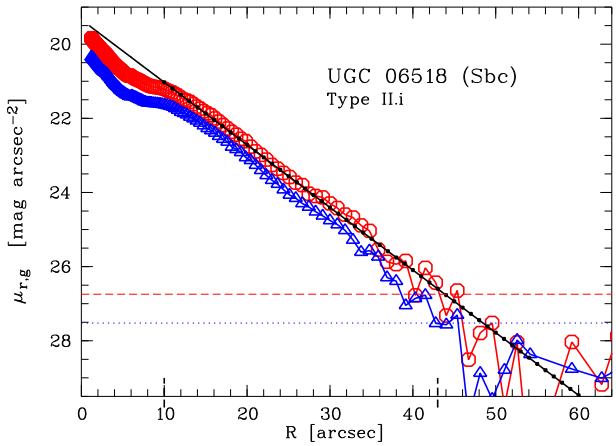

UGC 06903 : Type II.o-CT
`J115536.9+011415 .SBS6. 5.8 -18.80 2.5 1916`

Very bright star in FOV but galaxy not influenced. Final profile shows clearly a downbending break around $\sim 65''$ corresponding roughly to the end of the visible spiral arm structure and classified Type II.o-CT, since the size of the bar with $R \lesssim 17$ is too small. The extended bump between $R \sim 20-40''$ is related to the inner two, highly wrapped (pseudoring?) spiral arms. The downbending shape is consistent with the profile shown in Jansen et al. (2000) (cf. ID 99).

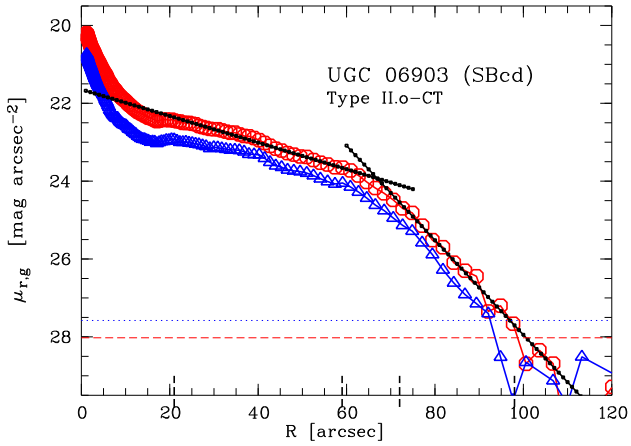

UGC 07700 : Type II.o-CT
`J123232.8+635238 .SBS8. 7.8 -18.50 1.8 3239`

There is a very bright star in the FOV but the galaxy is not influenced. On same image there is an edge-on companion (S0/a galaxy NGC 4512) at similar distance (v = 2536km s^{-1}) visible. Ellipticity obtained from the very outer isophotes and not by the usual 1σ criterion. The final profile shows clearly a downbending behaviour outside the bar region. The bar is about $R \sim 17''$ in size and slightly off-centered (by $\sim 5''$) compared to the center obtained from the outer, symmetric isophotes. This causes the dip at the center. The extended break region is not exponential but shows a curvature, but still one could define two break radii at $\sim 40''$ and $\sim 50''$. The region in between corresponds to a single spiral arm extending towards the north-east. Although the first one would roughly classify as a Type II.o-OLR break we used a single break slightly further out and classified the galaxy as Type II.o-CT.

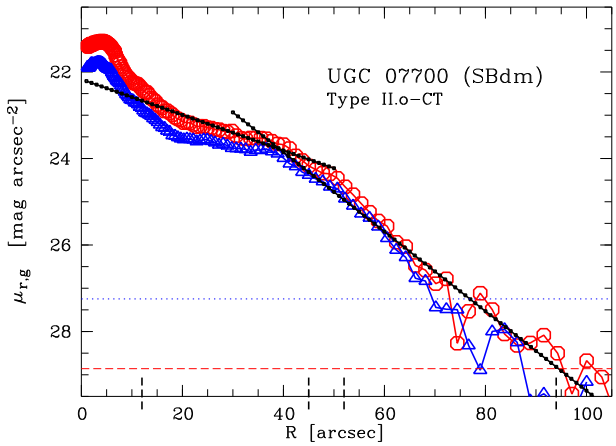

UGC 08041 : Type II.o-CT
`J125512.7+000700 .SBS7. 6.8 -18.62 3.2 1376`

Galaxy close to our high axis ratio limit and not influenced by the very bright star in FOV. The inner disk with a bright nucleus in the bar and weak spiral arm structure extends to about $\sim 100''$, followed by a rather asymmetric, lopsided outer disk extending to the south-west. Centering on the outer isophotes ($R \gtrsim 100''$) would be off by more than $\sim 10''$. The final profile shows a downbending break at $\sim 75''$roughly corresponding to the end of the spiral structure. Since the bar is only of size $R \lesssim 12''$ the break, at significantly more than twice the bar radius, is classified as Type II.o-CT. The fixed ellipse leaves the inner symmetric disk at about $\sim 100''$ into the asymmetric outer part causing the apparent upbending in the profile, which probably increases the fitted outer scalelength.

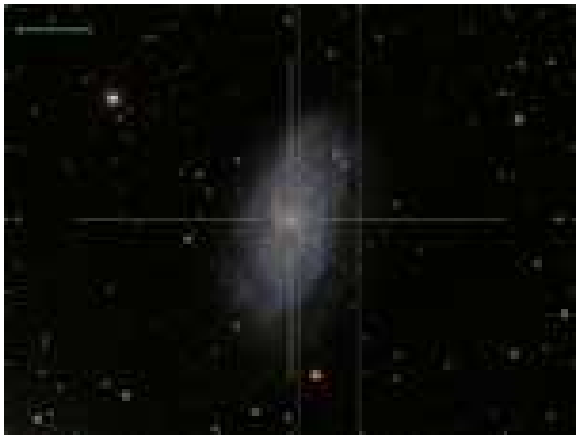

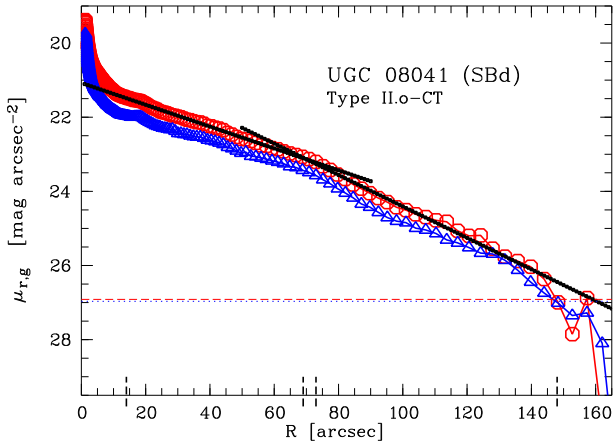

UGC 08084 : Type II.o-OLR
`J125822.4+024733 .SBS8. 8.1 -18.61 1.3 2824`

Small galaxy dominated by an inner offcentered, asymmetric bar of size $R \sim 17''$, which appears to be z-shaped together with the two spiral arms. The center is obtained from outer isophotes ($\sim 50''$) and is about $\sim 12''$ away from the brightest pixel in bar, which is responsible for the flat inner profile. The final profile shows clearly a downbending break at $\sim 40''$corresponding to the spiral arms forming a kind of pseudoring in the outer parts. Since the break is at about twice the bar size the galaxy is classified as Type II.o-OLR.

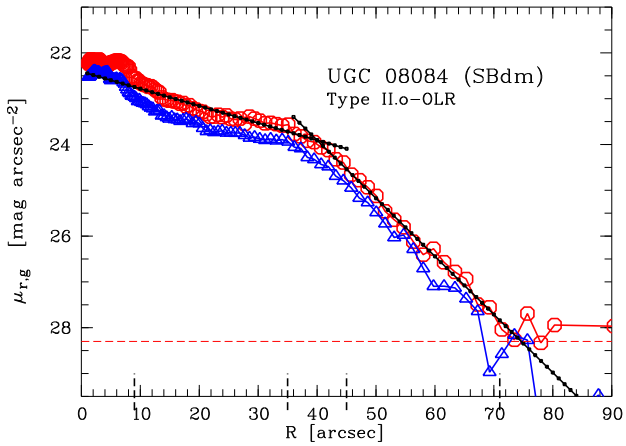

UGC 08237 : Type II.o-OLR
`J130854.5+621823 PSB.3* 3.2 -19.61 0.9 3120`

Galaxy is isolated according to Prada et al. (2003). The similar sized companion, only 2.3′ away, is a confirmed background galaxy (UGC 08234, $v = 8100\,\mathrm{km\,s^{-1}}$). Background needs extended mask due to straylight from a very bright star off the field. UGC 08237 is a small galaxy dominated by a bright, thick bar of size $R \lesssim 12''$ (producing the shoulder in the final profile) followed by two nearly symmetric, wrapped spiral arms forming a pseudoring peaking at $\sim 20''$. Similar to NGC 5701 (an early-type SB0/a galaxy from Erwin et al. (2006)) one could define a break at $\sim 25''$ just outside of the pseudoring forming the region $R \sim 12-25$ which is no longer well fitted by an exponential profile. Erwin et al. (2006) call these systems 'extreme' OLR breaks, so we also classify the galaxy as Type II.o-OLR and apply a crude fit to obtain an inner scalelength.

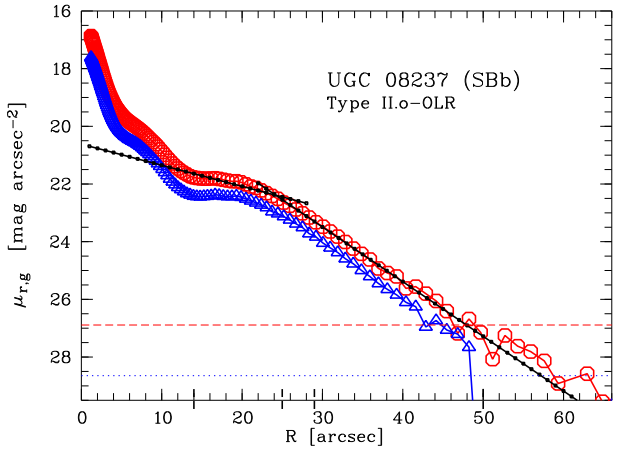

UGC 08658 ≡ Holmberg V : Type II-CT
`J134039.9+541959 .SXT5. 5.1 -19.91 2.6 2285`

Galaxy close to the border of the SDSS field but almost complete. Although classified as SAB, the bar size is not obvious from the image, but could be restricted by the spiral arms to be maximal $R \lesssim 10''$. The shoulder in the final profile at $\sim 20''$ is due to the inner spiral arms being aligned with the ellipse. There is a weak break at $\sim 65''$ visible which roughly coincides with the end of the inner spiral arm structure, although there are maybe two faint extensions into the outer disk. Since being at significantly more than two bar radii we classify the break as Type II-CT.

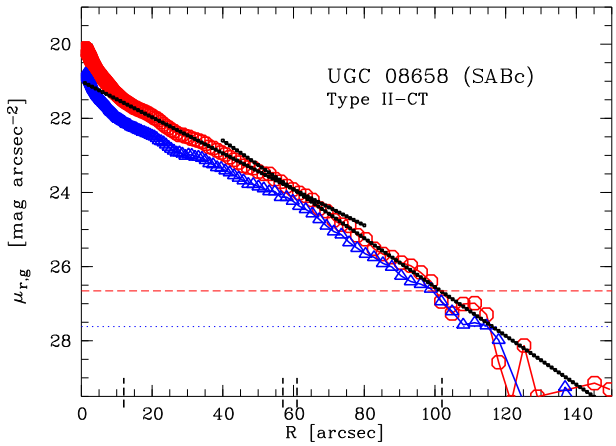

UGC 09741 ≡ NGC 5875A : Type III
`J150833.5+521746 .S?... 6.0 -18.54 0.9 2735`

The patch of faint light on the image towards the north-west is caused by straylight from a very bright star off field, but the galaxy is not affected. Very small galaxy dominated by a long, narrow bar of size $R \sim 9''$, enclosed by a ring like structure building the inner $R \lesssim 17''$ disk. The photometric inclination (ellipticity) and PA is obtained from the outer disk at $\sim 45''$ and not from the 1σ ellipse. Although it is possible to fit the profile beyond $\sim 17''$with a single exponential the offset inside would be too large to be assigned solely to a bulge component of a typical Sc galaxy. In addition, an extended bulge component is also not visible on the image inside the narrow bar. Thus we argue for a break, classified as Type III, at $\sim 25''$ followed by an upbending profile into the symmetric featureless outer disk. The shape of the profile is consistent with the one shown by Jansen et al. (2000) (cf. ID 166).

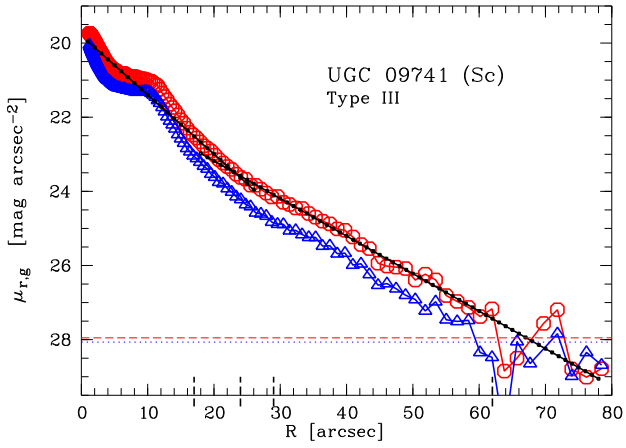

UGC 09837 : Type II-CT
`J152351.7+580311 .SXS5. 5.1 -19.45 1.8 2938`

Although classified as SAB, the bar size is not obvious from the image, but could be restricted to be maximal $R \lesssim 9''$by the two symmetric spiral arms starting beyond the bulge/bar region out to $R \sim 25''$. Further out, there is more asymmetric spiral arm structure visible, with one arm almost forming a ring-like section, which makes the photometric inclination (ellipticity) and PA determination impossible at the 1σ ellipse. Since the ring like section extends to the end of our free ellipse fit, we set the ellipticity to 0.05 (round). In the final profile there is a break visible at $\sim 50''$ just beyond the bump produced by the ring-like spiral arm. Since this break is at significantly more than two times the upper limit for the bar radius we classify the break as Type II-CT. The deep surface photometry from Pohlen et al. (2002) is consistent with the results here (cf. Fig. 3) aside from this bump produced by the outer spiral arm, which seems to be suppressed in their averaged profile. The downbending shape with a break at $\sim 50''$ is consistent with the profile shown by van der Kruit (1987).

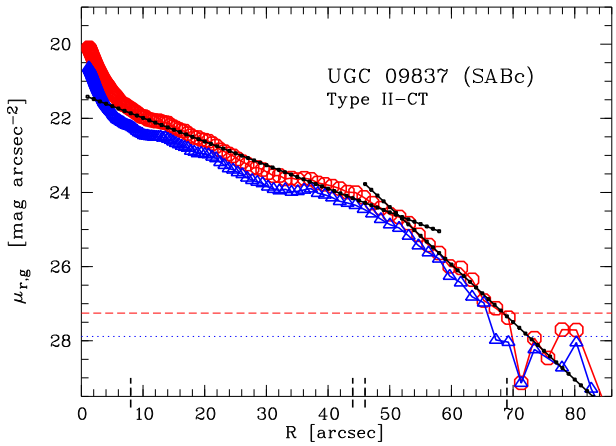

UGC 10721 : Type III
`J170825.6+253103 .S..6? 5.8 -19.68 1.2 3118`

Small galaxy close to our high axis ratio limit so the dust may get important. Galaxy shows an inner apparently inclined disk with a nucleus and some thin spiral arms sitting in an almost round outer isophote most probably related to a vertical structure (halo or thick disk). Thus the photometric inclination (ellipticity) and PA are highly uncertain since continously changing with radius. The shoulder at $\sim 12''$ in the final profile corresponds to an aligned spiral arm. There is a clear break visible at $\sim 40''$ followed by an upbending profile which is classified as Type III, associated to the transition between inner and outer disk (vertical structure?), so to be taken with some caution. The sharp transition in the profile argues against a thick disk. The upbending behaviour is confirmed by the profile from Courteau (1996).

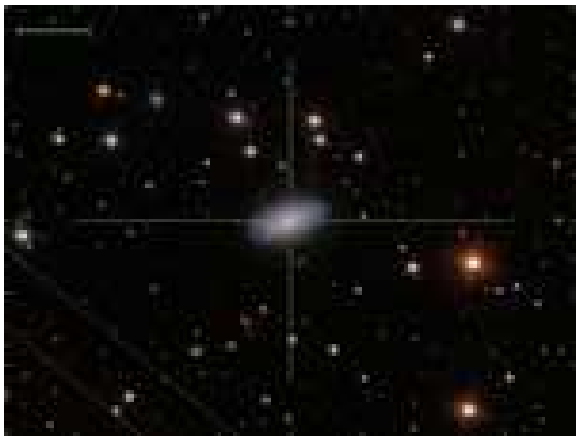

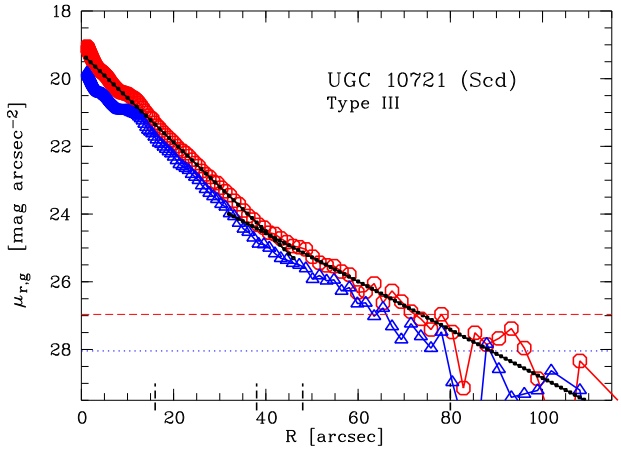

UGC 12709 : Type II-CT
`J233724.0+002327 .SXS9. 8.3 -19.05 3.0 2672`

This is a faint, low surface brightness galaxy without a well defined center, so the centering (obtained from the ~ 80″ellipse) and the photometric inclination (ellipticity) and PA (obtained at ~ 70″) are uncertain. The offcentered outer disk is reflected by the central dip in the final profile, which shows a clear downbending break at ~ 70″ corresponding roughly to the end of the flocculent starforming patches. Although classified as SAB the central region (~ 10″) is too fuzzy to argue for or against a bar, but in both cases it is to small to be responsible for the break, which is therefore classified as Type II-CT.

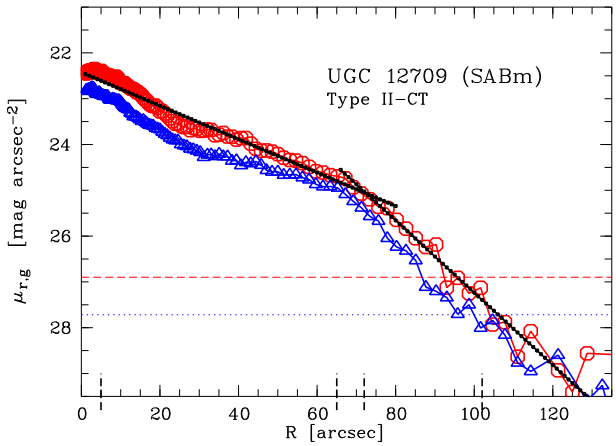

Appendix B: Rejected galaxies

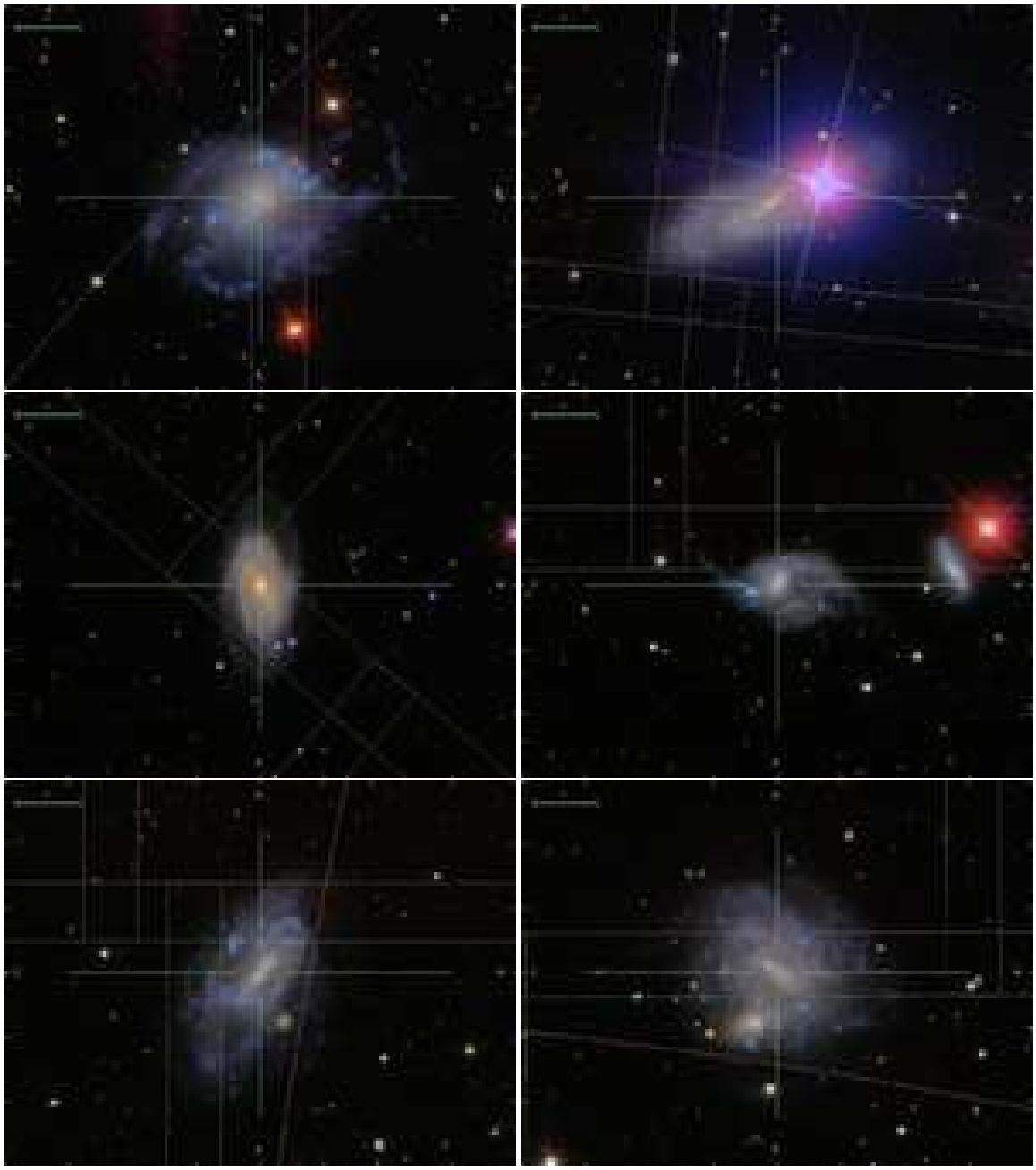

Fig. B.1. Galaxies rejected from the original LEDA-SDSS(DR2) sample: SDSS colour plates of NGC 0428, NGC 0988, NGC 2712, NGC 3023, NGC 4116, and NGC 4496A *(from left to right and top to bottom)*

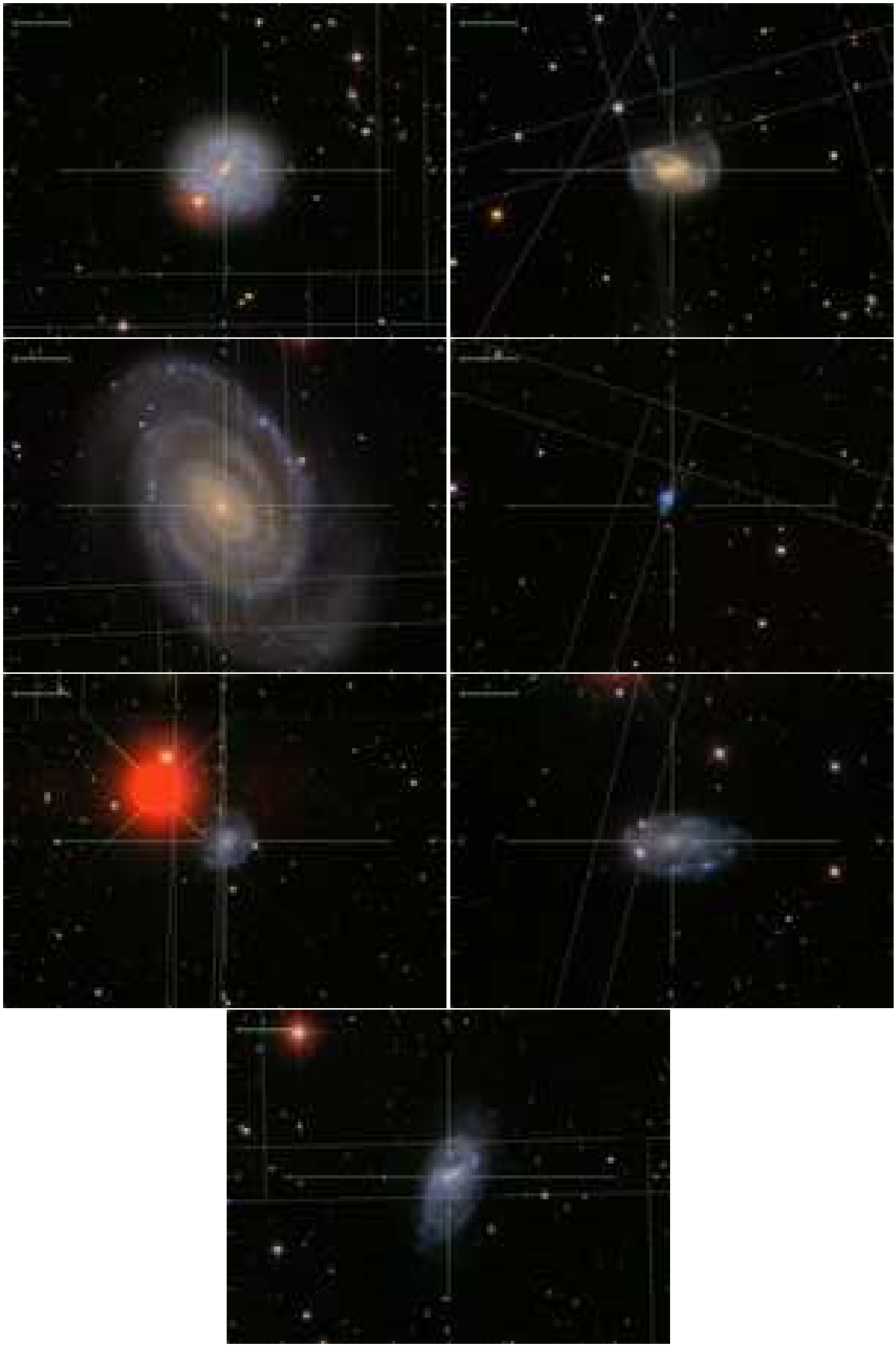

Fig. B.1. (continued): Galaxies rejected from the original LEDA-SDSS(DR2) sample SDSS colour plates of NGC 4900, NGC 5218, NGC 5364, PGC 032356, UGC 04684, UGC 06162, and UGC 09215 *(from left to right and top to bottom)*